The Dissertation Committee for Kaustubh Ramesh Thirumalai Certifies that this is the approved version of the following dissertation:

Surface-ocean variability in the northern Gulf of Mexico during the late Holocene

Committee:

Terrence M. Quinn, Supervisor

Timothy M. Shanahan

Sean P. S. Gulick

Yuko Okumura

Judson W. Partin

Cliff Frohlich

Surface-ocean variability in the northern Gulf of Mexico during the late Holocene

by

Kaustubh Ramesh Thirumalai, B.E.; M.S.Geo.Sci.

Dissertation

Presented to the Faculty of the Graduate School of

The University of Texas at Austin

in Partial Fulfillment

of the Requirements

for the Degree of

Doctor of Philosophy

The University of Texas at Austin

May 2016

Dedication

This body of work is dedicated to all extant foraminiferans in the Gulf of Mexico, whose number is estimated to be roughly equivalent to the number of bugs encountered via coding for this research.

Acknowledgements

As a 1st-year undergraduate student at the National Institute of Technology Karnataka in Surathkal, India, based on my erstwhile (woeful) progress towards a bachelor's degree in chemical engineering (and otherwise), I never thought that I would pursue (and complete) a graduate degree, moreover in an academic area that I would find enjoyable. During engineering off-time over the next two years, after having completed fledgling research stints at Ahmedabad's Physical Research Laboratory and Bangalore's Indian Institute of Science, I was astonished to discover that I was not only motivated to apply for graduate programs (lackluster chemical engineering scorecard notwithstanding) but had also stumbled upon an academic pursuit that charged my bones with curiosity. Looking back, foraying into the field of Earth sciences at the time was very fortuitous and the journey ever since has been richly rewarding and frankly, a whole lot of fun. Looking forward, I am confident of continually being fascinated by the Earth sciences well into the future.

Many thanks are due to the myriad number of people who have helped me along the way. Firstly, I must thank Dr. R. Ramesh (PRL) and Dr. Prosenjith Ghosh (IISc) who were instrumental in supporting and fostering my interests in stable isotopes, paleoclimatology, and the geosciences in general.

After I moved to Austin, Texas, perhaps nobody has been as helpful to me (scientifically or otherwise) as Dr. Jud Partin. Jud, who is a committee member of my dissertation, has also been a colleague, mentor, friend, brother, field work companion, and landlord amongst other roles during my Ph.D. I owe

him a token of deep gratitude and anticipate many more adventures in the future. On a similar note, Dr. Fred Taylor has helped me out by playing numerous roles as well and has instilled in me a great interest in corals, earthquakes, and neotectonics. Fred has also taught me countless lessons in the field and spending time with him in the Solomon Islands was an invaluable life-experience. I cherish all my UTIG lunches with Jud and Fred.

This body of research would not have been possible without the help of my USGS colleagues at the St. Petersburg Coastal and Marine Science Center, Dr. Richard Poore and Dr. Julie Richey. Dick has been an outstanding source of knowledge and support. Him, along with Jess Spear, taught me how to 'pick bugs' and for this I am very grateful. Julie has been a fantastic colleague and I am indebted to her for her sage advices and opportunities that she has provided me, including several chances to be a ship-going scientist in the Gulf of Mexico; here's to doing research in many more gulfs across the world.

The field of geochemistry and field work related to paleoceanography are inherently technical in nature and involve heavy machinery. During my Ph.D., I have had the opportunity to learn many laboratory and field techniques and to this I owe sincere, heartfelt thanks to Mark Woodworth and Jim Burdett from Thermo, and to Eric Tappa from USC.

I extend thanks to my committee members who have contributed significantly to my dissertation and my research. Dr. Tim Shanahan has been very helpful as a colleague with whom I have bounced off several ideas (most bad, some good!) and discussed paleoclimate hypotheses into the late hours of the evening. Dr. Yuko Okumura has been incredibly helpful in advancing my knowledge of climate dynamics and data analysis. I thank Dr. Sean Gulick for

providing knowledge on the marine geology and sedimentology aspect of my dissertation, and Dr. Cliff Frohlich who has been insightful on statistics and aided me greatly in my tectonics project. I also thank Dr. Charles Jackson, Dr. Luc Lavier, and Dr. John Goff from UTIG for their input as well.

I acknowledge all members of Team Paleo over the years who have helped me in one way or another – many thanks to Dr. Chris Maupin, Dr. Deborah Khider, Dr. Kelly Hereid, Allison Lawman, Victoria Fortiz, Meaghan Gorman, Natasha Sekhon, and Rindy Ostermann.

Several friends have been a constant source of support throughout my Ph.D. A big thank you to John Swartz, Sebastian Ramirez, Pedro DiNezio, Gail Gutowski, Maureen LeVoir Walton, Annie Miller, Abhijeet Rao, Allyson Plantz, Priya Mukherjee, Marie Cavitte, Enrica Quartini, David Walton, Brandon Hanna, and to my brother, Sriranjan Thirumalai. Thanks for listening to me vent and wax poetic about my research, hurdles, and progress!

My parents T. K. Ramesh and Harini Ramesh have been endlessly supportive and encouraging despite being two oceans apart, and I am very thankful for their reinforcement.

Last but certainly not least, I am indebted to Dr. Terry Quinn. If it hadn't been for a phone call that Terry made to a small, sleepy coastal town in southwestern India in 2010, I would not be graduating with a Ph.D. from UT Austin. I have learned many valuable lessons in paleoceanography, science, and life in general from Terry and am extremely grateful to have worked with him. For your support and all your insights – thank you Terry!

I am thankful to have stumbled upon paleoclimatology and Earth science. At this stage of life, I am pleased to count myself as someone who lives to work.

Surface-ocean variability in the northern Gulf of Mexico during the late Holocene

Kaustubh Ramesh Thirumalai, Ph.D.

The University of Texas at Austin, 2016

Supervisor: Terrence Quinn

The surface waters of the Gulf of Mexico (GOM) are a major moisture source for North America and play an important role in modulating the hydroclimate of the region. Predictions of future changes in surface-ocean variability in the GOM and hydroclimatic changes in response to greenhouse gas forcing must be placed in context of past changes. However, the instrumental record of sea-surface temperature (SST) and salinity (SSS) observations in the GOM is too brief to examine climate variability on multidecadal-to-centennial timescales; thus, proxy records of SST and SSS variability as encoded in marine sedimentary archives must be used to extract information about climate change on these timescales. In this work, I produce a near-decadal-resolution record of SST and SSS variability in the northern GOM over the last 4,400 years. These paleo-records are based on the measurement of the stable isotopic and trace metal composition of planktic foraminifer *Globigerinoides ruber* (White) shells in a suite of multicores from the Garrison Basin, northern GOM (26º 40.19'N,93º 55.22'W). The fidelity of this proxy is assessed by performing geochemical measurements on *in-situ* samples from a nearby sediment trap and by

performing statistical data-model comparisons with a foraminiferal forward model that can simulate different calcification depth habitats and seasonal productivity. Next, I construct a computational algorithm that characterizes uncertainty in foraminiferal reconstructions including age, analytical, calibration, ecological, sampling, and preservation errors. The utility of this algorithm is shown by applying it to several previously published records. It is also used to place the new Garrison Basin SST and SSS reconstructions in a quantitative uncertainty framework. I diagnose the controls of multidecadal-to-centennial-scale SST and SSS variability in the GOM (and establish its relationship with Atlantic Ocean circulation) by performing correlation analyses using observations, reanalysis datasets, and transient models. Several other marine and terrestrial proxy records spanning the last millennium are synthesized to document a coordinated linkage between Atlantic Ocean circulation and Western Hemisphere precipitation. This work hypothesizes that a century-scale linkage between ocean circulation and precipitation variability occurred over the last millennium, and perhaps the late Holocene, thereby providing a new perspective on long-term climate change.

Table of Contents

List of Figures

Introduction

The Gulf of Mexico (GOM) is a significant moisture source for the North American continent and plays an important role in modulating the climate of the southern United States, Mexico, and the northern Caribbean [*Biasutti et al.*, 2011; *Ryu and Hayhoe*, 2014]. GOM waters are also part of North Atlantic surface circulation through the Loop Current, a precursor current to the Gulf Stream, which brings warm Caribbean waters into the GOM and alters its surface-ocean conditions on subannual-to-decadal timescales [*Liu et al.*, 2012b; *Chang and Oey*, 2013; *Gopalakrishnan et al.*, 2013]. The brevity of the instrumental record requires the use of proxy data to understand variability of the Loop Current and its relationship with GOM climate change on multidecadal-to-centennial timescales. Furthermore, there is no consensus among general circulation models (GCMs) on how GOM oceanography and regional hydroclimate will evolve in response to rising levels of greenhouse gases [*Biasutti et al.*, 2011; *Liu et al.*, 2012a; 2012b]. Thus, there is a need to develop paleoclimate records that can characterize the century-scale variability of surface-ocean conditions in the GOM and thereby have the potential to improve future predictions of regional climate change.

This work reconstructs sea-surface temperature (SST) and sea-surface salinity (SSS) from marine sediments in the Garrison Basin, northern GOM (26° 40.19'N,93° 55.22'W), over the last 4,400 years at ~15-30 year resolution. The stable oxygen isotope composition ($\delta^{18}O$) and magnesium-to-calcium (Mg/Ca) ratios of planktic foraminifer *Globigerinoides ruber* (White variety; W) are used as proxies of SST and SSS. In this dissertation, I first assess the fidelity of *G. ruber*

(W) geochemistry in recording temperature and salinity, test how these signals are preserved in the sedimentary record, and finally reconstruct surface-ocean variability in the GOM over the late Holocene.

This dissertation is divided into three chapters as follows: (1) analysis and discussion of *in-situ* sediment trap observations detailing the ecology of *G. ruber* (W) and its relevance to downcore reconstructions in the GOM; (2) development and discussion of a Monte-Carlo-based algorithm that incorporates multiple sources of errors to produce SST and SSS estimates with appropriate uncertainty constraints; and (3) the application of previous results to generate paleo-records of surface-ocean variability in the GOM and the diagnosis of their controls and linkages with Atlantic Ocean circulation and Western Hemisphere hydroclimate.

Chapter 1 focuses on the use of stable isotopic measurements on different morphotypes of *G. ruber* (W) to examine their seasonal preferences and calcification depth habitats, and ultimately, to test whether the choice of morphotype can bias downcore reconstructions. I test these hypotheses using sediment trap, core-top, and downcore samples from the northern GOM. These results are coupled with a foraminiferal forward model, INFAUNAL [*Thirumalai et al.*, 2013], to robustly assess discrepancies in *G. ruber* (W) productivity and depth habitats in the northern GOM. Importantly, in this work, the suitability of this species' geochemistry for reconstructing mean-annual SST and SSS in the GOM is confirmed. The results are applied in the subsequent chapters to facilitate accurate reconstruction of SST and SSS in the northern GOM.

Chapter 2 focuses on the construction of a computational algorithm that quantifies overall uncertainty in paired Mg/Ca-$\delta^{18}O$ data generated from

foraminifera including sampling, analytical, calibration, ecological, preservation, and age errors. The algorithm, entitled Paleo-Seawater Uncertainty Solver (PSU Solver), is also capable of assessing the influence of salinity on Mg/Ca variability [*Hönisch et al.*, 2013] and can be applied to records of any resolution, with several built-in sea-level curves to correct for the influence of ice-volume on $\delta^{18}O$ variability. The applicability of PSU Solver, whose input conditions can are user-specified, is demonstrated for several previously published records that span different timescales. PSU Solver can be coupled to output obtained from other codes that characterize uncertainty in foraminiferal reconstructions including TURBO2 (bioturbation; [*Trauth*, 2013]), INFAUNAL (sampling error; [*Thirumalai et al.*, 2013]), and BACON (radiocarbon age-depth modelling; [*Blaauw and Christen*, 2011]). I show that the influence of salinity in Mg/Ca and the choice of sea-level curve can change the structure of the resulting reconstruction and hence affect paleoclimate interpretation.

Chapter 3 builds on results from the previous two chapters to provide robust and accurate reconstructions of SST and SSS variability in the northern GOM over the last 4,400 years. These reconstructions are based on paired Mg/Ca-$\delta^{18}O$ analyses on *G. ruber* (W) in three independently dated multicores from the same cast in the Garrison Basin. A replicated stack record is constructed using these three multicore records which is placed in a quantitative uncertainty framework and indicates marked centennial-scale SST and SSS variability (up to 1ºC and 0.3 PSU). I perform several field correlation analyses using observations, reanalysis datasets, and a fully-coupled transient simulation of the last millennium to assess and diagnose the controls on GOM surface-ocean variability and its linkages with global climate variability. With these

analyses, I demonstrate that the GOM is ‘part and parcel’ of the greater circulation of the Atlantic Ocean and find that on multidecadal-to-centennial timescales, the strength of Gulf Stream transport appears to be linked with precipitation variability in the Western Hemisphere. This relationship between circulation and hydroclimate is investigated in the proxy record by synthesizing marine and terrestrial records of the last millennium, including the new Garrison Basin reconstructions. The results not only reaffirm the role of a slowdown in the Gulf Stream during the Little Ice Age, but also demonstrate a coordinated hydroclimate linkage across the Western Hemisphere, a feature of the climate system that might have been at play throughout most of last 4,400 years. The newly generated records of SST and SSS variability from the northern GOM offer new insights into late Holocene climate change that may help us understand what could be possible for the future.

Globigerinoides ruber morphotypes in the Gulf of Mexico: a test of null hypothesis

K. Thirumalai[1,2], J. N. Richey[3], T. M. Quinn[1,2], R. Z. Poore[3]

[1] *Institute for Geophysics, Jackson School of Geosciences, University of Texas at Austin*

[2] *Department of Geological Sciences, Jackson School of Geosciences, University of Texas at Austin*

[3] *United States Geological Survey, St. Petersburg Coastal and Marine Science Center*

* Chapter 1 has been published as is in the open-access journal *Scientific Reports* (doi:10.1038/srep06018)

ABSTRACT

Planktic foraminifer *Globigerinoides ruber* (*G. ruber*), due to its abundance and ubiquity in the tropical/subtropical mixed layer, has been the workhorse of paleoceanographic studies investigating past sea-surface conditions on a range of timescales. Recent geochemical work on the two principal white *G. ruber* (W) morphotypes, sensu stricto (ss) and sensu lato (sl), has hypothesized differences in seasonal preferences or depth habitats, implying that reconstructions using a non-selective mixture of morphotypes could potentially be biased. Here, we test these hypotheses by performing stable isotope and abundance measurements on the two morphotypes in sediment trap, core-top, and downcore samples from the northern Gulf of Mexico. As a test of null hypothesis, we perform the

same analyses on couplets of *G. ruber* (W) specimens with attributes intermediate to the holotypic ss and sl morphologies. We find no systematic or significant offsets in coeval ss-sl $\delta^{18}O$, and $\delta^{13}C$. We also find comparable offsets in the intermediate couplets. Contrary to previous work, coupling our results with foraminiferal statistical model INFAUNAL, we find no evidence for discrepancies in ss-sl depth habitat or seasonality in the Gulf of Mexico.

1. Introduction

The geochemistry of foraminiferal tests from marine sediment is utilized extensively as a tool to infer paleoceanographic variability on timescales ranging from decades to millennia, thereby playing an integral role in our understanding of climate change [*Poore et al.*, 2003; *Spero et al.*, 2003; *Schmidt et al.*, 2004; *LoDico et al.*, 2006; *Richey et al.*, 2007; *Ganssen et al.*, 2010; *Mohtadi et al.*, 2014; *Weldeab et al.*, 2014]. In reconstructing geochemically derived estimates of paleoceanographic parameters, attention must be paid to the ecology and taxonomy of the foraminifera selected for analysis. Inaccurate identification of species could potentially bias or distort reconstructions and add an unknown dimension of uncertainty to quantitative estimates of paleoceanographic parameters [*Srinivasan et al.*, 1974; *Robbins and Healy-Williams*, 1991].

Planktic foraminifer *Globigerinoides ruber* (*G. ruber*) is perhaps one of the most widely used species for reconstructing past sea-surface conditions [*Poore et al.*, 2003; *Spero et al.*, 2003; *LoDico et al.*, 2006; *Richey et al.*, 2007; *Ganssen et al.*, 2010; *Mohtadi et al.*, 2014; *Weldeab et al.*, 2014]. *Globigernoides ruber* is ubiquitous in the mixed layer of tropical/subtropical waters and is known to live

throughout the year [*Schmidt and Mulitza*, 2002; *Farmer et al.*, 2007]. Thus, its geochemistry is an attractive proxy for past sea-surface temperature (SST) and $\delta^{18}O$ of seawater ($\delta^{18}O_{sw}$).

Apart from its pink chromotype, *G. ruber* (P), multiple morphotypical variants of its white variety, *G. ruber* (W), have been identified and described in micropalentological literature. These include *Globigerinoides elongatus* [*d'Orbigny*, 1826], *Globigerinoides pyramidalis* [*Van den Broeck*, 1876], *Globigerinoides cyclostomus* [*Galloway and Wissler*, 1927], and the holotypic normalform of *G. ruber* (W), first described as *Globigerina rubra* {dOrbigny:1839vh}. More recently, stable isotopic and trace metal geochemistry studies have placed the former three variants under *G. ruber* sensu lato (sl) while the latter has been termed *G. ruber* sensu stricto (ss), albeit acknowledging a large range of transitional forms between the morphotypes [*Wang*, 2000; *Lin et al.*, 2004; *Kawahata*, 2005; *Löwemark et al.*, 2005; *Steinke et al.*, 2005; *Mohtadi et al.*, 2009] (Fig. 1). These studies compared the stable isotopic oxygen and carbon composition of the two morphotypes in core-tops, downcore sediments, and sediment traps from the South China Sea, Indo-Pacific, and Japanese seas [*Wang*, 2000; *Lin et al.*, 2004; *Kawahata*, 2005; *Löwemark et al.*, 2005; *Steinke et al.*, 2005; *Mohtadi et al.*, 2009].

Understanding the ecology of modern *G. ruber* (W) sets up the expectation for interpreting signals derived from downcore geochemical variations. Previous studies based on core-tops and downcore samples, despite small sample numbers (5-23 pairs), inferred that differences in stable isotopes were the result of either distinct calcifying depth habitats (ss: ~0-25 m, sl: ~25-50 m), seasonal preferences (sl: winter-biased), or vital effects between *G. ruber*

(W) ss and sl, and concluded that the sl morphotype was a cold-biased specimen [*Wang*, 2000; *Kawahata*, 2005; *Löwemark et al.*, 2005; *Steinke et al.*, 2005]. These results have critical implications for paleoceanographic reconstructions using a non-selective mixture of the two morphotypes, as they can be biased or distorted due to the averaging of signals from different depths or seasons. The sediment trap studies, where the age of the samples are known with weekly/monthly precision, were more equivocal in their conclusions, finding little-to-no differences in the stable isotopes [*Lin et al.*, 2004; *Mohtadi et al.*, 2009]. Hence it is important to study both the modern ecology and geochemistry of these morphotypes using large sample numbers and different sampling archives in order to quantify the degree of bias that may occur due to morphotypical variability in *G. ruber* (W).

In this work, we study the stable isotopic differences between coeval ss and sl from core-tops, downcore samples, and a sediment trap in the northern Gulf of Mexico (Fig. 2; Table 1). As a geochemical test of the null hypothesis, we also analyze mixed *G. ruber* (W) couplets with morphologies intermediate to the ss and sl holotypes (hereafter 'intermediate' *G. ruber* (W) tests) to systematically investigate the composition of different *G. ruber* (W) subsets: if the geochemical composition of all subsets are comparable, we fail to reject the null hypothesis that morphotypical variability has a significant effect on *G. ruber* (W) geochemistry; if they are consistently different, then we reject the null hypothesis and conclude that morphotypical variability has a significant effect on *G. ruber* (W) geochemistry. We couple these results with INFAUNAL, a recently published foraminiferal statistical model [*Thirumalai et al.*, 2013], to gain

insight into the use of the two morphotypes as paleoceanographic recorders in the Gulf of Mexico.

2. METHODS

2.1. Specimen Selection

We chose *G. ruber* (W) sensu stricto (ss) and sensu lato (sl) specimens in the 212- We chose *G. ruber* (W) sensu stricto (ss) and sensu lato (sl) specimens in the 212-300μm size for all sampling archives. Sensu lato (Fig. 1a, b) was characterized as a kummerform having three compressed spherical chambers in the final whorl where the final chamber was smaller and flattened compared to the others, forming a moderate to high trochospiral form, with a rounded primary aperture situated asymmetrically over the previous suture. Sensu stricto (Fig. 1c, d) was characterized as having three spherical chambers in the final whorl that progressively increased in size and had a moderate trochospire shape, with radial sutures containing supplementary apertures and a primary aperture that was wide and more arched than the sl morphotype, symmetric over the previous suture. Intermediate specimens include tests with morphotypical variability transitional to that between ss and sl (for example, a normalform containing compressed chambers in the final whorl and a wide, highly-arched primary aperture that sat asymmetrically over the previous suture or a normalform containing a narrow, rounded, primary aperture sitting symmetrically over the previous suture, with depressed radial sutures with ancillary suture apertures).

2.2. Stable Isotope Analysis

We selected 6-20 specimens of each *G. ruber* (W) morphotype from the sediment trap samples and ≥50 specimens for the downcore/core-top samples.

Specimens were crushed and homogenized, and cleaned with methanol before geochemical analysis. Stable isotopes were measured using a Thermo-Finnigan MAT 253^{TM} isotope ratio mass spectrometer coupled to a Kiel IV Carbonate Device housed in the Analytical Laboratory for Paleoclimate Studies (ALPS) at the Jackson School of Geosciences, University of Texas at Austin. The 1σ precision of the stable isotopic measurements in this study based on multiple analyses of an in-house carbonate standard (n = 28) is 0.03‰ for $\delta^{13}C$ and 0.06‰ for $\delta^{18}O$, consistent with the long-term precision for this instrumental setup (0.06‰ for $\delta^{13}C$ and 0.08‰ for $\delta^{18}O$). All stable isotope values are reported relative to Vienna Pee Dee Belemnite (VPDB) in standard notation.

2.3. Year-normalized Flux

We calculated year-normalized flux from the sediment trap using:

$$\frac{Monthly\ count\ of\ particular\ morphotype}{Yearly\ total\ of\ all\ morphotypes} \times 100\ \% \qquad (1)$$

2.4. Binomial Expansion for Intermediate Couplet Combinations

While computing the mean and standard deviation of the offsets between coeval intermediate pairs for an archive, we considered all possible combinations by interchanging samples of the intermediate couplets. In offset space, this effectively reduces to a change in sign before computing the mean and standard deviation of all the offsets in an archive, thereby following a binary 'on-off' pattern. The number of unique combinations *n* possible for a given number of samples *s* in an archive is obtained by binomial expansion:

$$n = 2^{s-1} + 1 \qquad (2)$$

After generating *n* combinations, we computed the mean (μ_c) and standard deviation (σ_c) of the offsets for each combination. We report the average mean offset of all the combinations with its associated standard deviation ($\langle\mu_c\rangle\pm\sigma_\mu$; (b1) and (d1) in Table 2) and the average standard deviation of all the offsets with its associated standard deviation ($\langle\sigma_c\rangle\pm\sigma_\sigma$; (b2) and (d2) in Table 2) in the binomially generated combinations to compare the variability of offsets in the intermediate couplets and compare them to the ss-sl offsets.

2.5. INFAUNAL model

Bootstrap Monte Carlo simulations (n = 10000) were performed to generate a population of means that incorporated analytical uncertainty (±2σ) and sampling uncertainty involved with utilizing 50 pseudo-foraminifera in a virtual sediment sample representing 50 years using the Individual Foraminiferal Approach Uncertainty Analysis (INFAUNAL) model for multi-test foraminiferal analysis as described by Thirumalai et al. [*Thirumalai et al.*, 2013]. We applied the algorithm to perform picking experiments on a $\delta^{18}O$ time series generated from temperature and salinity data at depths of 5 m and 55 m using the ECMWF ORA-S4 ocean reanalysis dataset [*Balmaseda et al.*, 2012] with data extracted from 26.7°N, 93.9°W (the location of our core-top and downcore samples) in the Gulf of Mexico. 5 and 55 m depths were chosen from the reanalysis dataset because they were the closest to the extremes of the previously hypothesized calcification depths (0-25 m for ss and 25-50 m for sl). To ensure the robustness of these results, we also performed the same INFAUNAL picking experiments at 35 m and 45 m. Similar to the resulting offsets between 5 and 55 m, we observed that there was a high probability (≥70%) that pseudo-foraminifera

calcifying at 5 m versus 45 m can resolve depth-specific $\delta^{18}O$ signals. The probability of resolving depth-specific signals using idealized pseudo-foraminifera became lower at 35 m (≥25%), limiting our ability to test hypothesis of selective ss-sl calcification depths using a model-data comparison. However, all offsets produced by INFAUNAL between 5 and 35 m, 45 m, and 55 m are still significantly distinct from zero ($p<0.001$) and from the $\delta^{18}O$ data ($p<0.001$), the latter of which is not significantly different from zero (we also tested this at 100 and 5000 Monte Carlo simulations and obtained the same outcome). This indicates that it is statistically unlikely that most ss and sl specimens are calcifying deeper than 35 m. Furthermore, since the mixed layer at the sediment trap site extends well beyond 55 m for most months of the year (Fig. 3), our results hold that both *G. ruber* (W) morphotypes in the northern Gulf of Mexico calcify in the upper portion of the mixed layer.

3. Results

We report here 130 $\delta^{18}O$ and $\delta^{13}C$ measurements on 37 pairs of *G. ruber* (W) ss and sl along with 28 pairs of intermediate *G. ruber* (W) tests from three sampling archives in the northern Gulf of Mexico (Fig. 2): core-tops, downcore samples, and a sediment trap (Figs. 1.4, 1.5, and 1.6). Table 1 lists the mean and standard deviation of ss-sl measurements in each archive. Here, the mean and standard deviation reflect the overall (time-dependent) variability in our selected samples of each archive; for example, sediment trap standard deviation is high due to the greater variance of annual temperature/salinity in the sampling interval. This variability notwithstanding, the mean and standard

deviation of the ss morphotypes are similar to the sl morphotypes. To statistically test these comparisons, we chose to perform Welch's *t* test [*Welch*, 1947] (paired *t* test with unknown and unequal variance) on the ss-sl pairs with no *a priori* assumptions about the variance of the underlying populations [*Ruxton*, 2006]. All populations were found to be normal based on a Shapiro-Wilk test [*Shapiro and Wilk*, 1965], except for downcore $\delta^{13}C$ of ss and sl, where we used the non-parametric Mann–Whitney–Wilcoxon ranksum test [*Mann and Whitney*, 1947]. From this exercise, we failed to reject the null hypothesis for ss-sl pairs across all archives, that is, the $\delta^{18}O$ and $\delta^{13}C$ difference between ss and sl morphotypes is not statistically significant ($p<0.05$; Table 1). We also pooled all the ss-sl pairs across the different sampling archives and tested for regressions using the maximum likelihood estimate method [*York et al.*, 2004] incorporating bivariate analytical uncertainty [*Thirumalai et al.*, 2011], where $1\sigma_{analytical}$ = 0.08‰ in $\delta^{18}O$, and 0.06‰ in $\delta^{13}C$. Within uncertainty, both $\delta^{18}O$ and $\delta^{13}C$ slopes and intercepts were not significantly different ($p<0.05$) from the 1:1 line, where the slope is unity and intercept is zero (Fig. 5).

We use offsets between coeval samples as a metric to statistically compare the ss-sl measurements with the intermediate couplets. The absolute offsets between coeval ss-sl samples ranged from 0-0.52‰ in $\delta^{13}C$ and 0-0.56‰ in $\delta^{18}O$, while the intermediate couplets ranged from 0-0.50‰ in $\delta^{13}C$ and 0.01-0.53‰ in $\delta^{18}O$ (See Table 3 for the range in each archive). The mean ss-sl offset and standard deviations in all archives are not systematic, and closely cluster around zero. We tested for mean ss-sl offsets significantly different from zero using a Student's *t* test in a Monte Carlo framework (n = 5000) to account for analytical error at the 95% confidence level (i.e. $\pm 2\sigma_{analytical}$)

incorporated as a Gaussian distribution. All archives failed the test with probabilities ≥70% that both carbon and oxygen stable isotopic offsets were not significantly distinct from zero thus corroborating our initial Welch *t* test outcomes and regression analysis that ss-sl couplets have statistically similar variability in stable isotopic composition.

As the intermediate *G. ruber* (W) pairs are interchangeable amongst coeval couplets (their transitional form inhibits selective categorization), we generated all possible combinations of the couplets in each archive using binomial expansion (See Methods for details). Next, we computed the mean (μ_c) and standard deviation (σ_c) of the offsets for each combination. To gain insight into the variability of the intermediate couplets, we report the average mean offset of all the combinations with its associated standard deviation ($\langle\mu_c\rangle\pm\sigma_\mu$; (b1) and (d1) in Table 2) and the average standard deviation of all the offsets with its associated standard deviation ($\langle\sigma_c\rangle\pm\sigma_\sigma$; (b2) and (d2) in Table 2) in the binomially generated combinations. We note that the average standard deviation of the intermediate *G. ruber* (W) offset ($\langle\sigma_c\rangle$), a measure of non-morphotypical variability, is statistically similar to the corresponding mean and standard deviation of the ss-sl offset within analytical error ($p<0.05$; Table 2).

Apart from stable isotope analysis, the sediment trap allows us to quantify the monthly abundance of each morphotype. Over our sampling interval, in general, we observe the sl morphotypes to be more abundant than the other morphotypes. Concerning seasonal preferences, the census data indicate that neither ss, sl, nor the intermediate *G. ruber* (W) specimens prefer any particular season in our sampling window (Fig. 6). Moreover, we found no persistent season where one morphotype dominates over the others.

Ruling out a seasonal bias in morphotype, we investigated whether the ss and sl morphotypes had preferential calcifying depth habitats as suggested in previous studies: ss preferring 0-25 m and sl preferring 25-50 m. To assess the potential for resolving depth-specific signals in marine sediment, we applied INFAUNAL [*Thirumalai et al.*, 2013] at surface and subsurface depths in the Gulf of Mexico to construct idealized virtual sediment samples for the two habitats. We constructed two 50-year-long pseudo-$\delta^{18}O_{carbonate}$ time series using monthly temperature and salinity from the ECMWF ORA-S4 reanalysis dataset [*Balmaseda et al.*, 2012] at depths of 5 m (ss) and 55 m (sl; see Figs. 1.7). These depths were chosen based on those available in the ORA-S4 dataset that were closest to the extremes of the previously hypothesized calcification depths (we also performed the experiment using 35 m and 45 m depths; see Methods). Next, we performed bootstrap Monte Carlo picking experiments (n = 10000) on these virtual sediment samples with 50 pseudo-foraminifera to determine whether the offset produced in INFAUNAL would be comparable to the offset observed in the ss-sl data. We chose 50-year-long time series and 50 pseudo-foraminifera for the experiment based on approximately equivalent sample resolution and number of foraminifera analyzed in the core-top and downcore samples (the high temporal resolution and abundance of the sediment trap samples does not allow for a one-to-one downcore analog). The INFAUNAL results indicated that 50 foraminifera picked from the 5 m pseudo-$\delta^{18}O_{carbonate}$ time series and 50 from the 55 m time series could resolve these depth-specific signals with a high probability (≥90%) and that the offset between the picked means of the idealized time series was significantly distinct from zero ($p<0.001$). However, this idealized population of offsets is significantly different than the ss-

sl offset observed in the core-top and downcore $\delta^{18}O$ data ($p<0.001$), the latter of which is not distinct from zero ($p<0.05$; Fig. 8).

4. Discussion and Conclusion

Our observations and statistical tests indicate that there are neither significant nor systematic stable isotopic differences between *G. ruber* (W) ss and sl populations across three different sampling archives in the Gulf of Mexico (Fig. 5). The variability in $\delta^{13}C$ and $\delta^{18}O$ of both morphotypes is statistically indistinguishable (Table 1). The intermediate *G. ruber* (W) samples display very similar variability and contain intra-sample variability comparable to the ss-sl populations (Table 2), thereby preventing us from rejecting the geochemical test of the null hypothesis. Taken together, our observations imply that morphotypical variability in *G. ruber* (W) has little if any control on its $\delta^{13}C$ and $\delta^{18}O$ composition.

Though the $\delta^{13}C$ variability in the sediment trap samples is seemingly chaotic, the $\delta^{18}O$ variability is distinctly controlled by climate. Despite steep rates of change in SST during boreal spring and fall at the northern Gulf of Mexico (~10°C seasonal cycle), the $\delta^{18}O$ of both morphotypes in the sediment trap samples reliably capture SSTs (Fig. 4). The same is true for the intermediate couplets. In examining coeval offsets, the $\delta^{18}O$ standard deviation is reduced by ~50% compared to the overall standard deviation of each morphotype (~0.6‰ vs. ~0.2‰; Tables 1 and 2), whereas the overall $\delta^{13}C$ standard deviations are similar to that of the offset (~0.2‰ vs. 0.2‰; Tables 1 and 2). This implies that intra-morphotype $\delta^{13}C$ is as variable as inter-morphotype $\delta^{13}C$, a result that is in

line with previous studies highlighting the complex controls on stable isotopic carbon in foraminifera [*Spero and Williams*, 1989; *Spero et al.*, 1997]. We observe similar variability in the intermediate *G. ruber* (W) couplets (±0.23‰), supporting this interpretation.

What are the ecological implications of our observations concerning the habitat of *G. ruber* (W) morphotypes and its effect on paleoceanographic reconstructions? From our sediment trap flux data, we find no evidence that ss, sl, or the intermediate *G. ruber* (W) samples prefer one season over another (Fig. 6). The data also indicate that no particular morphotype is persistently more abundant than any other morphotype. This supports the inference that all morphotypes of *G. ruber* (W) live throughout the year and that paleoceanographic records generated using the species should be representative of annual conditions, substantiating previous studies in the Gulf of Mexico [*Spear and Poore*, 2011; *Poore et al.*, 2013] and elsewhere [*Deuser*, 1987]. Using INFAUNAL, we show that pseudo-foraminifera calcifying exclusively at 5 m and 55 m can resolve depth-specific $\delta^{18}O$ (temperature and salinity) signals with a very high probability (≥90% with 50 specimens in 50-year sample resolution and ≥70% at 45 m; See Methods and Fig. 9). We also show that the resulting distribution of pseudo-foraminifera is significantly different from our core-top and downcore data, which is centered on zero (Fig. 8). This result implies that ss and sl morphotypes must dwell and migrate to similar depths in the Gulf of Mexico. We infer that these depths are restricted to the upper portion of the mixed layer due to the excellent correlation between both morphotypes and SST in the sediment trap samples (r_{ss} = 0.92, r_{sl} = 0.86; Fig. 4). Thus, our observations and modeling results unequivocally indicate that *G. ruber*

(W)-based paleoceanographic records, regardless of morphotype, reflect annual surface water conditions in the Gulf of Mexico.

Contrary to previous *G. ruber* (W)-morphotype studies based on core-tops and downcore samples in the South China Sea and Japanese seas [*Wang*, 2000; *Kawahata*, 2005; *Löwemark et al.*, 2005; *Steinke et al.*, 2005], our findings suggest no morphotype-based biases in utilizing a non-selective mixture of *G. ruber* (W) ss and sl for paleoceanographic reconstructions. Nevertheless, our findings are corroborated by previous work utilizing sediment traps in the Indo-Pacific seas [*Mohtadi et al.*, 2009] and plankton tow samples around Japan [*Kuroyanagi and Kawahata*, 2004], where no geochemical and flux differences were observed in the former and sea-surface peaks in abundance for both morphotypes were observed in the plankton tows. We feel that this inconsistency may arise either due to the influence of the large latitudinal extent of sample selection in the previous studies resulting in dissimilar seasonal cycles across all the sampling locations, loose temporal constraints on core-tops and/or possibly from limited sample numbers and a non-rigorous treatment of uncertainty. For example, we note that the core-top samples from the South China Sea in a previous study [*Wang*, 2000] are obtained from a large latitudinal transect spanning from 6°N-22°N where the seasonal cycle changes from a tropical (smaller seasonal cycle) to sub-tropical (larger seasonal cycle) setting. The thermocline and other oceanographic features are variable over this latitudinal range as well [*Qu et al.*, 2000; *Liu et al.*, 2001]. Quantifying this spatially varying influence of uncertainty and focusing solely on ss-sl-based isotopic variability is non-trivial and outside the scope of this work. Though preliminary sediment trap work in the South China Sea region is equivocal [*Lin et*

al., 2004] about the two morphotypes, a more comprehensive spatially-invariant sediment trap/plankton tow study would potentially yield more insight into the earlier core-top/downcore studies.

We demonstrate the advantage and application of using a comprehensive dataset in tandem with a forward modeling statistical approach to glean insights into modern ecological variability. Such data-model comparisons characterized with robust uncertainty constraints are useful in discerning the effect of ecological parameters on paleoceanographic reconstructions. In this study, we show that all lines of evidence (observations, null hypothesis testing, and data-model comparisons) indicate that *G. ruber* (W) ss, sl, and intermediate morphotypes live throughout the year and dwell in the upper portion of the mixed layer in the Gulf of Mexico. Hence, downcore reconstructions using non-selective mixtures of *G. ruber* (W) specimens should reflect annual surface water conditions.

5. Acknowledgements

We thank the crew of the R/V Pelican for assisting us in the collection and redeployment of the sediment trap, and the crew of the R/V Cape Hatteras for aid in obtaining the cores utilized in this study. We acknowledge Caitlin Reynolds for aiding sample preparation and Jennifer Flannery for help with the SEM images. The authors are thankful to Judson Partin for helpful discussion and for critiquing a preliminary draft of this manuscript along with Deb Willard. K. T. thanks the UTIG Ewing-Worzel fellowship for support. This research was

funded by the U.S. Geological Survey Climate and Land Use Research & Development program and the National Science Foundation (OCE-0902921).

	Sediment Trap	Core-Tops	Downcore
No. of Pairs	17	5	13
$\delta^{18}O_{ss}$ (‰)	-1.58 ± 0.64	-1.22 ± 0.32	-1.12 ± 0.21
$\delta^{18}O_{sl}$ (‰)	-1.50 ± 0.56	-1.24 ± 0.35	-1.10 ± 0.39
H	H_o	H_o	H_o
$\delta^{13}C_{ss}$ (‰)	0.01 ± 0.21	0.84 ± 0.19	1.06 ± 0.28
$\delta^{13}C_{sl}$ (‰)	-0.12 ± 0.2	0.77 ± 0.18	0.92 ± 0.34
H	H_o	H_o	H_o*

Table 1. Mean and Standard Deviation of ss-sl Isotopic Measurements in Each Sampling Archive with Outcomes of Welch's *t* test at $p<0.05$ level, where $H = H_o$ implies null hypothesis cannot be rejected; $H = H_a$ implies null hypothesis can be rejected. * - $H = H_o$ based on Mann–Whitney–Wilcoxon due to the non-parametric nature of underlying populations.

		Sediment Trap	Core-Tops	Downcore
$\langle\Delta\delta^{18}O_{ss\text{-}sl}\rangle$ (‰)	(a) $\mu_{ss\text{-}sl}\pm\sigma_{ss\text{-}sl}$	-0.08 ± 0.20	0.01 ± 0.15	-0.02 ± 0.33
$\langle\Delta\ \delta^{18}O_{Null}\rangle$ (‰)	(b1) $\langle\mu_c\rangle\pm\sigma_\mu$ ±	0.01±0.04 ±	-0.02±0.06 ±	0±0.07 ±
	(b2)$\langle\sigma_c\rangle\pm\sigma_\sigma$	0.14±0.01	0.14±0.02	0.26±0.01
$\langle\Delta\ \delta^{13}C_{ss\text{-}sl}\rangle$ (‰)	(c) $\mu_{ss\text{-}sl}\pm\sigma_{ss\text{-}sl}$	0.13 ± 0.18	0.07 ± 0.18	0.14 ± 0.22
$\langle\Delta\ \delta^{13}C_{Null}\rangle$ (‰)	(d1) $\langle\mu_c\rangle\pm\sigma_\mu$ ±	-0.02±0.07 ±	0.03±0.08 ±	0.01±0.08 ±
	(d2) $\langle\sigma_c\rangle\pm\sigma_\sigma$	0.23±0.02	0.18±0.02	0.29±0.02

Table 2. Mean and Standard Deviation (1σ) of Offsets Between Coeval ss-sl Samples (a and c) and Corresponding Mean (b1 and d1), Standard Deviation (b2 and d2), and their Standard Deviation for all Combinations of Intermediate *G. ruber* (W) Couplets.

	Sediment Trap	Core-Tops	Downcore
$\lvert\Delta^{18}O_{ss\text{-}sl}\rvert$ (‰)	0.00 – 0.49	0.02 – 0.28	0.04 – 0.56
$\lvert\Delta^{18}O_{Null}\rvert$ (‰)	0.01 – 0.27	0.09 – 0.34	0.05 – 0.53
$\lvert\Delta^{13}C_{ss\text{-}sl}\rvert$ (‰)	0.02 – 0.49	0.00 – 0.35	0.02 – 0.52
$\lvert\Delta^{13}C_{Null}\rvert$ (‰)	0.01 – 0.45	0.00 – 0.20	0.04 – 0.50

Table 3. The Range of Absolute Offsets Between Coeval ss-sl Samples and Intermediate Samples in each Archive.

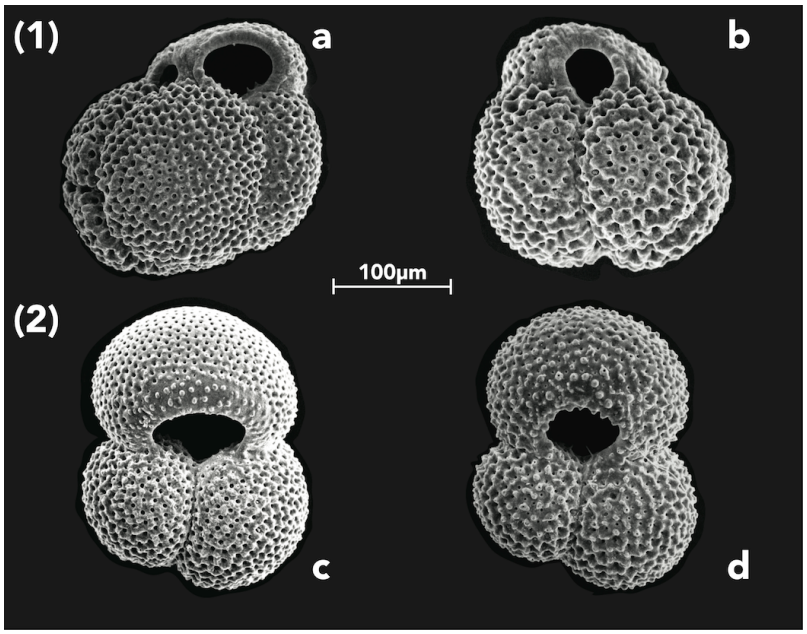

Figure 1. Scanning Electron Micrographs of *Globigerinoides ruber* (White) morphotypes. (1) a and b: *G. ruber* (W) sensu lato; (2) c and d: *G. ruber* (W) sensu stricto.

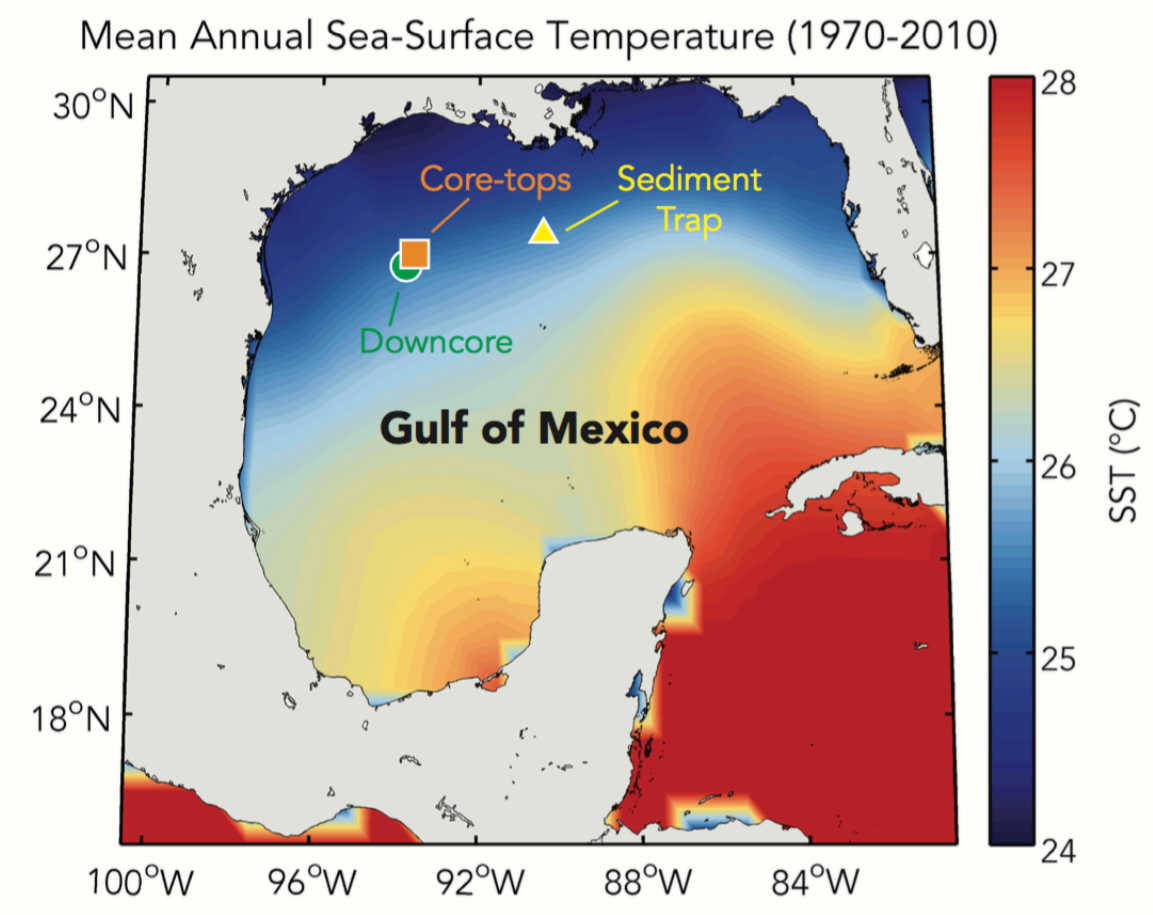

Figure 2. Map of Study Area. Map of mean annual sea-surface temperatures (SSTs) in the Gulf of Mexico with locations of sampling archives used in the study. Downcore samples are all late Holocene in age while all core-top samples are modern. This figure was generated using the M_Map mapping package in MATLAB™ with SST data from HadISST.

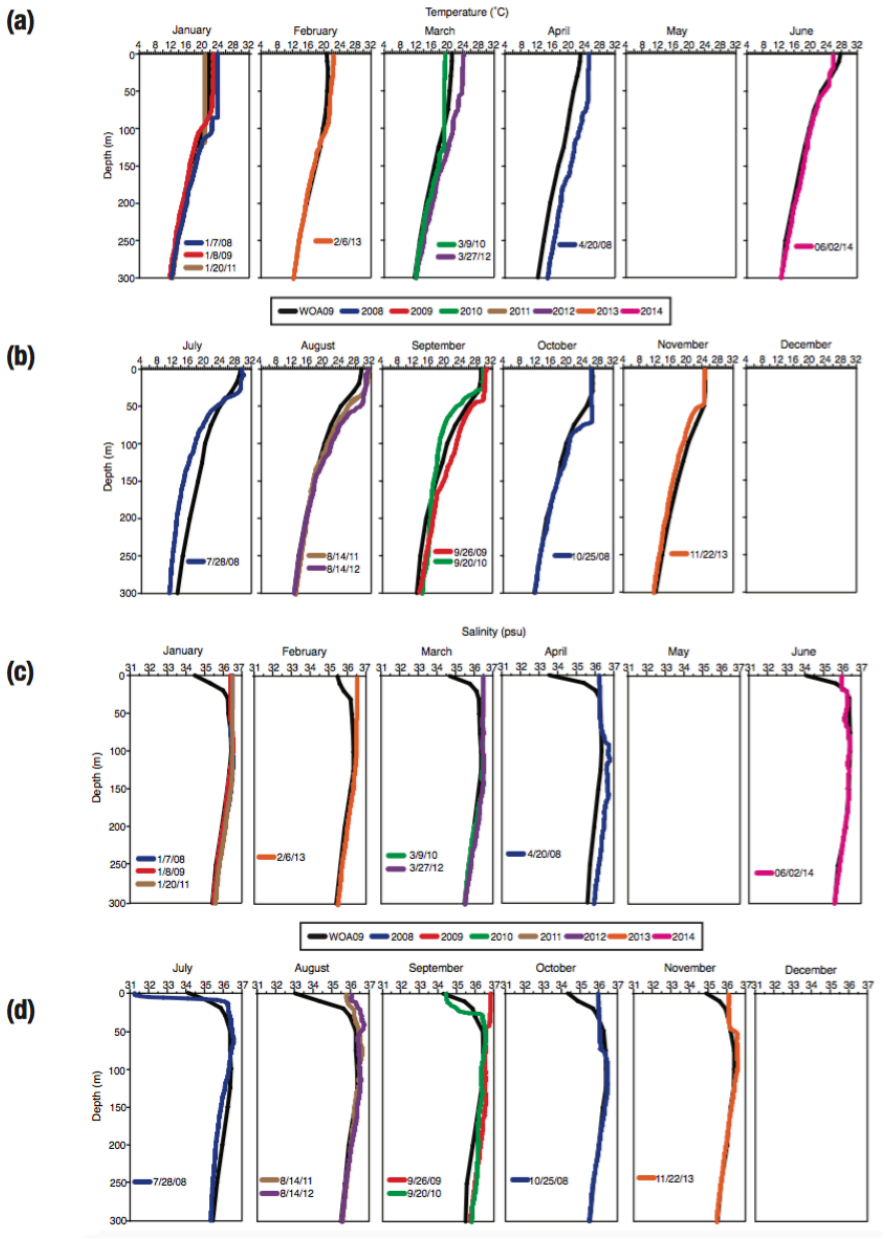

Figure 3. Monthly Temperature and Salinity Profiles in the Upper 300 m of the Northern Gulf of Mexico. Vertical temperature (a and b) and salinity (c and d) profiles in the water column at the sediment trap site in the northern Gulf of Mexico. Note that the thermocline in most months is deeper than 55 m. WOA09 indicates World Ocean Atlas data while all other data are from CTD measurements. CTD data up to the 2012 casts are from Poore et al., 2013.

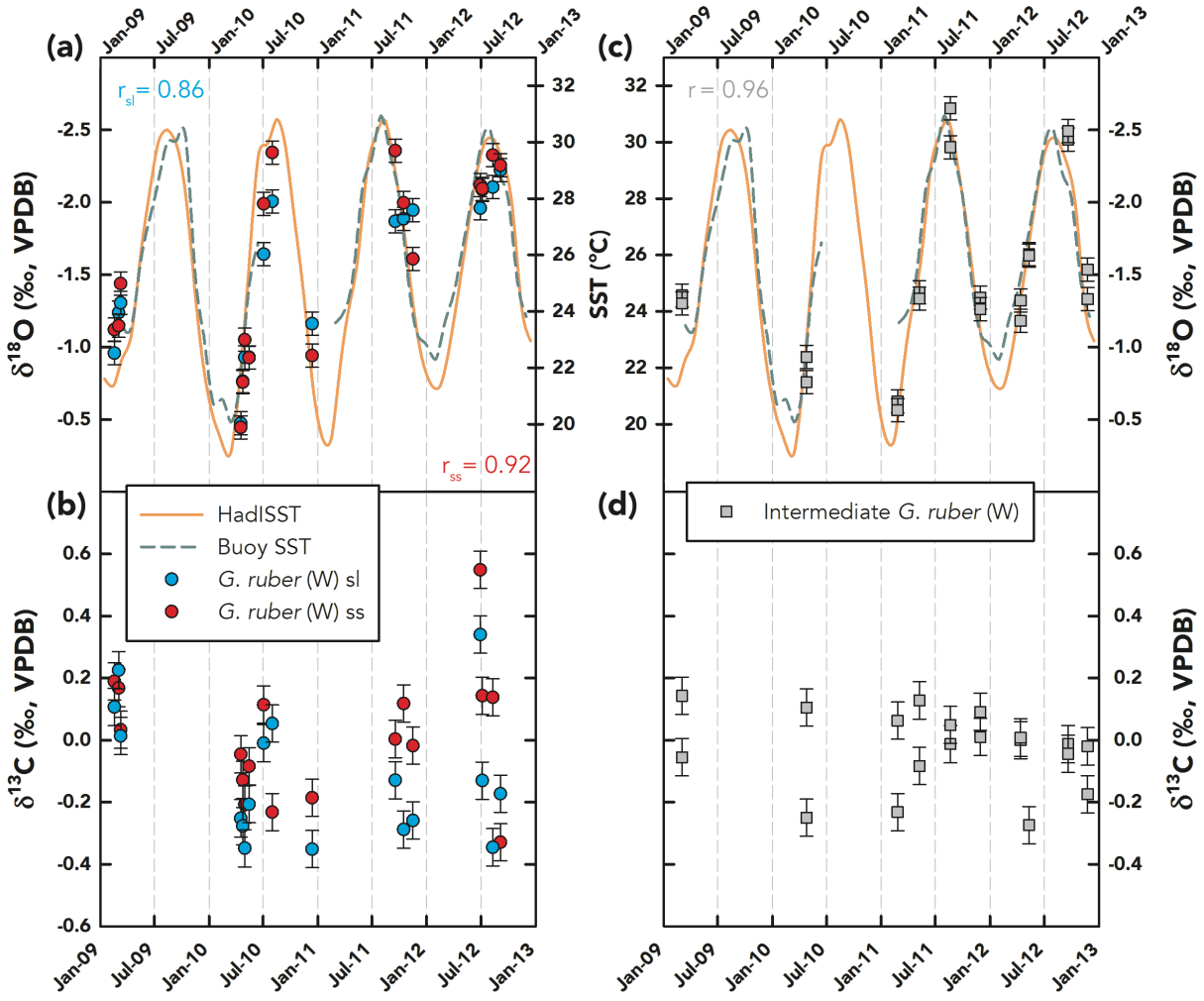

Figure 4. Stable Isotopic Results from the Sediment Trap. $\delta^{18}O$ (a) and $\delta^{13}C$ (b) of *G. ruber* (W) sl (blue circles) and ss (red circles) morphotypes along with $\delta^{18}O$ (c) and $\delta^{13}C$ (d) of intermediate *G. ruber* (W) morphotypes (gray squares) reported relative to VPDB (‰) with error bars based on analytical precision (±1σ; $\delta^{18}O$ – 0.08‰ and $\delta^{13}C$ – 0.06‰) over 2009-2013. Sea-surface temperature (SST) from HadISST [*Rayner et al.*, 2003] (orange line) and nearby NDBC Buoy SST (27.795°N, 90.648°W – Green Canyon; green dashed line) over the same time period are plotted in (a) and (c), scaled according to the $\delta^{18}O$ axis, based on the slope from Bemis et al., 1998[*Bemis et al.*, 1998]. Correlation coefficients are calculated with buoy SSTs when available and HadISST-based SSTs when the former are unavailable.

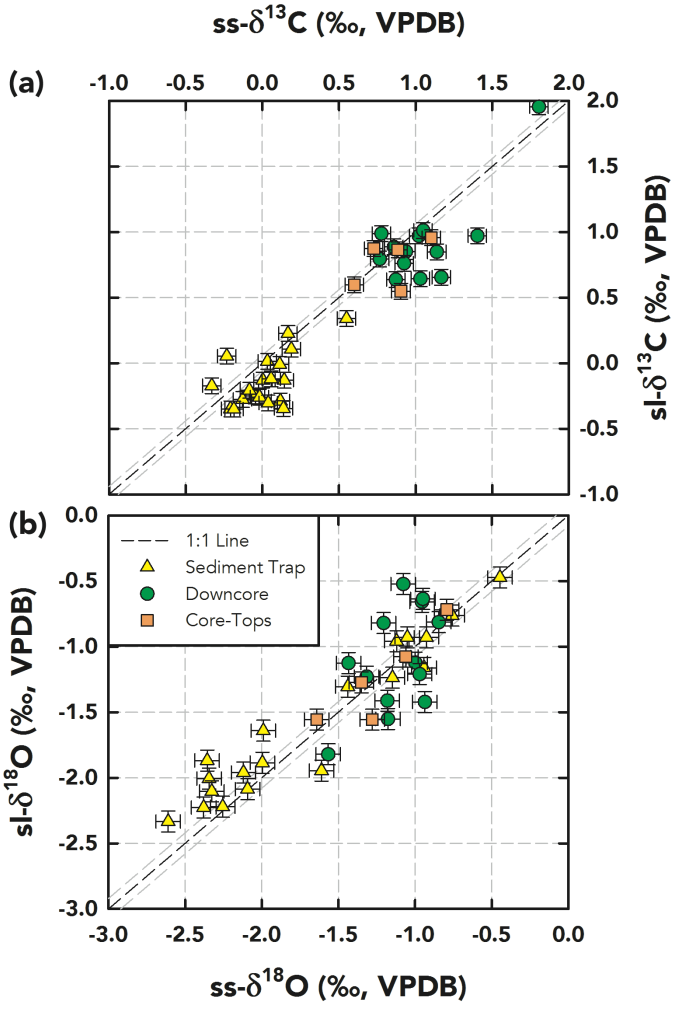

Figure 5. Regression Analysis of ss-sl Samples Across Three Sampling Archives. *G. ruber* (W) $\delta^{13}C$ (a) and $\delta^{18}O$ (b) results for ss (abscissa) versus sl (ordinate) from the sediment trap (yellow triangles), core-top (orange squares), and downcore samples (green circles) with error bars based on analytical precision ($\pm 1\sigma_{analytical}$; $\delta^{13}C$ – 0.06‰ and $\delta^{18}O$ – 0.08‰). The 1:1 line (black dashed line) along with uncertainty limits (grey dashed lines based on $\pm 1\sigma_{analytical}$) is also plotted. The maximum likelihood regression lines incorporating bivariate uncertainty are: 1) sl-$\delta^{13}C$ = (-0.11 ± 0.06) + (0.96 ± 0.06)*ss-$\delta^{13}C$ and 2) sl-$\delta^{18}O$ = (-0.01 ± 0.05) + (0.96 ± 0.04)*ss-$\delta^{18}O$.

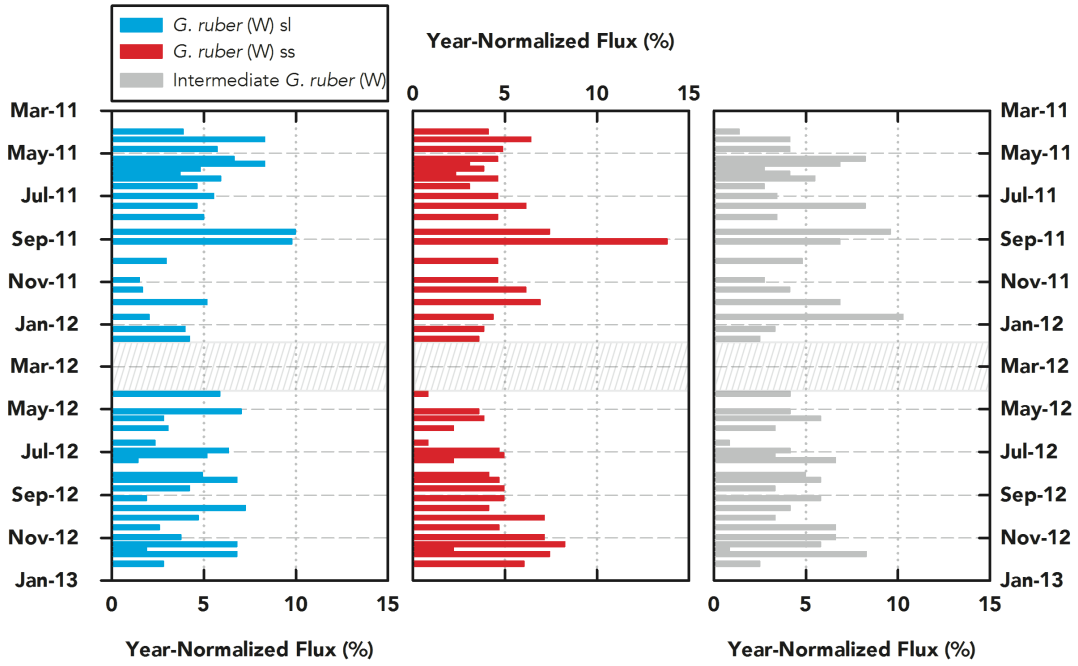

Figure 6. Year-Normalized Flux. Sediment trap-based year-normalized flux (%) measurements for *G. ruber* (W) sl (blue), ss (red), and intermediate (grey) morphotypes. Persistent seasonal preferences or abundance of one morphotype over another are not observed. Box containing hatched lines indicates a gap in data collection.

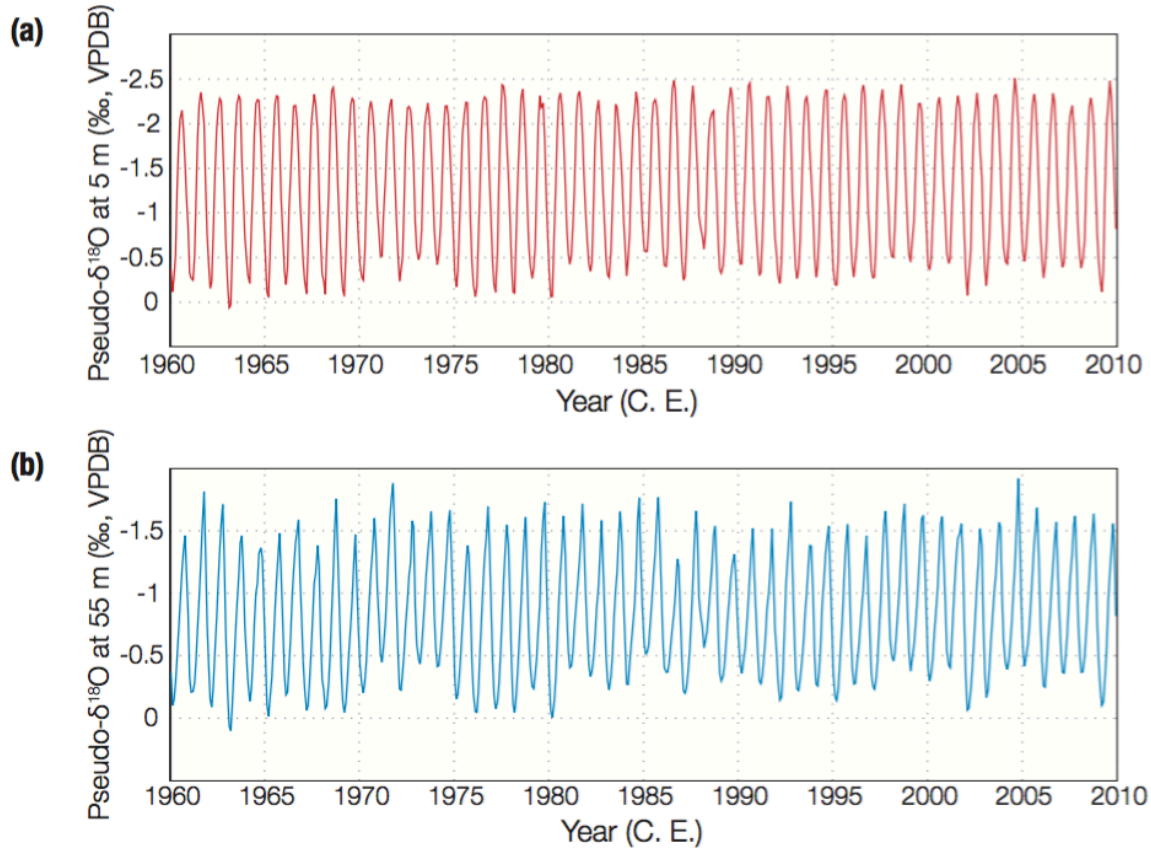

Figure 7. Pseudo-$\delta^{18}O$ Time Series Generated with INFAUNAL. Monte Carlo picking experiments were performed on pseudo-$\delta^{18}O$ time series at 5 m (a) and 55 m (b) generated as a function of temperature and salinity extracted from the ORA-S4 reanalysis dataset at 26.7°N, 93.9°W in the northern Gulf of Mexico.

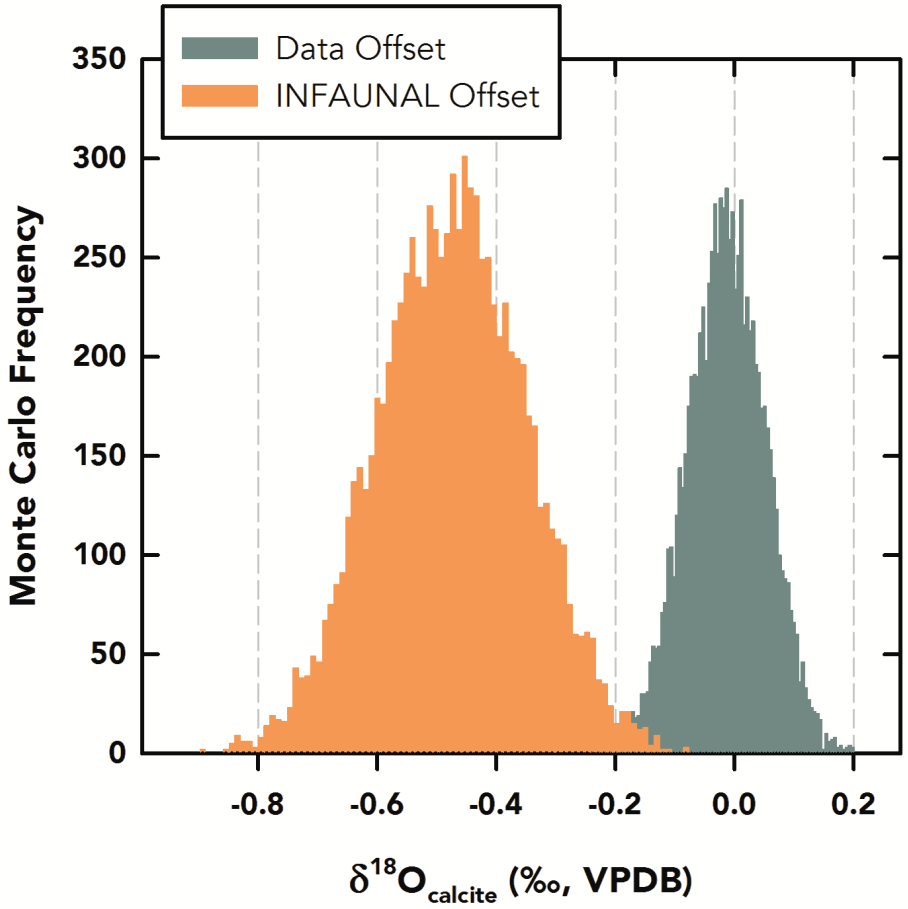

Figure 8. Data-Model Comparison of Simulated Offsets with Uncertainty Constraints. Monte-Carlo-based histogram of mean offsets from the ss-sl data (green) in core-top/downcore samples compared to a histogram of mean offsets between pseudo-$\delta^{18}O$ time series from 5 m and 55 m depth generated using INFAUNAL [*Thirumalai et al.*, 2013] (orange). Both populations incorporate analytical and sampling uncertainty and are significantly different from each other ($p<0.001$). Note that the model-offset population is significantly distinct from zero ($p<0.001$) while the data-offset population is not different from zero ($p<0.05$).

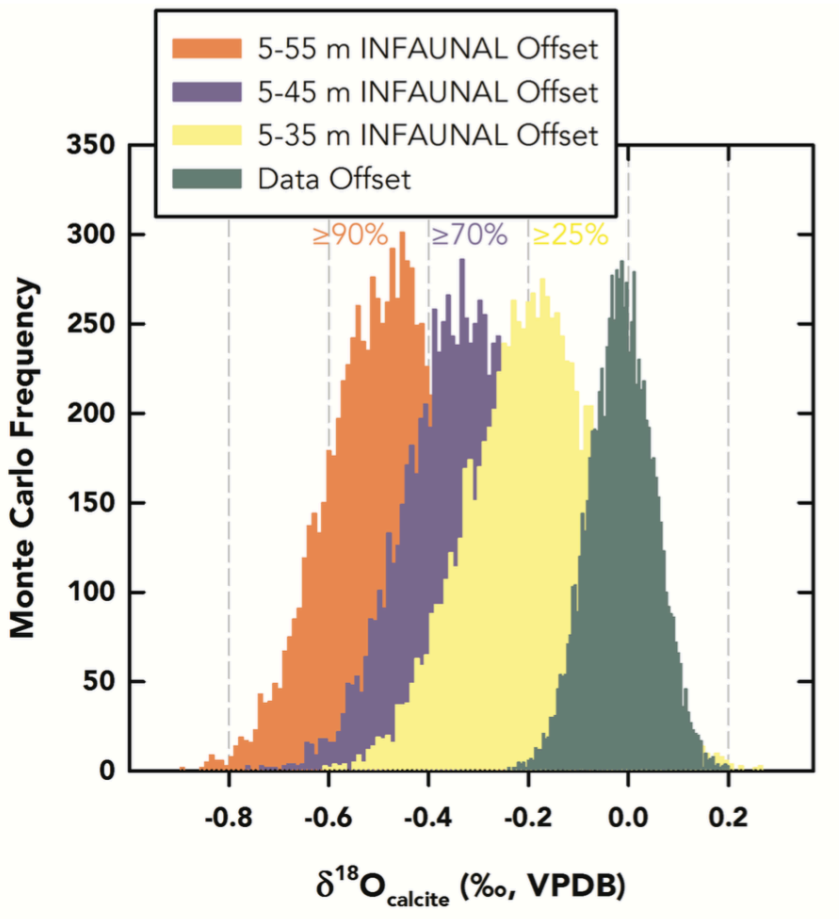

Figure 9. Data-Model Comparison of Simulated Offsets with Uncertainty Constraints at Various Depths. Histogram of mean offsets in ss-sl data (green histogram) from core-top/downcore samples compared with populations of mean $\delta^{18}O$ time series at 5 m and 55 m (orange), 5 m and 45 m (purple), and 5 m and 35 m (yellow) depths generated using INFAUNAL. Percentages above the modeled histograms indicate the minimum probabilities that depth-specific signals can be resolved using picked means of 50 pseudo-foraminifera, as given by INFAUNAL. All three model-based histograms are significantly different from the data offset ($p<0.001$) incorporating both analytical and sampling uncertainty, and are significantly distinct from zero ($p<0.001$), while the data-based histogram is not different from zero ($p<0.05$).

Constraining past seawater $\delta^{18}O$ and temperature records developed from foraminiferal geochemistry

Kaustubh Thirumalai[1,2], Terrence M. Quinn[1,2], Gianluca Marino[3]

[1] *Institute for Geophysics, Jackson School of Geosciences, University of Texas at Austin*

[2] *Department of Geological Sciences, Jackson School of Geosciences, University of Texas at Austin*

[3] *Research School of Earth Sciences, The Australian National University*

* Chapter 2 has been submitted for publication.

ABSTRACT

Paired measurements of magnesium-to-calcium ratios (Mg/Ca) and the stable oxygen isotopic composition ($\delta^{18}O$) in foraminiferal shells have provided significant insights into Cenozoic paleoceanography over the last two decades. Temperature and seawater $\delta^{18}O$ ($\delta^{18}O_{sw}$, a proxy for salinity and ice volume) reconstructions using these measurements have advanced our knowledge of past climate change. However, multiple sources of uncertainty exist in transferring these depth-based geochemical signals into climate variables within a discrete time domain. Here, we develop a computational toolkit entitled Paleo-Seawater Uncertainty Solver (PSU Solver) that performs bootstrap Monte Carlo simulations to constrain these various sources of uncertainty. PSU Solver offers simultaneous solutions for temperature and $\delta^{18}O_{sw}$ and their respective uncertainty envelopes using an iterative approach with user-defined errors,

calibrations, and sea-level curves. In this work, we demonstrate the applicability of PSU Solver for four published records covering three different timescales: late Holocene, the last deglaciation, and the last glacial period. We show that the influence of salinity in Mg/Ca and the choice of sea-level curve can change the structure of the resulting reconstruction and hence affect paleoclimate interpretation. PSU Solver offers an expeditious yet rigorous approach to test the robustness of past climate variability derived from paired Mg/Ca-$\delta^{18}O$ measurements.

1. Introduction

The magnesium-to-calcium ratio (Mg/Ca) of foraminiferal calcite is widely used as a proxy for past water mass temperature on a variety of timescales. Commonly, the stable oxygen isotopic composition ($\delta^{18}O$) of foraminiferal shells from the same depth in the marine sediment core, also dependent on the temperature, is analyzed to isolate the seawater $\delta^{18}O$ ($\delta^{18}O_{sw}$) signal, a proxy for the salinity of the water mass which can be affected by significant changes in global ice volume. This method of coeval measurements on foraminiferal shells picked from the same depth interval in a marine sediment core is usually termed as coupled or paired Mg/Ca-$\delta^{18}O$ analysis [*Elderfield and Ganssen*, 2000; *Lea et al.*, 2000; *Nürnberg et al.*, 2000]. The development of the foraminiferal Mg/Ca paleothermometer [*Nürnberg et al.*, 1996; *Lea et al.*, 1999; *Dekens et al.*, 2002; *Anand et al.*, 2003] and the resultant application of paired Mg/Ca-$\delta^{18}O$ analysis has enabled several critical insights into past climate change regarding ocean-atmosphere processes [*Weldeab et al.*, 2007; *Elderfield et al.*, 2012; *Arbuszewski*

et al., 2013; *Moffa-Sanchez et al.*, 2014a; *Marino et al.*, 2015], abrupt climate change [*Leduc et al.*, 2007; *Anand et al.*, 2008; *Marcott et al.*, 2011; *Ezat et al.*, 2014; *Tierney et al.*, 2015a], and climate sensitivity [*Lear et al.*, 2000; *Billups and Schrag*, 2003; *Zachos et al.*, 2003; *Lea*, 2004; *Medina-Elizalde et al.*, 2008].

The quantitative merit of these interpretations relies on the strength of calibrations that detail the relationships between Mg/Ca, $\delta^{18}O$, $\delta^{18}O_{sw}$, temperature, and salinity. However, there are multiple sources of uncertainty inherent in transferring the paired Mg/Ca-$\delta^{18}O$ signal into deconvolved time series of temperature and salinity. Propagating analytical, sampling [*Thirumalai et al.*, 2013; 2014], and calibration errors [*Khider et al.*, 2015] along with age uncertainty [*Trauth et al.*, 1997; *Blaauw and Christen*, 2011] into a climatic time series is complex [*Schmidt*, 1999a; *Rohling*, 2000] due to the non-linear nature of the associated Mg/Ca and $\delta^{18}O$ relationships [*Dekens et al.*, 2002; *Anand et al.*, 2003], the potential effect of salinity and post-depositional effects on Mg/Ca [*Ferguson et al.*, 2008; *Kısakürek et al.*, 2008; *Arbuszewski et al.*, 2010; *Dueñas-Bohórquez et al.*, 2011; *Hertzberg and Schmidt*, 2013; *Hönisch et al.*, 2013; *Khider et al.*, 2015], the effect of ice volume on $\delta^{18}O_{sw}$ [*Shackleton*, 1967; *Mix and Ruddiman*, 1984; *Shackleton*, 1987; *Elderfield et al.*, 2012], and the potential non-stationarity of the $\delta^{18}O_{sw}$-salinity relationship [*Rohling and Bigg*, 1998; *Bigg and Rohling*, 2000; *Caley and Roche*, 2015; *Holloway et al.*, 2016]. Each of these factors can complicate the interpretation of downcore foraminiferal geochemistry, depending on the signal-to-noise ratio being reconstructed. As the interaction between these different sources of uncertainty is not straightforward [*Schmidt*, 1999a; *Rohling*, 2000], there is a need to test the sensitivity of the reconstructed temperature and salinity signal to these factors in

order to derive robust records of climate variability. Furthermore, as these relationships are refined with more nuanced observational studies [*Arbuszewski et al.*, 2010; *Hertzberg and Schmidt*, 2013; *Hönisch et al.*, 2013; *Thirumalai et al.*, 2014; *Spero et al.*, 2015], updated statistical constraints [*Tierney et al.*, 2015a], sea-level records of increased resolution and better chronological constraints [*Grant et al.*, 2012; *Rohling et al.*, 2014; *Schneider*, 2014], and improved spatiotemporal $\delta^{18}O_{sw}$ data coverage [*Conroy et al.*, 2014], there is also a need to revisit interpretations of previously published geochemical records. Finally, model-data comparisons and large-scale data assimilation [*McGregor et al.*, 2015; *Wang et al.*, 2015] stand to benefit from comprehensive uncertainty analysis of temperature and salinity reconstructions from foraminiferal geochemistry.

In this work, we probabilistically constrain the errors associated with temperature, $\delta^{18}O_{sw}$, and salinity reconstructions developed from foraminiferal geochemistry. We use bootstrap Monte Carlo simulations to quantify the overall uncertainty in these reconstructions which includes age, analytical, calibration, and sampling errors in a framework where the effects of salinity on Mg/Ca, and the effect of ice-volume on $\delta^{18}O_{sw}$ can also be incorporated (Fig. 10). We apply our algorithm, entitled Paleo-Seawater Uncertainty Solver (PSU Solver), to several previously published reconstructions of sea-surface temperature (SST) and salinity (SSS) to demonstrate its utility in testing the robustness of climate reconstructions to the aforementioned sources of uncertainty. The aim of this study is not to emphasize the advantage or disadvantage of particular sets of transfer functions or input conditions for foraminiferal geochemistry. Rather, we demonstrate how reconstructions can be affected by various input conditions

and aim to provide a platform where users can obtain rigorous uncertainty constraints and explore the effect of different combinations of equations on the underlying geochemical records. A MATLAB™ version of PSU Solver, whose runtime is typically less than a minute, is publicly available for future use.

2. METHODS AND DATA

PSU Solver constrains uncertainty in paired Mg/Ca-$\delta^{18}O$ data using a bootstrap resampling approach within an iterative Monte Carlo framework [*Efron*, 1979; *Hall and Martin*, 1988]. Using the paired dataset, user-specified errors, and a user-specified set of input conditions, PSU Solver produces *n* realizations of temperature, $\delta^{18}O_{sw}$, and salinity time series, where *n* is the number of Monte Carlo iterations. The median and its errors, represented by the 68/95th percentiles, are calculated at each time step for the *n* time series. The temperature, $\delta^{18}O_{sw}$, and salinity time series along with their errors are then furnished as output for user interpretation (Fig. 10).

2.1. Data Input

As input, PSU Solver is written to accept discrete time data (unevenly or evenly spaced) with corresponding Mg/Ca (in mmol/mol) and $\delta^{18}O$ (in ‰, VPDB) measurements at each timestep. PSU Solver also has the capability to directly couple output from BACON, a code that generates numerous age-depth distributions for radiocarbon ages based on a Bayesian methodology [*Blaauw and Christen*, 2011]. These age-depth distributions can be used to produce an age-depth model (with associated uncertainty) for the core based on user-specified functions (where the default fit is a spline). If the BACON option is

employed, PSU Solver requires a vector of depths as input instead of age-related timesteps.

2.2. Error Input

After the age (or depth) and paired Mg/Ca-$\delta^{18}O$ data are entered, the user can specify constant or time-varying errors associated with these data including 1) age error, 2) analytical error, and 3) sampling error. The age error, which is the mean error around a particular time domain, serves to smooth the resulting time series, and can include uncertainty related to bioturbation [*Trauth et al.*, 1997], whose range can be quantified from mixing models such as TURBO2 [*Trauth*, 2013], and/or the effects of sediment compaction [*Huybers and Wunsch*, 2004]. Thus, even if age uncertainty is constrained by employing the BACON option, the age error parameter may be used to quantify time uncertainty related to bioturbation and/or compaction. Next, analytical error is prescribed to the Mg/Ca (either in mmol/mol or as a percentage) and $\delta^{18}O$ (in permil) data. Lastly, a sampling error term is entered as a percentage of the analytical error. This parameter is mainly related to the the seasonal signal at the core location, the ecology and growth habitat of the foraminiferal species utilized, and the number of foraminifera used in the reconstruction at each timestep [*Killingley et al.*, 1981; *Schiffelbein and Hills*, 1984; *Thirumalai et al.*, 2013]. Forward models such as INFAUNAL [*Thirumalai et al.*, 2013] can be used to obtain viable estimates of the sampling error term [*Schmidt*, 1999b; *Evans et al.*, 2013; *Thirumalai et al.*, 2014; *Wicks et al.*, 2015]. These three sources of error specify the potential range of the Monte Carlo sample space at each timestep and become important in parameterizing the overall uncertainty.

2.3. Initialization

PSU Solver requires the user to specify a set of input conditions after they have entered the downcore data and have prescribed their corresponding errors. These include 1) the number of total Monte Carlo simulations to be performed, 2) a choice of sea-level curve (or the option to not correct for ice volume), and 3) the desired set of climate-geochemistry relationships. We recommend that the number of Monte Carlo simulations is kept low (100-500) for initial runs of PSU Solver, while they can be increased to a more suitable number (1000-10000) after it is ensured that the program functions efficiently. In the present version, PSU Solver contains three different sea-level curves which can be used for different scenarios: 1) a high-resolution curve based on the inversion of ~1,000 global observations spanning the Last Glacial Maximum (LGM) and the Holocene [*Lambeck et al.*, 2014] (hereafter L14), 2) a probabilistically constrained sea-level curve with independent chronology that spans the last 150 kyrs with sufficient resolution to investigate millennial-scale events [*Grant et al.*, 2012] (hereafter G12), and 3) a lower resolution curve based on regressions using benthic foraminiferal isotopes that spans the past ~430 kyrs [*Waelbroeck et al.*, 2001] (hereafter W01). PSU Solver can interpolate the input sea-level curve to match the input timestep and is also capable of accepting a custom sea-level curve as well. The user can also choose to refrain from correcting for ice-volume-related changes in $\delta^{18}O_{sw}$ and not choose any sea-level curve. Finally, as the last step prior to the Monte Carlo simulations (Fig. 10), the user can choose the inversion equations that are used for the reconstructions. These inversions are performed in the following framework (using the Symbolic Toolbox in MATLAB™):

1. $\delta^{18}O = f(\delta^{18}O_{sw}, T)$
2. $Mg/Ca = g(T)$ OR $Mg/Ca = h(T, S)$
3. $\delta^{18}O_{sw} = j(S) + k(SL)$

where $\delta^{18}O$ and Mg/Ca are the measured stable isotopic and trace metal content of the foraminiferal shell, $\delta^{18}O_{sw}$ is the stable oxygen isotopic composition of the seawater, T and S are the temperature and salinity of the water mass respectively, SL is the sea-level curve utilized and *f*, *g*, *h*, *j*, and *k* are the transfer functions that describe these relationships. These functions can vary based on the type and habitat of the foraminiferal species used, the core location and/or depth, the choice of calibration applied, and whether the influence of salinity on Mg/Ca is considered. With these set of input-conditions, PSU Solver proceeds to iteratively and simultaneously solve these equations to produce time series of temperature, salinity, and $\delta^{18}O_{sw}$ along with their bootstrap-based errors. We stress that we do not recommend one set of relationships over the other and urge the user to judiciously choose an appropriate set of equations and conditions.

In summary, PSU Solver accepts the following parameters as user input (Fig. 10):

1. Data input
    a. Age (or depth) data
    b. Mg/Ca data
    c. $\delta^{18}O$ data
2. Error input
    a. Age error
    b. Analytical error

c. Sampling error

3. Initialization
    a. Number of Monte Carlo Simulations
    b. Choice of sea-level curve
    c. Transfer Functions

2.4. Example Datasets

We applied PSU Solver to four paired Mg/Ca-$\delta^{18}O$ records investigating sea-surface conditions spanning three different timescales: 1) a late Holocene record (Figs. 2.2 and 2.3) from the Gulf of Mexico (GOM; Pigmy Basin [*Richey et al.*, 2007]), 2) another late Holocene record (Fig. 13) from the Indo-Pacific Warm Pool (IPWP; Makassar Straits [*Oppo et al.*, 2009]), 3) a deglacial record (Figs. 2.5 and 2.6) from the GOM (Orca Basin [*Williams et al.*, 2010; 2012]), and 4) a record from the Caribbean Sea (Colombian Basin [*Schmidt et al.*, 2004]) that captures a full glacial cycle. All four of these studies utilized the geochemistry of planktic foraminiferal species *Globigerinoides ruber*, a commonly used proxy for mean-annual, sea-surface conditions [*Fairbanks et al.*, 1982; *Schmidt and Mulitza*, 2002; *Farmer et al.*, 2007; *Thirumalai et al.*, 2014]. While the white variety, *G. ruber* (W) was used in the Makassar Strait, Colombian and Pigmy basin studies, a pink variety, *G. ruber* (P), was used for the deglacial Orca Basin study. Each of these studies used a different set of Mg/Ca-SST and $\delta^{18}O$-$\delta^{18}O_{sw}$-SST transfer functions (Table 4). We demonstrate the utility of PSU Solver by replicating the published datasets and testing the sensitivity of these records to different $\delta^{18}O_{sw}$-salinity relationships, different sea-level curves, and the influence of salinity on Mg/Ca variability.

3. Results and Discussion

3.1. Late Holocene GOM Record

Figure 11 displays the original Mg/Ca (orange circles) and $\delta^{18}O$ measurements (green circles) on *G. ruber* (W) from core PBBC-1 and the resulting temperature and $\delta^{18}O_{sw}$ reconstructions (black line) as presented in the original study [*Richey et al.*, 2007] (Table 4). Uncertainty envelopes consisting of analytical, sampling, and age errors are plotted with the Mg/Ca and $\delta^{18}O$ time series while the PSU Solver median is plotted along with its uncertainty envelope which consists of the previous errors as well as calibration uncertainties. In this case, the input conditions were set such that PSU Solver would replicate the published dataset: no ice-volume correction, no correction for the influence of salinity on Mg/Ca and the same *G. ruber*-(W)-specific transfer functions as used in the study [*Bemis et al.*, 1998; *Anand et al.*, 2003]. This exercise demonstrates that PSU Solver is capable of replicating the transformations of paired Mg/Ca-$\delta^{18}O$ data computed in previously published studies.

We observe discrepancies from published values if we use a transfer function *h* that corrects for the influence of salinity on Mg/Ca [*Tierney et al.*, 2015a] with all the other conditions remaining the same (Fig. 2.3). Here, we also require a definition of a $\delta^{18}O_{sw}$-salinity relationship in order to solve for all the unknowns (See Section 2.3). We investigated the use of two different equations to describe this relationship including one for the northern Atlantic Ocean (Fig. 2.3a, b), and another for the tropical Atlantic Ocean (Fig. 2.3c, d) based on a

gridded model [*LeGrande and Schmidt*, 2006]. In both cases, the temperature reconstructed using PSU Solver is warmer on average than the published values, which do not consider the influence of salinity (0.8°C for the tropical Atlantic case and 1.4°C for the north Atlantic case on average). Similarly, the reconstructed $\delta^{18}O_{sw}$ in both cases is lower than average relative to the published values (0.29‰ for the tropical Atlantic case and 0.16‰ for the north Atlantic case on average). We also note that the variability (as inferred from standard deviations) in both temperature and $\delta^{18}O_{sw}$ reconstructions is muted compared to the published datasets when an influence from salinity on Mg/Ca is considered in the PSU Solver output (Fig. 2.3). While comparing core-top values from the PSU Solver output with instrumental observations (yellow stars in Fig. 11 and 2.3), we find the best match for both temperature and $\delta^{18}O_{sw}$ reconstructions in the case using the tropical Atlantic $\delta^{18}O_{sw}$-salinity equation (Fig. 2.3a, b). However, it should be noted that all PSU Solver outputs for the core-top agree with the instrumental data within error.

3.2. Late Holocene IPWP Record

We applied PSU Solver to another highly-resolved late Holocene record of *G. ruber* (W) [*Oppo et al.*, 2009] from a gravity core in the IPWP (Fig. 13). We first ensured that PSU Solver replicates the published dataset and then derived uncertainty constraints for the reconstructions (Fig. 13a, b) using reported analytical and errors, and sampling errors calculated using INFAUNAL [*Thirumalai et al.*, 2013]. To examine how the influence of salinity on Mg/Ca would affect the paleoclimatic reconstructions, we chose a Mg/Ca-temperature-salinity equation [*Tierney et al.*, 2015a] and a $\delta^{18}O_{sw}$-salinity equation based on

biweekly observations from the western Pacific [*Morimoto et al.*, 2002]. In this case, reconstructed temperatures from PSU Solver are warmer than the reported values (Fig. 13c) whereas $\delta^{18}O_{sw}$ estimates are greater (Fig. 13d). Though this record ends at ~400 yrs BP (Fig. 13), paired Mg/Ca-$\delta^{18}O$ data at the top of this gravity core, BJ8-03-34GGC, is comparable to the core-top values of multicore BJ8-03-31MCA which overlaps with the instrumental record [*Oppo et al.*, 2009]. It is worth noting that the core-top values of the PSU Solver output agree better with instrumental measurements (yellow stars in Fig. 13) of mean-annual temperature [*Rayner et al.*, 2003] and available $\delta^{18}O_{sw}$ measurements from the IPWP [*Epstein and Mayeda*, 1953; *Bigg and Rohling*, 2000; *LeGrande and Schmidt*, 2006]. This contrasts with the interpretation in the original study that *G. ruber* (W) downcore record is representative of the cold, upwelling season in the IPWP [*Oppo et al.*, 2009]. However, sediment trap studies in the IPWP indicate a year-round preference of the *G. ruber* (W) species [*Kawahata et al.*, 2002; *Mohtadi et al.*, 2009], thereby implying that downcore reconstructions should be representative of mean-annual conditions. Thus, by using different transfer functions, the PSU Solver output offers a potential reconciliation of the observed discrepancy between the sediment trap results and the downcore late Holocene record in the IPWP.

3.3. Deglacial GOM Record

We plot the results from a replication experiment and two sensitivity experiments on the deglacial *G. ruber* (P) record from the Orca Basin [*Williams et al.*, 2010; 2012] in Figure 14. Initially, we replicated the published values with transfer functions used in the study [*Bemis et al.*, 1998; *Anand et al.*, 2003] and

produced uncertainty envelopes (Fig. 14a, b) using error values reported therein [*Williams et al.*, 2010] where we used the W01 sea-level curve. Next, with all other parameters being equal, we used L14, a sea-level curve of higher resolution that focused on the deglaciation, to correct for the effect of ice-volume on $\delta^{18}O_{sw}$ (Fig. 14c, d). In this case, while the median temperature, uncertainty in temperature, and median $\delta^{18}O_{sw}$ estimates do not significantly deviate from the published values, the $\delta^{18}O_{sw}$ uncertainty envelope is visibly reduced compared to that produced from the lower resolution sea-level curve (compare Fig. 14b with Fig. 14d). At times during the record, this improvement is up to 50% of the overall uncertainty range. The median temperature reconstruction nor their corresponding uncertainties are affected by choice of sea-level input, although, the temperature estimates deviate significantly outside uncertainty from published values (Fig. 14e) if the effect of salinity on Mg/Ca variability is considered [*Tierney et al.*, 2015a]. Most notably, there are warmer SST values during the 16-12 kyr BP interval, with SST running 1-2.5°C higher than published values after 14 kyr BP, during the Bølling-Allerød [*Williams et al.*, 2012]. However, the median $\delta^{18}O_{sw}$ reconstruction and their uncertainties for these input conditions do not significantly deviate from the previous uncertainty estimates (although the range of median values is slightly decreased; Fig. 14f). This implies that the structure of $\delta^{18}O_{sw}$ variability as reconstructed from the paired Mg/Ca-$\delta^{18}O$ data is robust, despite different sea-level curves and despite the influence of salinity on foraminiferal Mg/Ca ratios.

3.4. Late Quaternary Caribbean Sea Record

To demonstrate the applicability of PSU Solver on longer timescales, we applied PSU Solver to a paired Mg/Ca-$\delta^{18}O$ record from the Colombian basin [*Schmidt et al.*, 2004] that uses *G. ruber* (W) geochemistry and spans the past ~130 kyr (Fig. 15). First, we replicated the reported values using the W01 sea-level curve, errors, and relationships utilized in the original study [*Schmidt et al.*, 2004] (Fig. 15a, b). This study utilized an Mg/Ca-SST relationship [*Dekens et al.*, 2002] which is dependent on the depth of the core, a capability that is built into PSU Solver. Next, we used an Mg/Ca-SST equation that considered the influence of salinity on Mg/Ca variability [*Tierney et al.*, 2015a] and also used the G12 sea-level curve as input for PSU Solver (Fig. 15c, d). This exercise yielded temperature and $\delta^{18}O_{sw}$ estimates offset from the published values with discrepancies as large ~4°C in SST and ~1‰ in $\delta^{18}O_{sw}$ (Fig. 15), where millennial-scale and glacial-interglacial variability in the latter is considerably reduced. Most strikingly, the originally reported LGM-Holocene temperature difference is ~2°C compared to ~5°C in the PSU Solver output (Fig. 15c). Moreover, the trends in $\delta^{18}O_{sw}$ variability over the past ~60 kyr to the present are reversed in both cases, where Caribbean Sea $\delta^{18}O_{sw}$ values become lower in the original dataset over time whereas the values become greater when the effect of salinity on Mg/Ca is considered (Fig. 15d). Interestingly, mean annual SST and $\delta^{18}O_{sw}$ in observations from the Caribbean Sea [*Epstein and Mayeda*, 1953; *Rayner et al.*, 2003; *Robbins et al.*, 2012] match better with the latter case than the former (yellow stars in Fig. 15). Along with improved uncertainty estimates and better agreement with modern observations, reconstructed $\delta^{18}O_{sw}$ variability in the PSU Solver output compared to the originally reported dataset (Fig. 15d)

are more muted and are easier to reconcile with theoretical and modeling constraints for the LGM [*Wunsch*, 2003; 2010]. These results arguably render the application with the influence of salinity on Mg/Ca variability as a more "realistic" reconstruction from the geochemical data. If accurate, since the LGM-to-Holocene difference of ~5°C is likely too large of a mean annual SST change alone [*Mix et al.*, 1999; *Waelbroeck et al.*, 2009], varying seasonality and/or productivity of *G. ruber* (W) in the past [*Laepple and Huybers*, 2014; *Timmermann et al.*, 2014], as opposed to (or along with) mean annual SST changes could explain such large reconstructed SST changes. Thus, PSU Solver can be applied to records that span multiple marine isotopic stages, and that it can assess the sensitivity of such paired Mg/Ca-$\delta^{18}O$ records to various sea-level curves, calibrations, and the influence of salinity on Mg/Ca variability.

3.5. Summary of Four Initial Applications

We have demonstrated the utility of PSU Solver in replicating previously published reconstructions with different foraminiferal transfer functions that span different timescales and have different sample resolutions. We have shown that PSU Solver can identify the robustness of temperature and $\delta^{18}O_{sw}$ estimates to various sources of uncertainty. Slightly different $\delta^{18}O_{sw}$-salinity relationships can alter the reconstructed parameters and their underlying uncertainty (Figs. 2.3, 2.4), whereas well-dated and highly resolved sea-level curves can significantly reduce uncertainty in $\delta^{18}O_{sw}$ reconstructions requiring a correction due to ice-volume (Fig. 14, 2.6). Input for PSU Solver can be coupled to other code utilized in foraminiferal reconstructions such as BACON [*Blaauw and Christen*, 2011], TURBO2 [*Trauth*, 2013], and INFAUNAL [*Thirumalai et al.*, 2013]

whereas the output time series and corresponding uncertainty estimates can be readily transformed as necessary including the use of filters [*Clemens et al.*, 2010], smoothing functions [*Marino et al.*, 2015], or empirical orthogonal functions [*Anchukaitis and Tierney*, 2012]. The underlying code can be suitably modified to address problems on timescales or foraminiferal species outside our example datasets, including important paleoclimate targets where seawater Mg/Ca was different from the modern ocean [*O'Brien et al.*, 2014; *Ravelo et al.*, 2014; *Zhang et al.*, 2014; *Lear et al.*, 2015] or scenarios where modeling studies provide constraints on the stationarity of past $\delta^{18}O_{sw}$-salinity relationships [*Caley and Roche*, 2015; *Tindall and Haywood*, 2015; *Holloway et al.*, 2016]. Importantly, PSU Solver can be useful in large-scale data assimilation studies where several paleoceanographic records are being processed with updated uncertainty constraints and/or calibrations [*McGregor et al.*, 2015; *Tierney et al.*, 2015b]. Taken together, we have established that PSU Solver is a toolkit that can not only quantify uncertainty in these reconstructions, but can also provide important constraints on the interpretation of past seawater $\delta^{18}O$ and temperature variability.

4. Conclusions

We provide an algorithm (PSU Solver) to probabilistically constrain and quantify records of temperature and $\delta^{18}O_{sw}$ developed from paired Mg/Ca-$\delta^{18}O$ data in foraminifera. We demonstrate that the application of PSU Solver can replicate previous reconstructions, assess robustness to various sources of uncertainty, and furnish median estimates and corresponding uncertainty

envelopes using a bootstrap Monte Carlo methodology. Using a suite of user-specified input PSU Solver can incorporate age (including bioturbation/compaction), analytical, calibration, and sampling errors in its estimates of temperature and $\delta^{18}O_{sw}$ variability where the user can also specify the influence of salinity on Mg/Ca and select from several published sea-level curves. In general, PSU Solver is an uncertainty quantification toolkit that can be easily implemented to offer constraints on records developed from foraminiferal geochemistry, for paleoceanographers and other scientists interested in past changes in ocean history.

5. Acknowledgements

We thank the International Ocean Discovery Program for helping facilitate this project. K. T. thanks the UTIG Ewing-Worzel fellowship, the JSG Lagoe Micropaleontology Fund, and the National Science Foundation under a cooperative agreement with the Consortium for Ocean Leadership as a U.S. Science Support Program for support. GM acknowledges support from the Australian Laureate Fellowship project FL120100050 (to E.J. Rohling). This work was supported by the National Science Foundation grant OCE-0902921 to TMQ.

Dataset	Mg/Ca-SST	D18O
Richey et al. 2007	Mg/Ca = 0.449exp(0.09*T) [*Anand et al.,* 2003]	T = 14.9 - 4.8*($\delta^{18}O$ - $\delta^{18}O_{sw}$) [*Bemis et al.,* 1998]
Oppo et al. 2009	Mg/Ca = 0.38exp(0.09*T) [*Anand et al.,* 2003]	T = 16.5 - 4.8*($\delta^{18}O$ - $\delta^{18}O_{sw}$) [*Bemis et al.,* 1998]
Williams et al. 2010/2012	Mg/Ca = 0.38exp(0.09*T) [*Anand et al.,* 2003]	T = 14.9 - 4.8*($\delta^{18}O$ - $\delta^{18}O_{sw}$) [*Bemis et al.,* 1998]
Schmidt et al. 2004	Mg/Ca = 0.38exp(0.09*(T – 0.61*Core Depth) [*Dekens et al.,* 2002]	T = 16.5 - 4.8*($\delta^{18}O$ - $\delta^{18}O_{sw}$) [*Bemis et al.,* 1998]

Table 4. Transfer functions used in the example datasets.

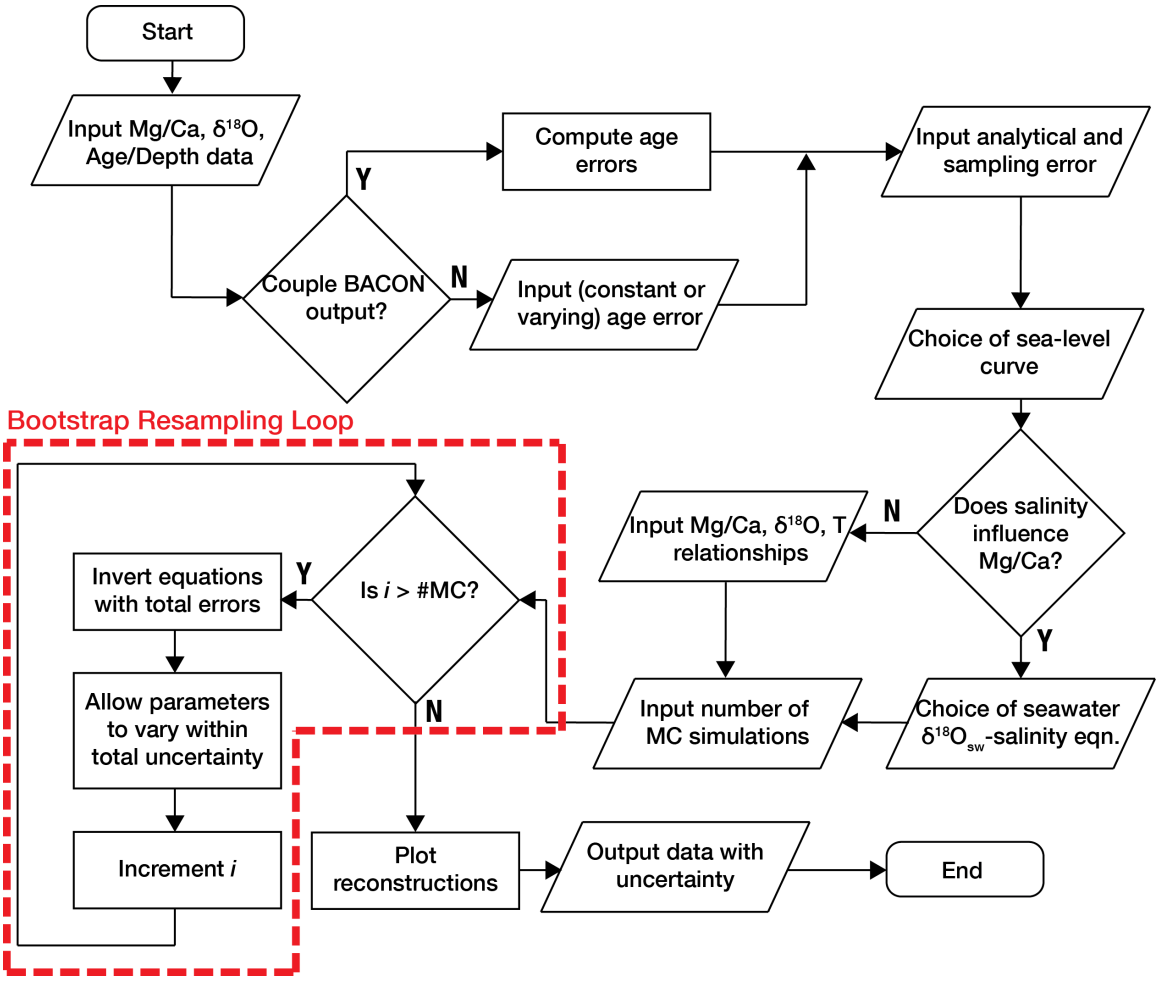

Figure 10. Flowchart for PSU Solver, a toolkit to constrain past seawater $\delta^{18}O_{sw}$ and temperature reconstructions that are generated from foraminiferal geochemistry using a bootstrap resampling approach (red dashed line). The code is written in MATLAB™ and has a runtime typically under a minute, even for high numbers (>1000) of Monte Carlo simulations.

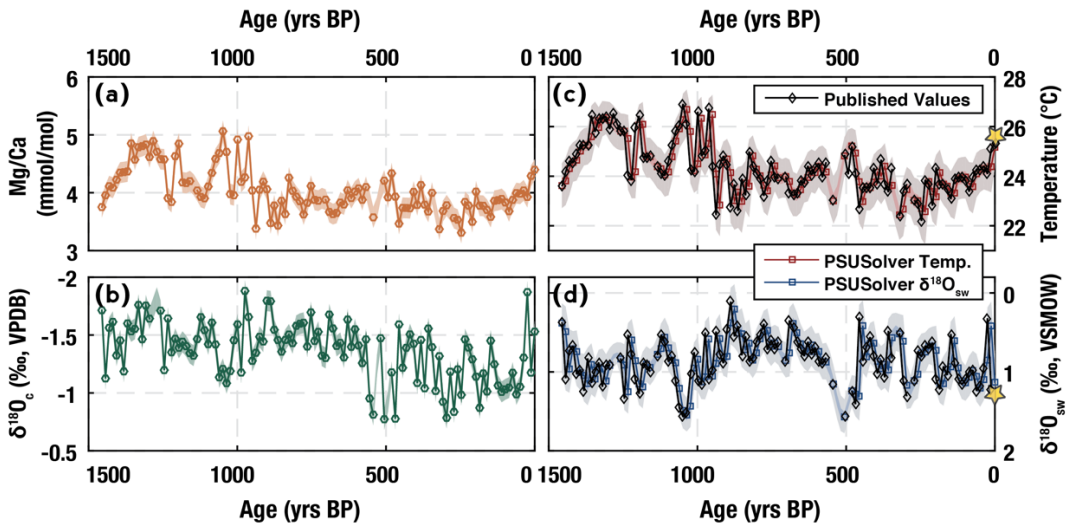

Figure 11. Initial application of PSU Solver to a paired Mg/Ca-$\delta^{18}O$ record from the Gulf of Mexico (Pigmy Basin [*Richey et al.*, 2007]) using the geochemistry of *G. ruber* (W). The published Mg/Ca (orange; a) and $\delta^{18}O$ (green; b) measurements are shown with age, analytical and sampling errors on the left hand side. The published reconstructions are plotted on the right (black line with diamonds in c and d) along with the PSU Solver output where the SST (red), $\delta^{18}O_{sw}$ (blue), and corresponding uncertainty envelopes are based on transfer functions reported in the original study. Yellow stars indicate mean-annual SST (1970-2015; HadISST) and available $\delta^{18}O_{sw}$ data in the northern Gulf of Mexico. Age values are reported in year before present (yrs BP).

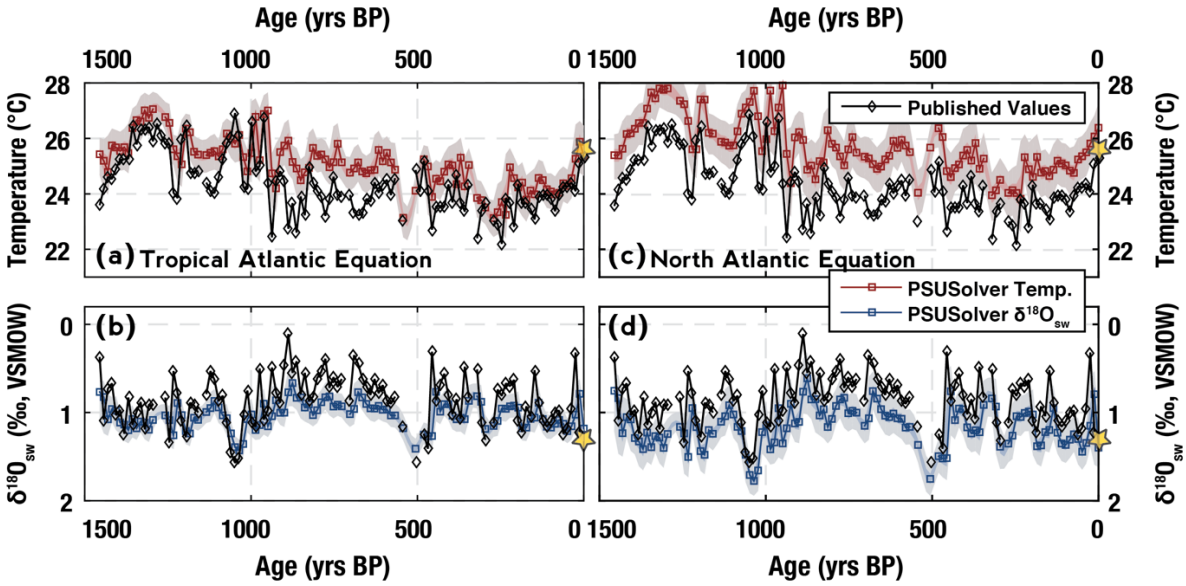

Figure 12. Application of PSU Solver to the late Holocene Gulf of Mexico record from the Pigmy Basin [*Richey et al.*, 2007] where different $\delta^{18}O_{sw}$-salinity relationships are used when the influence of salinity on Mg/Ca variability is considered. Both cases use the $\delta^{18}O$-$\delta^{18}O_{sw}$-T "high-light" equation [*Bemis et al.*, 1998] and a new Mg/Ca-SST-SSS calibration equation based on a compilation of cultured data [*Tierney et al.*, 2015a]. The tropical Atlantic and northern Atlantic equations are derived from a gridded $\delta^{18}O_{sw}$ dataset [*LeGrande and Schmidt*, 2006]. Note that the median estimates computed using the tropical Atlantic equation yield a better match with mean-annual observations (yellow stars), although both cases match the observations within overall uncertainty.

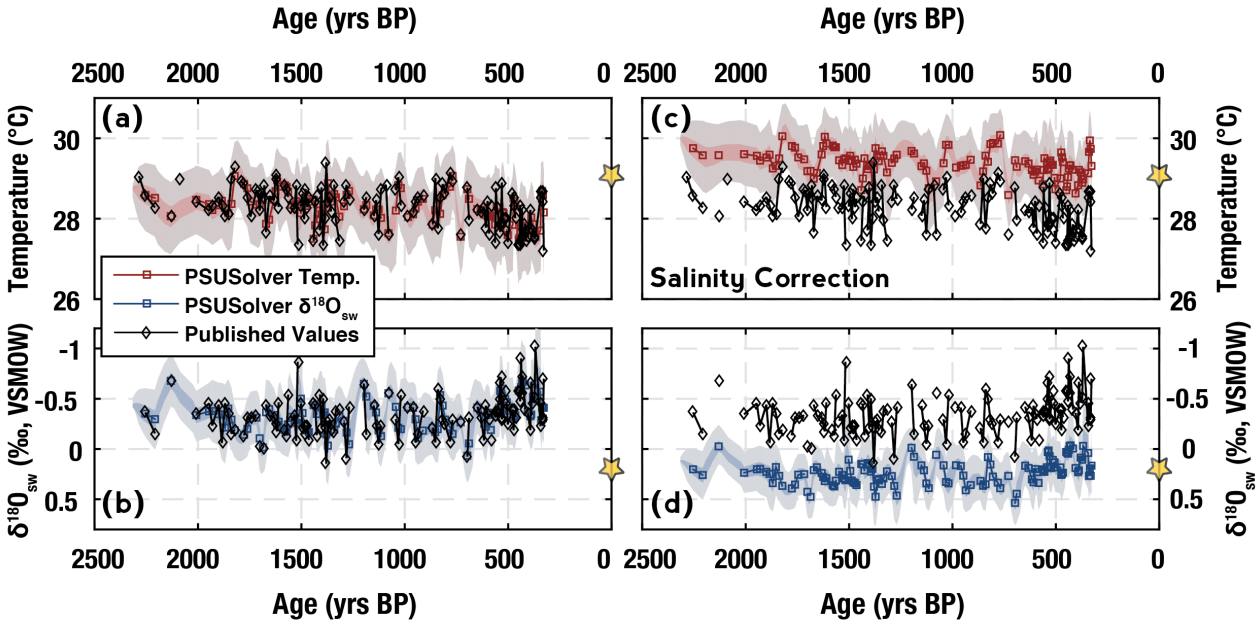

Figure 13. Application of PSU Solver to a late Holocene record from the Indo-Pacific Warm Pool [*Oppo et al.*, 2009]. (a) and (b) replicate the originally reported SST and $\delta^{18}O_{sw}$ values (original data in black; PSU Solver SST - red; $\delta^{18}O_{sw}$ – blue) using the "low-light" equation [*Bemis et al.*, 1998] and an Mg/Ca-SST calibration based on a sediment trap in the Sargasso Sea [*Anand et al.*, 2003]. (c) and (d) are the PSU Solver output using the "high-light" equation, a compilation-based Mg/Ca-SST-SSS calibration equation, and a local $\delta^{18}O_{sw}$-SSS relationship [*Bemis et al.*, 1998; *Morimoto et al.*, 2002; *Tierney et al.*, 2015a]. Yellow stars indicate mean-annual sea-surface observations.

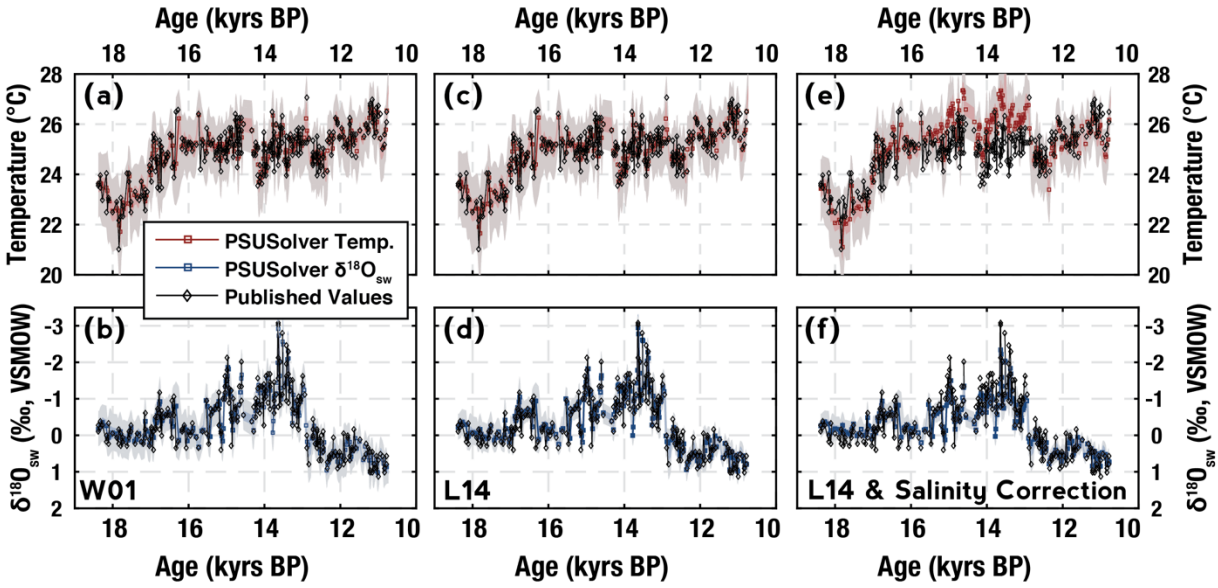

Figure 14. Application of PSU Solver to a deglacial record of paired *G. ruber* (P) data from the Gulf of Mexico (Orca Basin [*Williams et al.*, 2010; 2012]) where different sea-level curves are applied to correct for the fractionation of $\delta^{18}O_{sw}$ due to ice-volume changes. In (a) and (b) we applied a lower-resolution sea-level curve [*Waelbroeck et al.*, 2001] based on regressions with benthic isotopes whereas the reconstructions in (c) and (d) utilize a higher-resolution deglaciation-specific sea-level curve [*Lambeck et al.*, 2014]. The reconstructions in (e) and (f) were computed considering the effect of salinity on Mg/Ca along with the same input conditions as in (c) and (d). Note that the uncertainty envelopes in (d) and (e) are reduced compared to that in (b).

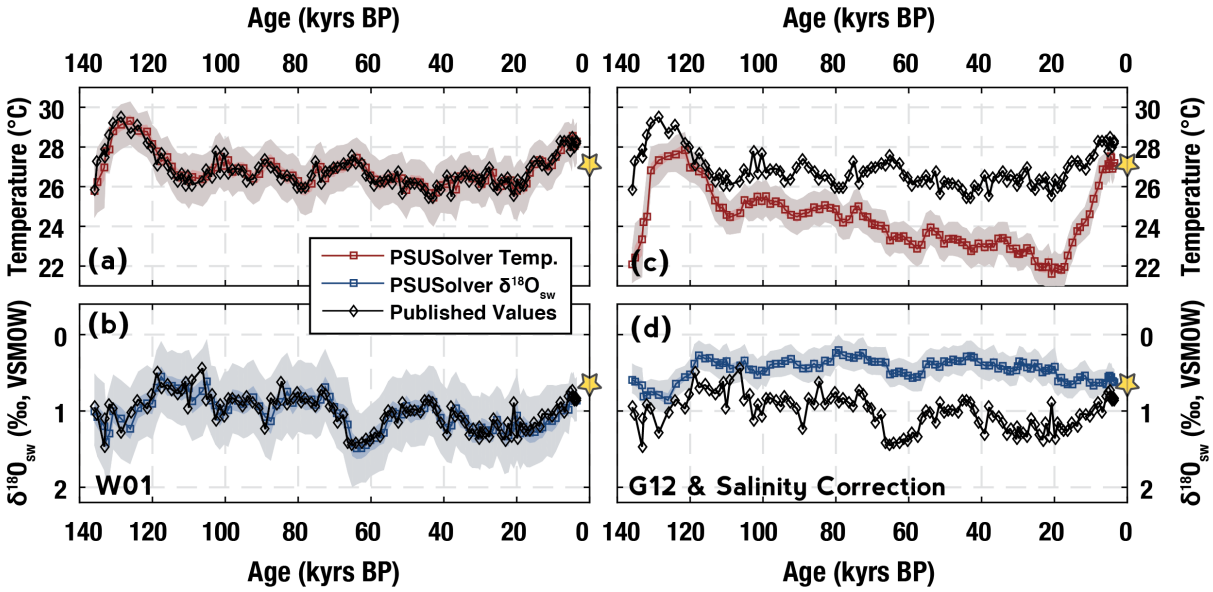

Figure 15. Reconstructed $\delta^{18}O_{sw}$ and SST variability (black lines with diamonds) from a site in the Caribbean Sea (Colombian Basin [*Schmidt et al.*, 2004]) based on paired Mg/Ca-$\delta^{18}O$ in *G. ruber* (W) and corresponding output from PSU Solver (red – SST; blue - $\delta^{18}O_{sw}$) with available mean-annual observations at the core location (yellow stars). While (a) and (b) follow a replication exercise in PSU Solver, (c) and (d) depict reconstructions where the influence of salinity on Mg/Ca variability, and a higher resolution sea-level curve is considered as input. Note that the significantly different reconstructions using the PSU Solver output in (c) and (d) are a better match with the observations and contain improved uncertainty estimates.

Centennial-scale links between Gulf Stream variability and Western Hemisphere hydroclimate

Kaustubh Thirumalai[1,2] Terrence M. Quinn[1,2], Yuko Okumura[1], Julie N. Richey[3], Judson W. Partin[1], Richard Z. Poore[3], Eduardo Moreno-Chamarro[4]

[1] *Institute for Geophysics, Jackson School of Geosciences, University of Texas at Austin*

[2] *Department of Geological Sciences, Jackson School of Geosciences, University of Texas at Austin*

[3] *United States Geological Survey, St. Petersburg Coastal and Marine Science Center*

[4] *Max Planck Institute for Meteorology, Hamburg, Germany*

* Chapter 3 has been submitted for publication.

ABSTRACT

The Gulf Stream, a surface ocean current associated with the Atlantic Meridional Overturning Circulation (AMOC), is an important medium of heat transfer in the global climate system. Yet, its variability on centennial timescales is poorly constrained due to insufficient long, high-resolution records. Here we present a fully replicated reconstruction of sea-surface temperature and salinity from a site the northern Gulf of Mexico sensitive to Atlantic Ocean circulation to improve our understanding of climate variability over the last 4,400 years. We use a suite of instrumental and proxy records in tandem with modeling simulations to demonstrate a link between Gulf Stream strength and Western

Hemisphere hydroclimate over the last millennium. Our results suggest marked centennial variability (up to 1°C and 0.3 PSU) in the Gulf of Mexico during the last 4,400 years and are consistent with a slowdown of the Gulf Stream and a more southward intertropical convergence zone during the Little Ice Age.

1. Introduction

The Gulf Stream, a surface current linked with the Atlantic Meridional Overturning Circulation (AMOC), transports heat and salt poleward into the North Atlantic basin, influencing North American and European climate [*Palter*, 2015; *Srokosz and Bryden*, 2015]. Variability of AMOC and its components on decadal-to-centennial timescales constitutes a major source of uncertainty in predicting future global climate [*Park and Latif*, 2008; *Srokosz and Bryden*, 2015]. However, comprehensive, continuous observations of AMOC variability only span the last decade[*Srokosz and Bryden*, 2015]. A recent synopsis of these measurements [*Srokosz and Bryden*, 2015] revealed interannual variability larger than intermittent, ship-based historical estimates [*Bryden et al.*, 2005] and concluded that future observations would yield “inevitable surprises”. Climate models predict that on the timescale of centuries, AMOC variability may be even larger [*Cheng et al.*, 2013], underscoring the need for proxy data that allows quantitative reconstructions of centennial-scale variability associated with AMOC, its multiple branches, and its effects on climate.

Although previous paleoceanographic studies have implicated changes in the AMOC as a driver of climate variability on glacial-interglacial and millennial timescales [*Nürnberg et al.*, 2008; *Marino et al.*, 2013; *Böhm et al.*, 2014], there exist few marine records of sufficient resolution to investigate centennial-scale

changes in the late Holocene [*Lund et al.*, 2006; *Wanamaker et al.*, 2012; *Moffa-Sanchez et al.*, 2014a]. This time period is an important paleoclimatic target to understand natural climate and AMOC variability, owing to the relative similarity of its background conditions to the preindustrial era. The last millennium in particular has emerged as a powerful testbed for model-data intercomparison due to well-known external forcings [*Landrum et al.*, 2013] and characteristic global oceanic [*McGregor et al.*, 2015] and terrestrial [*Ahmed et al.*, 2013] fingerprints of surface temperature variability.

Over the past millennium, reconstructions of seawater density gradients inferred from benthic foraminiferal $\delta^{18}O$ from a sediment core transect [*Lund et al.*, 2006] below the passage of the Florida Current (purple stars in Fig. 16), a precursor current that directly feeds into the Gulf Stream, indicate a ~10% decrease in transport volume during the Little Ice Age (LIA; 1450-1850 C.E.) [*Masson-Delmotte et al.*, 2013]. If accurate, this reduction in the surface branch of AMOC should be evident in ocean circulation systems both upstream and downstream of the Gulf Stream [*Palter*, 2015; *Srokosz and Bryden*, 2015]. Northward of the path of the Gulf Stream, a ^{14}C record of water mass variability from the North Iceland shelf (purple star in Fig. 16), interpreted to record variations in the North Atlantic Current, corroborates this reduction in Gulf Stream circulation during the LIA [*Wanamaker et al.*, 2012]. The Loop Current is situated upstream of the Gulf Stream and feeds warm, salty Caribbean waters into the Florida Current via the Yucatan Channel [*Liu et al.*, 2012b]. Through eddy-shedding processes, the Loop Current also transports water masses into the Gulf of Mexico (hereafter GOM) and affects the sea-surface temperature (SST), salinity (SSS), and circulation of the region [*Liu et al.*, 2012b;

Gopalakrishnan et al., 2013]. No records exist that directly capture the strength of the Loop Current over the LIA. Additional marine records are required to validate and to track the spatiotemporal expression of Gulf Stream variability during time periods that are similar to the pre-industrial era: the LIA and the late Holocene.

Towards this endeavor, we reconstructed SST and SSS variability over the last 4,400 years using foraminiferal geochemistry in sediments from the Garrison Basin (26° 40.19'N,93° 55.22'W, Blue circle with yellow border in Fig. 16), northern GOM, to investigate variability related to the Gulf Stream. We measured magnesium-to-calcium ratios (Mg/Ca) and the stable oxygen isotope composition ($\delta^{18}O_c$) of the planktic foraminifer *Globigerinoides ruber* (white variety; *G. ruber* (W) hereafter). Based on sediment trap results from a mooring close to the core location, we are confident that *G. ruber* (W) is a suitable specimen for reconstructing mean annual sea-surface conditions from its geochemistry [*Thirumalai et al.*, 2014]. To assess the fidelity and preservation of these proxy signals in the geological record, and to replicate our results, we performed paired Mg/Ca-$\delta^{18}O_c$ analyses on three multicores from the same cast in the Garrison Basin (2010-GB2-MCA, 2010-GB2-MCB, 2010-GB2-MCC; hereafter MCA/MCB/MCC; Fig. 17). Radiocarbon measurements on planktic foraminifera revealed sedimentation rates of 14-15 cm/kyr allowing for 15-35-year sampling resolution (Fig. 3.3). We utilized a bootstrap Monte Carlo procedure that incorporated the Bayesian posterior distributions of calibrated radiocarbon ages, analytical and calibration errors for the $\delta^{18}O_c$ and Mg/Ca measurements, foraminiferal sampling error [*Thirumalai et al.*, 2013], and replication errors to develop stacked records with appropriate uncertainty

bounds from the multicore suite (Fig. 17; see Methods and Fig. 19). This iterative approach allowed us to simultaneously compute both SST and $\delta^{18}O$ of seawater ($\delta^{18}O_{sw}$), a proxy for SSS [*Lund et al.*, 2006; *Nürnberg et al.*, 2008; *Marino et al.*, 2013], over the last ~4,400 years (Fig. 17), and to quantitatively characterize the overall uncertainty in our reconstructions.

2. Materials and Methods

2.1. Multicore Collection and Sample Processing

Multicores 2010-GB2-MCA, 2010-GB2-MCB, and 2010-GB2-MCC (hereafter MCA, MCB, and MCC) were collected in the Garrison Basin, northern GOM (26° 40.19'N,93° 55.22'W) during the summer of 2010 aboard the R/V Cape Hatteras at a water depth of 1776 m. Cores MCA (core depth = 60 cm) and MCC (core depth = 58 cm) were both extruded and sectioned every 0.5 cm over their entire depths. MCB (core depth = 57 cm) was sectioned at 0.25 cm and analyzed up till 18 cm to obtain higher-resolution sampling over the last millennium. After extrusion, the mud samples from the three cores were disaggregated and gently sieved through a 63μm mesh size sieve using ultra-pure water, and subsequently dried. X-ray computed tomography and visual examinations of the cores revealed minimal bioturbation.

2.2. Age-Depth Modeling and Uncertainties

The three cores were independently dated using AMS radiocarbon measurements (n = 12: MCA = 6, MCB = 3, MCC = 3: no age inversions; Fig. S1) on upper-ocean planktic foraminiferal species (primarily *Globigerina sacculifer*, *Globigerinoides ruber* (white), and *Globigerinoides conglobatus*). Each multicore

contained intact and excellently preserved sediment-water interfaces and the tops of all three cores contained bomb radiocarbon, confirming that the core-tops contained the most recently deposited sediments and were not significantly bioturbated. Resultant sedimentation rates of ~14-15 cm/kyr allowed for ~30-year sampling resolution (for MCA and MCC; MCB was sectioned every 0.25 cm for ~15-year resolution over the last millennium).

The radiocarbon dates for each multicore were individually calibrated into calendar years using the R code BACON [*Blaauw and Christen*, 2011]. This code uses a Bayesian Monte Carlo Markov Chain (MCMC) methodology to produce numerous age-depth models with inherent reservoir-age-based and past-^{14}C-variability-based uncertainty. In this process, we applied the Marine13 curve [*Reimer et al.*, 2013] to calibrate for marine reservoir ages and used a correction (ΔR) of -32 ± 25 years, based on coral radiocarbon ages from the nearby (~100 km) Flower Garden Banks Sanctuary [*Wagner et al.*, 2009]. With post-bomb core-top ages and the BACON output, we built 5,000 age-depth models for each of the three cores based on a monotonic Monte Carlo procedure that included the full extent of their calendar age probability distributions (Fig. 3.3).

To investigate the robustness of the individual age-depth models against the combined ages of all three cores, we calibrated and built a set of 5,000 age-depth models using all of our ages (n = 12; black line in Fig. 3.3) based on the aforementioned procedure. This exercise showed that, within uncertainty, the three individual age-depth models were indistinguishable from the combined age model and validated the assumption that all three cores from the same multicore cast also had the same sedimentation rates. We used the age-depth model and inherent uncertainties containing all the ages (most informative) to

subsequently transform stratigraphic depth into calibrated ages. To investigate the potential effects of bioturbation we used smoothing filters larger than the size of our calibrated age error (3 cm - ~150 years) and used TURBO2 [*Trauth*, 2013] on our replicated stacks. These results matched each other, revealing that centennial-scale variability would still be preserved, despite bioturbation rates, which appear to be very minimal in our cores. Thus, through replication and error propagation, we constrain all components of age uncertainty, and include them in our confidence bounds prior to interpreting our downcore reconstructions.

2.3. Stable Isotopic and Mg/Ca Analyses

70-100 individual specimens of the white variety of planktic foraminifer *Globigerinoides ruber* (*G. ruber* (W)) were picked from the 250-300μm fraction in each sample for geochemical analysis. This narrow fraction window (50μm) minimizes size-based ontogenetic effects [*Peeters et al.*, 1999]. The geochemical variability of different morphotypes of *G. ruber* (W) was found to be insignificant in the northern GOM, based on sediment trap, core-top, and downcore samples [*Thirumalai et al.*, 2014]. The picked tests were visibly inspected for manganese and organic-based contaminants prior to analysis, gently crushed, homogenized, and separated into two aliquots for stable isotopic and trace metal measurements.

$\delta^{18}O$ and $\delta^{13}C$ measurements (n = 408) were carried out using one of the aforementioned aliquots (which usually contained enough material for replicate analysis) after ultrasonicating briefly in methanol and analyzed on a Kiel IV Carbonate Device coupled to a Thermo Scientific MAT 253 Isotope Ratio Mass

Spectrometer, housed at the Analytical Laboratory for Paleoclimate Studies (ALPS), University of Texas at Austin. The resulting stable isotope values are all reported in permil relative to the Vienna Pee Dee Belemnite standard notation (‰, VPDB). Two external standards, Estremoz (n = 36) and NBS-19 (n = 50) were routinely analyzed to monitor the accuracy of the measurements. The 1σ analytical precision of standard analysis during this study was ±0.03‰ for carbon and ±0.06‰ for oxygen, consistent with the long-term precision of the instrumental setup (0.06‰ for $\delta^{13}C$ and 0.08‰ for $\delta^{18}O$). Sampling uncertainty was determined to be 0.1‰ for carbon and oxygen, based on inter-sample replicate isotopic measurements (n = 100) of different sets of foraminifera from the same depth, consistent with forward modeling experiments in the northern GOM [*Thirumalai et al.*, 2013; 2014], and incorporated into our overall uncertainty analysis.

Trace element analysis (n = 350) was performed following routine foraminiferal cleaning protocols [*Barker et al.*, 2003] and measured using a Perkin-Elmer Optima 4300 dual view inductively coupled plasma-optical emission spectrophotometer [*Olesik*, 1991], also housed at the ALPS. All Mg/Ca values are reported in mmol/mol. An internal gravimetric standard (n = 90 per run; Mg/Ca = 3.2 mmol/mol) was run after every sample to monitor accuracy, precision and was used to correct raw Mg/Ca data for drift [*Schrag*, 1999]. A series of gravimetric standards and an external standard (ECRM 752-1) were also analyzed with every batch of samples to assess the accuracy and precision of the instrument, whose accuracy was confirmed by an interlaboratory calibration [*Greaves et al.*, 2008; *Hathorne et al.*, 2013]. We found no relationships between Al/Ca and Mg/Ca, nor Fe/Ca and Mg/Ca, and all samples

in this study contained less than detectable Mn/Ca. The average 1σ analytical precision was ±0.15% (0.010 mmol/mol) for samples in this study, based on repeated analysis of standards and 20% sample replicates. The sampling uncertainty, inferred from replicate measurements of different sets of *G. ruber* (W) tests from the same sample depth (n = 50), was found to be ±3% (0.10 mmol/mol). These two sources of uncertainty were incorporated into our error propagation analysis.

2.4. Sea-surface Temperature/ Seawater $\delta^{18}O$ Reconstructions and Error Propagation

The paired Mg/Ca and $\delta^{18}O$ measurements of *G. ruber* (W) were used to reconstruct sea-surface temperatures (SST) and seawater $\delta^{18}O$ ($\delta^{18}O_{sw}$) using published calibration equations in a bootstrap Monte Carlo framework [*Efron*, 1979; *Hall and Martin*, 1988; *Thirumalai et al.*, 2013; 2014]. This procedure accounts for inherent analytical error, sampling uncertainty obtained from replicates and forward modeling experiments in INFAUNAL [*Thirumalai et al.*, 2013], and age uncertainty as modeled above.

At each sampling depth, we allowed Mg/Ca and $\delta^{18}O$ values to vary between their associated combined analytical and sampling uncertainty [*Thirumalai et al.*, 2013] to produce probability distributions around the measured value (n = 5000). Each sampling depth was also associated with a probability distribution of calibrated calendar age (n = 5000). Figure 19 displays the uncertainty cloud for Mg/Ca measurements on 2010-GB2-MCA. Using these uncertainty distributions, we acquired simultaneous solutions for SST and $\delta^{18}O_{sw}$ at each depth by inverting the following relationship equations:

1. ln(Mg/Ca) = 0.084*T + 0.051*S - 2.54 ([*Tierney et al.*, 2015a])
2. T = 16.5 - 4.8($\delta^{18}O_c$ - $\delta^{18}O_{sw}$ + 0.27) (Low-light equation; [*Bemis et al.*, 1998])
3. $\delta^{18}O_{sw}$ = 0.55S – 18.98 (North Atlantic; [*LeGrande and Schmidt*, 2006])

where T is the temperature of the water mass, S is the salinity, and $\delta^{18}O_c$ is the $\delta^{18}O$ of foraminiferal carbonate. The 0.27‰ term is subtracted from the $\delta^{18}O_{sw}$ term to convert from the VPDB scale to the Vienna Standard Mean Ocean Water (VSMOW) scale. All $\delta^{18}O_{sw}$ values are reported in permil relative to this scale (‰, VSMOW).

This methodology accounts for the influence of salinity on foraminiferal Mg/Ca [*Arbuszewski et al.*, 2010; *Hertzberg and Schmidt*, 2013; *Khider et al.*, 2015] by using a newly published equation [*Tierney et al.*, 2015a] that is built using a collation of culture-based relationships [*Nürnberg et al.*, 1996; *Kısakürek et al.*, 2008; *Dueñas-Bohórquez et al.*, 2011; *Hönisch et al.*, 2013]. A potential drawback of using this methodology is the assumption of stationarity in using the salinity-$\delta^{18}O_{sw}$ relationship back in time [*Rohling and Bigg*, 1998]. However, this assumption should be valid considering the lack of abrupt changes in the late Holocene. This assumption is further validated by an isotopic modeling study that shows little-to-no salinity bias in the salinity-$\delta^{18}O_{sw}$ relationship in the GOM during the Last Glacial Maximum and Heinrich Event 1, two time periods with significant changes compared to the late Holocene [*Caley and Roche*, 2015]. Furthermore, the structure of the resultant $\delta^{18}O_{sw}$ and SST reconstruction at the Garrison Basin is unchanged even if we use the conventional

methodology of a straightforward Mg/Ca-SST relationship [*Anand et al.*, 2003], though the absolute magnitudes differ.

For independence from the assumption of normality (which is generally not true for these uncertainty distributions due to age calibration error), after inverting for SST and $\delta^{18}O_{sw}$ from our multicore-based geochemical records, we used the median, and 32-68th and 5-95th percentiles, as the corresponding value and its confidence bounds at each sample depth, whose time uncertainty was also incorporated into the propagated uncertainty envelope. We also investigated a blanket bioturbation-related uncertainty [*Trauth et al.*, 1997] of ~2 cm and found no differences in the structure of the resultant time series.

2.5. Stacking Methodology

We produced a stacked record of Mg/Ca and $\delta^{18}O$ variability from the three Garrison Basin multicores and resultant stacked records of $\delta^{18}O_{sw}$ and SST variability over the past 4,400 years, maximizing accuracy in extracting climatic signals and minimizing the errors on the reconstructions (Fig. 17). The stacked record was also produced in a bootstrap Monte Carlo framework (n = 5,000) where the median values from the overall uncertainty probability distributions of MCA, MCC, and MCB (when available) are used as the stack values. The 32-68th, and 5-95th percentiles of this distribution were used as the subsequent confidence bounds (Fig. 19). This methodology 'rewards' the stack by reducing the uncertainty envelope when all three multicore distributions are closer together, and 'punishes' the stack with larger errors when they are different (Fig. 17). This ensures that the ensuing uncertainty envelopes minimize methodological and geological uncertainties where geochemical values from the

same depths in different cores can be dissimilar, a common occurrence in foraminiferal-based replication studies of cores from nearby basins [*Oppo et al.*, 2009; *Richey et al.*, 2009; *Mohtadi et al.*, 2014; *Thirumalai et al.*, 2014]. To our knowledge, this is the first study to produce paleoceanographic records from the same basin using three multicores from the same cast. No mean offsets or corrections were applied to any of the core data to produce stacked records of SST and $\delta^{18}O_{sw}$ variability.

2.6. Comparisons with Observations

We used available measurements of $\delta^{18}O_{sw}$ close to the Garrison Basin to compare with the stacked $\delta^{18}O_{sw}$ reconstruction. These measurements were made on surface waters in the northern GOM taken from CTD-casts, analyzed on a Thermo Scientific Gasbench II coupled to a Thermo Scientific Delta V isotope ratio mass spectrometer housed at the ALPS. Since these measurements do not span a complete year, we also included $\delta^{18}O_{sw}$ data from the proximal Flower Garden Banks to produce a modern data point (orange) plotted in Figure 2e.

Where overlap was available, we compared the Garrison Basin SST stack with instrumental observations from the HadISST dataset [*Rayner et al.*, 2003]. To facilitate an apples-to-apples comparison, after extracting monthly observations from 1870-2010 from the Garrison Basin gridpoint (26.5°N,93.5°W), we divided the dataset into sets of 30 years (the average sampling resolution of the stack). Next, with n = 50 months, we employed a bootstrap picking procedure which produced a set of 5,000 distributions for the average of 50 random months selected from each 30-year set. We used n = 50 months to

simulate 50 *G. ruber* (W) specimens that might have lived during the time period [*Thirumalai et al.*, 2013]; this is a conservative estimate of the homogenization procedure of the actual 70-100 foraminifera used in the study, however the resulting medians for n=30 or n=100 were statistically indistinguishable. The median and 95% confidence bounds of these distributions are plotted in orange in Figure 2h.

2.7. Changepoint Algorithm and SST-$\delta^{18}O_{sw}$ Running Correlation

We used a Bayesian changepoint algorithm in MATLAB [*Ruggieri*, 2012] to find the posterior probability of a statistically significant changepoint in the median $\delta^{18}O_{sw}$ time series. The Little Ice Age peak (Fig. 17e) is statistically robust even if we minimize the minimum distance between adjacent change points, or the number of changepoints to be detected.

To perform a running correlation between SST and $\delta^{18}O_{sw}$, we used the uncertainty envelopes for each of the respective time series and produced a probability distribution of 5,000 running correlation values whose median and 95% confidence bounds are plotted in purple in Figure 2e. The timestep we used was 180-200 years to investigate centennial-scale variability and to minimize high-frequency structure in the running correlations.

2.8. Marine Proxy Screening and Reprocessing

To investigate regional SST variability over the last millennium, we compiled published records from the GOM: Pigmy Basin: PBBC-2 [*Richey et al.*, 2007], Fisk Basin: PE07-5I and (previously published) Garrison Basin: PE07-2, Dry Tortugas: W167-79GGC and Grand Bahama Bank: KNR166-2-118MC-A [*Lund and Curry*, 2006]. As detailed above for the multicores used in this study,

we used the ^{14}C ages on each of these cores and reprocessed them through BACON to produce calendar age distributions at each depth. Sampling uncertainty calculated using INFAUNAL [*Thirumalai et al.*, 2013; 2016] and the reported analytical uncertainty was used to produce error distributions for these datasets. With the exception of PE07-5I and PE07-2, all other records used paired Mg/Ca-$\delta^{18}O$ analyses so we could use the same methodological uncertainty procedures as above to calculate SST and its uncertainty envelope (Fig. 20a). For PE07-5I and PE07-2, we used the straightforward equation of $Mg/Ca = 0.449e^{0.09*SST}$ [*Anand et al.*, 2003] along with the low-light equation [*Bemis et al.*, 1998] in an iterative bootstrap framework (n = 5000) to calculate SST and its associated uncertainty.

To investigate past $\delta^{18}O_{sw}$ variability (Fig. 21), we chose available records of surface water $\delta^{18}O_{sw}$ spanning the last millennium. Apart from the records mentioned above, we used a paired Mg/Ca-$\delta^{18}O$ record from the Carolina Slopes (CH07-98-MC22) and processed it in the same manner as above (BACON->bootstrap) to calculate median $\delta^{18}O_{sw}$ and its uncertainty envelope.

The Dry Tortugas, Great Bahama Bank, and Carolina Slopes had companion cores from nearby sites. For Figures 3.5 and 3.6, we used the cores with higher sampling resolution for comparison. However, these companion cores were similarly reprocessed and showed similar structures to their companion cores. This is also seen in Table S2. For centennial-scale comparisons, all proxies shown in Fig. 20a and Fig. 21 (including precipitation/NADA proxies), were smoothed with a 100-year lowpass filter [*Cook and Peters*, 1981]. The NADA tree ring records were initially smoothed with a 10-year lowpass filter, which was eventually filtered again This was also

performed in a bootstrap Monte Carlo framework to produce confidence bounds on the smoothed time series.

2.9. Observation-based Correlation Map and Data Analysis

We used the gridded ORA-S4 monthly salinity dataset (1958-2013) to correlate long-term sea-surface salinity (SSS) in the northern GOM (red box in Figure 1; 23.5ºN-28.5ºN, 83.5ºW-95.5ºW) with global ocean SSS [*Balmaseda et al.*, 2012]. The dataset was annually averaged, filtered with an 8-year lowpass filter to infer multidecadal variability and remove sensitivity to interannual variability, and then detrended prior to correlation. We used 8 years so as to optimize inferring multidecadal variability and to ensure sufficient degrees of freedom for correlation analysis due to the length of the dataset. The statistical significance of the resulting correlation coefficients was assessed by a one-tailed Student's t test at the 99% confidence level. We estimated the effective sample size (N_{eff}) by dividing the number of years (N) by the mean characteristic time scale (τ), defined as the minimum lag for which the autocorrelation falls below 0.2 [*Bretherton et al.*, 1999; *Okumura et al.*, 2012; *Goff et al.*, 2015]. This methodology is especially useful where N_{eff} tends to be low. Our significance analysis was verified using a Monte Carlo-based methodology [*Ebisuzaki*, 1997] which also yielded similar results. We also performed similar correlations with GOM SSS and evaporation-minus-precipitation at every gridpoint from the ERA dataset, which yielded low correlations and spatial patterns that were not similar to the SSS correlations at every grid point. Furthermore, the correlation between Mississippi outflow alone and the northern GOM salinity was also low. Thus, we

invoke oceanic current changes as the most plausible explanation for the initial correlation analysis.

Figure 22 was generated in the same manner, correlating 8-yr-bandpassed SST from the northern GOM box with SST in every grid box from the HadISST dataset [*Rayner et al.*, 2003] and the significance calculations were performed accordingly as well.

Using the same methodology, we also correlated long-term (8-year) SSS in the northern GOM with land-based rainfall observations using the gridded GPCC dataset [*Beck et al.*, 2005] over their time of overlap (1958-2010), which is plotted in green/brown in Figure 1. The statistical significance of these correlations were also performed as described above.

2.10. Last Millennium Simulation and Data Analysis

The Max Plank Institute Earth System Model for paleo-applications (MPI-ESM-P) contains the atmosphere general circulation model ECHAM6, run at a horizontal resolution of spectral truncation T63 (1.875°) with 47 vertical levels, as well as the ocean/sea-ice model MPIOM which is run at 1.5° resolution and contains 70 vertical layers [*Jungclaus et al.*, 2013; 2014; *Moreno-Chamarro et al.*, 2015]. The transient simulation was run from 850 to 2005 following the Paleo-Modeling Intercomparison Project Phase 3 (PMIP3) protocols [*Schmidt et al.*, 2011; *Braconnot et al.*, 2012] with prescribed external forcing factors including volcanic aerosols, greenhouse gases, total solar irradiance, orbital parameters, and changes in land-cover [*Jungclaus et al.*, 2013; 2014; *Moreno-Chamarro et al.*, 2015].

For the correlation analysis in Fig. 23, we used a 50-150 year bandpass to isolate the variability associated with centennial timescales. Here, we extracted monthly precipitation and salinity as simulated by the model from 1000 CE to 2000 CE and then annually averaged and bandpass-filtered the dataset. Statistical significance was assessed in the manner as stated above.

3. Results and Discussion

The three Garrison Basin multicores display excellent replication in SST and $\delta^{18}O_{sw}$, reflected in the small uncertainty estimates for the corresponding stacked records (Fig. 17). Replication greatly minimizes dating, analytical, preservation, sampling, ecological, and calibration uncertainties, which become significant sources of interpretation bias in time periods with small signal-to-noise ratios, like the late Holocene. To validate our SST reconstruction, we simulated the hypothetical SST variability at the site, by modeling how *G. ruber* (W) tests in a sediment core would record them, by performing INFAUNAL [*Thirumalai et al.*, 2013] picking experiments on the HadISST dataset [*Rayner et al.*, 2003]. This exercise found a highly skillful match between instrumental SSTs and our reconstruction, where overlap is available (orange points and line in Fig. 17h). Additionally, available measurements of $\delta^{18}O_{sw}$ in the northern GOM compared with $\delta^{18}O_{sw}$ computed at the core-top also validate our downcore $\delta^{18}O_{sw}$ results (orange datapoint in Fig. 17g) and suggest that both stacked reconstructions are robust. Our approach provides tangible estimates of SST and SSS variability that can be used for model-data intercomparison.

The Garrison Basin stacks indicate marked centennial-scale variability in SST and $\delta^{18}O_{sw}$ (up to 1°C and 0.25‰ respectively based on the running standard deviation of ~200 year bins) throughout the late Holocene. We performed centennial running correlations (purple line in Fig. 17h) between the stacked reconstructions to track the co-variability of SST and $\delta^{18}O_{sw}$. This yielded two distinct periods having high positive median correlations ($r > 0.7$, $p<0.001$; purple shaded boxes in Fig. 17h): [1] ~650-1100 C. E., characterized by rapid and highly variable centennial-scale shifts in SST and $\delta^{18}O_{sw}$, and [2] ~1450-1650 C. E., during the canonically defined LIA [*Masson-Delmotte et al.*, 2013], which shows a systematic century-scale cooling and freshening into the time period followed by subsequent warming and salinification. The LIA is also identified as a period containing a statistically significant changepoint (bottom grey histogram in Fig. 17g) in the overall $\delta^{18}O_{sw}$ time series using a Bayesian methodology [*Ruggieri*, 2012]. Thus, the LIA emerges as a statistically unique time period when the Garrison Basin was cooler by 1 ± 0.2°C and fresher by 0.23 ± 0.06‰ (equivalent to a 0.5 ± 0.2 PSU reduction in salinity) compared to the modern era (post-1850 C. E.).

We compiled published paleoceanographic records developed using *G. ruber* (W) in the GOM [*Lund and Curry*, 2006; *Richey et al.*, 2007; 2009] and compared them with the new Garrison Basin record to investigate regional centennial-scale SST variability over the last millennium (Fig. 20). To do so, we used our simultaneous Monte Carlo procedure to model uncertainty in the previous studies incorporating their age uncertainty, analytical and calibration errors, and number of foraminifera used for each record. The northern GOM records (Garrison Basin – this study and a previous one [*Richey et al.*, 2009],

Fisk Basin [*Richey et al.*, 2009], and Pigmy Basin [*Richey et al.*, 2007]) all display higher SST variability (average $1\sigma_{\text{last millennium}}$=0.68±0.06°C) than records from the Florida Straits (average $1\sigma_{\text{last millennium}}$=0.43±0.18°C; Grand Bahama Bank & Dry Tortugas [*Lund and Curry*, 2006]). However, more variable northern GOM SST versus those in the Florida Straits is in line with expectations (Fig. 20b) from multidecadal SST variability over the instrumental era [*Rayner et al.*, 2003] and suggest that the GOM, as a whole, was between 0.5-1.1 ± 0.7°C (95% confidence) cooler during the LIA compared to modern temperatures [*Lund and Curry*, 2006; *Richey et al.*, 2009]. Though our revised estimates of the cooler LIA SSTs is less than previous studies [*Richey et al.*, 2009] due to updated uncertainty constraints, *G. ruber* (W)-based SST reconstructions across different cores, different basins and different laboratories indicate a ~1°C magnitude cooler GOM.

Following our regional SST synthesis, we compiled available paired Mg/Ca-$\delta^{18}O_c$ records of *G. ruber* (W) proximal to the Garrison Basin that resolved the LIA and processed the data simultaneously to compute $\delta^{18}O_{sw}$ with all aforementioned uncertainty considerations (Fig. 21). While the SST stack indicates cooler LIA conditions in the Garrison Basin over the last millennium, the $\delta^{18}O_{sw}$ stack, a proxy for SSS, shows a reduction in salinity that begins around ~1350 C. E., is at its freshest at ~1450 C. E., and displays an increasing trend into the current era (Fig. 21a). This "fresher" LIA is observed in $\delta^{18}O_{sw}$-SSS records from the Dry Tortugas, Great Bahama Bank [*Lund and Curry*, 2006], and the Carolina slopes [*Saenger et al.*, 2011], all downstream of the GOM (Blue circles with white boundaries in Fig. 16) considering the path [*Srokosz and Bryden*, 2015] of the Gulf Stream (Fig. 21a-d).

We analyzed long-term (~multidecadal) observations in instrumental datasets to place our reconstructions into a global climatic context. The HadISST dataset [*Rayner et al.*, 2003] documents 0.4-0.7°C of multidecadal SST variability in the northern GOM over the last century (Fig. 20b). On multidecadal timescales, SSTs in the northern GOM correlate highly with SST in the Loop Current region (Fig. 22). In particular, long-term SST variability here is partly impacted by the Loop Current through its eddy shedding processes [*Liu et al.*, 2012b]: if Loop Current strength is anomalously low (high), then northern GOM SSTs are anomalously reduced (increased) due to decreased (increased) eddy penetration [*Nürnberg et al.*, 2008; *Liu et al.*, 2012b; *Gopalakrishnan et al.*, 2013]. Furthermore, the Loop Current, sitting upstream of where the Gulf Stream originates, correlates highly with SST associated with downstream currents, indicative of altered ocean currents rather than local wind forcing (Fig. 22).

Our reconstructions, and the synthesis and uncertainty analysis of other regional SST records support a basin-wide, cool GOM during the LIA [*Richey et al.*, 2009]. Cooler SSTs during the LIA are consistent with reduced Loop Current strength and support the inference of reduced Gulf Stream volume transport [*Lund et al.*, 2006]. For example, a recent high-resolution ocean modeling study that investigated the influence of reduced AMOC and Loop Current strength on GOM SSTs under a future warming scenario [*Liu et al.*, 2012b]: weakened Loop Current transport has a cooling effect on GOM SSTs which is particularly pronounced in the northern GOM, where the Garrison Basin is located. Although the LIA and current anthropogenic warming differ in their dynamical origins [*Landrum et al.*, 2013], the Garrison Basin SST stack and other GOM proxy records serve to extend our perspective on the effects of Gulf Stream and

potentially AMOC changes on regional variability allowing insights into long-term climatic processes [*Landrum et al.*, 2013; *McGregor et al.*, 2015].

To track the spatial covariance of long-term Garrison Basin SSS variations along these sites, we regressed reanalysis SSS data [*Balmaseda et al.*, 2012] in the northern GOM (red dashed box in Fig. 16) with SSS across the Atlantic Ocean (Fig. 16). The correlation analysis yields a dipolar structure with high, significant correlations ($|r|>0.7$; $p<0.01$) in the Atlantic Ocean with positive correlations (blue patch) in the subtropical north Atlantic, the GOM, and the western Caribbean Sea, and negative correlations (red patch) along the northern South American coastline and tropical Atlantic Ocean. These correlations cannot be explained by changes in local freshwater fluxes and are suggestive of altered oceanic currents. The reprocessed $\delta^{18}O_{sw}$-SSS reconstructions appear to match this correlation map remarkably well (Fig. 16). The $\delta^{18}O_{sw}$ changes over the LIA in these records are also coeval with changes in seawater density reconstructions from the Florida Straits [*Lund et al.*, 2006], and Greenland ice core $\delta^{18}O$ [*Vinther et al.*, 2006] (purple stars in Fig. 16) where both records indicate a reduction in poleward heat transport during the LIA (Fig. 21e-f).

Records of past SSS variability in addition to the aforementioned GOM and Carolina Banks sediment cores (Fig. 21) also match the correlation map. For example, SSS reconstructed from corals in Puerto Rico [*Kilbourne et al.*, 2008] and Bermuda [*Goodkin et al.*, 2008] that extend into the 1700s, and paired Mg/Ca-$\delta^{18}O_c$ analysis on planktic foraminifera from North Atlantic sediment cores [*Moffa-Sanchez et al.*, 2014a; 2014b], also show lower $\delta^{18}O_{sw}$ during the LIA, indicating reduced salinities (blue squares with white boundaries in Fig. 16). Unfortunately, the lack of last millennium $\delta^{18}O_{sw}$ records from the tropical

Atlantic preclude comparison with the correlation map. However, the proxy-observation match of anomalously fresh SSS in the northern Atlantic Ocean bolsters our confidence in implicating a weakened Gulf Stream as an important dynamical process during the LIA.

We examine potential linkages between Western Hemisphere hydroclimate and Gulf Stream changes evinced from SSS variability by correlating gridded, continental, precipitation data based on rain gauges [*Beck et al.*, 2005] and northern GOM SSS on decadal timescales (Fig. 16). Most notably, we find an anticorrelation between west African and southern North American rainfall when correlated with northern GOM SSS ($|r|>0.6$, $p<0.01$). In comparing available reconstructions of precipitation during the LIA with our correlation map, we find remarkable agreement with the proxy record: tree-ring-based PDSI reconstructions in southern North America [*Cook et al.*, 2010], and stalagmites from southern Mexico [*Lachniet et al.*, 2012] and Peru [*Reuter et al.*, 2009] capture a wetter LIA (Fig. 21g-i) compared to modern times whereas a lake record from southern Ghana [*Shanahan et al.*, 2009], titanium percent in Cariaco Basin sediments [*Haug et al.*, 2001], and reconstructed PDSI in the southeast U. S. indicate dry LIA conditions (Fig. 21j-l). Additional proxy records appear to corroborate this observation as well (brown and green squares in Fig. 16; Table 5). These mean state changes all appear to be coeval with an anomalously fresher northern Atlantic Ocean, indicative of weakened Gulf Stream strength. Taken together, these findings indicate a coordinated hydroclimate response in the Western Hemisphere that is tightly coupled with Gulf Stream and potentially AMOC variability.

Though the length of the instrumental record limits us from directly analyzing centennial-scale correlations, there is evidence to implicate similar atmosphere-ocean processes on multidecadal and multicentennial timescales [*Mignot and Frankignoul*, 2004; *Krebs and Timmermann*, 2007; *Park and Latif*, 2008]. We interpret past periods in the Garrison Basin reconstructions when both SST and $\delta^{18}O_{sw}$ variability were positively correlated (salty/warm or fresh/cool) as periods during which Loop Current strength and its related SST variability, advection-related salinity, and freshwater input interacted constructively to produce systematic changes in the northern GOM surface water $\delta^{18}O_{sw}$. This allows us to contextualize the Garrison Basin records and link them to Gulf Stream variability and Western Hemisphere hydroclimate (Fig. 16).

Coupled general circulation model (GCM) simulations show that weakened AMOC and associated reduced heat and salt transport [*Mignot and Frankignoul*, 2004] can arise from sustained sea-ice-ocean feedbacks [*Landrum et al.*, 2013] triggered either by external forcing [*Krebs and Timmermann*, 2007; *Miller et al.*, 2012] or through internal atmosphere-ocean interactions [*Park and Latif*, 2008; *Mahajan et al.*, 2011], both of which can result in a southward displacement of the Atlantic intertropical convergence zone (ITCZ) [*Krebs and Timmermann*, 2007; *Chang et al.*, 2008]. Despite this southward shift, positive SSS anomalies can occur in the tropical Atlantic (and negative anomalies in the northern Atlantic) due to reduced freshwater input resulting from decreased rainfall in the Amazon and west African regions [*Mignot and Frankignoul*, 2004]. This state of weakened AMOC, with cool and fresh north Atlantic anomalies, can induce increased rainfall over the southwest US via atmospheric teleconnections associated with the North Atlantic subtropical high overlying the

gyre [*Enfield et al.*, 2001; *Vellinga and Wood*, 2002; *Kushnir et al.*, 2010]. Eventually, the tropical positive salinity anomaly in the southern Atlantic propagates northward, thereby strengthening meridional oceanic transport [*Krebs and Timmermann*, 2007] and providing the delayed negative feedback. This provides a potential mechanism that might reconcile our late Holocene paleoclimatic and observational analysis with GCM simulations.

We investigated this centennial-scale link between salinity and precipitation variability in a transient simulation of the last millennium using the fully-coupled MPI-ESM-P model with prescribed external forcing [*Jungclaus et al.*, 2013; *Moreno-Chamarro et al.*, 2016]. We performed the same correlation analysis between GOM SSS in the model and 1) global oceanic SSS and 2) continental precipitation simulated by the model, this time on centennial time-scales (Fig. 23). The resultant correlation map contained features that strongly resembled those from the multidecadal correlation analysis performed using instrumental datasets (Fig. 16). For example, both analyses revealed a dipolar structure in Atlantic Ocean SSS that is consistent with the LIA proxies, and thereby supports our hypothesis linking meridional salt transport and tropical rainfall [*Krebs and Timmermann*, 2007]. Both analyses also displayed similarities in continental precipitation patterns over western Africa, northern South America, and the southwestern United States, which are also consistent with the LIA hydroclimate proxies (Fig. 23). However, differences between the correlation patterns also exist. Most notably, rainfall correlations over Canada, Europe, and western South America, and salinity patterns offshore Europe are in disagreement between the model output and the reanalysis data. Future work is required to investigate whether these occur due to biases in the model,

insufficient observations, or whether these might indicate significantly different responses on multidecadal versus centennial timescales. Regardless of these discrepancies, the broad agreement between the analyses supports similar ocean-atmosphere processes on multidecadal-to-centennial timescales [*Mignot and Frankignoul*, 2004; *Krebs and Timmermann*, 2007; *Park and Latif*, 2008] and provides additional evidence of a robust century-scale link between circulation changes in the Atlantic basin and precipitation in the adjacent continents. Finally, in concert with the proxy-synthesis and observational analysis, the model output also suggests a slowdown in the Gulf Stream and associated precipitation response as a feature of LIA climate.

The transient simulation indicates that a weaker gyre, increased sea-ice cover, and reduced interhemispheric heat transport causes the ITCZ to shift southward and produces anomalous rainfall over the Americas [*Vellinga and Wood*, 2002; *Kushnir et al.*, 2010; *Schneider et al.*, 2014]. During the onset of the LIA in the transient simulation, fresh anomalies are observed in the Arctic that serve to abruptly weaken the subpolar gyre [*Moreno-Chamarro et al.*, 2016]. Comparisons with control simulations of the same model indicate that though volcanic forcing can aid in inducing such conditions [*Miller et al.*, 2012], internal variability of the climate system by itself can produce a weakened subpolar gyre [*Moreno-Chamarro et al.*, 2016]. This weakening and resultant reduction in meridional oceanic transport induces fresh and cool anomalies in the northern Atlantic Ocean, consistent with our proxy synthesis of the LIA. Interestingly, the model indicates that such anomalous gyre strength and reduced meridional heat transport in the surface ocean need not be coupled with changes in AMOC-related deepwater formation [*Moreno-Chamarro et al.*, 2016]. More quantitative

and highly resolved proxies of North Atlantic deepwater formation are required to refute or confirm whether this was the case during the LIA. However, regardless of the specific physical mechanism concerning the onset of the LIA [*Miller et al.*, 2012; *Landrum et al.*, 2013; *McGregor et al.*, 2015; *Moreno-Chamarro et al.*, 2016] and whether AMOC changes were linked with circulation changes in the surface ocean, we suspect that the reported oscillatory feedback involving the Gulf Stream [*Lund et al.*, 2006; *Wanamaker et al.*, 2012] and Western Hemisphere hydroclimate occurred during the last millennium and perhaps, over the late Holocene.

4. Conclusions

The new, triplicated Garrison Basin paleoclimate records serve to extend the historical perspective of GOM sea-surface conditions over the last 4,400 years and provide important constraints for natural climate variability in the region. Robust uncertainty analysis of these reconstructions provides confidence in documenting substantial centennial-scale variability in SST and $\delta^{18}O_{sw}$ whose magnitude model simulations should be tested against. Our proxy synthesis not only reaffirms the role of a slowdown in the Gulf Stream during the LIA but also demonstrates a coordinated hydroclimate linkage across the Western Hemisphere offering new insights into late Holocene climate change that may help us understand what could be possible for the future.

5. Acknowledgements

Thanks are due to Johann Jungclaus for aiding interpretation in the last millennium simulation. We thank Thomas Guilderson for analyzing three AMS Radiocarbon dates which benefitted this study. We acknowledge Casey Saenger and David Lund for providing access to their published datasets, and thank all the authors who uploaded their records to the NCDC/NOAA portal. This manuscript greatly benefitted from discussions with Timothy Shanahan, Thomas Laepple, Kevin Anchukaitis, Pedro DiNezio, Jessica Tierney, Deborah Khider, Gianluca Marino, and finally, last but not least, Team Paleo at UT Austin. KT thanks the UTIG Ewing-Worzel Fellowship, the UTIG Gale White Fellowship, the JSG Lagoe Micropaleontology Fund, and the Consortium for Ocean Leadership for support. This work was supported by Grant #OCE-0902921 to TMQ from the National Science Foundation.

Location	Proxy Type	Expectation during LIA*	Proxy Record during LIA	Reference
Salinity Proxies				
Garrison Basin, GOM	*G. ruber* (W) $\delta^{18}O_{sw}$	Fresh	Fresh	This Study
Pigmy Basin, GOM	*G. ruber* (W) $\delta^{18}O_{sw}$	Fresh	Fresh	Richey et al. 2007
Dry Tortugas	*G. ruber* (W) $\delta^{18}O_{sw}$	Fresh	Fresh	Lund and Curry, 2006
Great Bahama Bank	*G. ruber* (W) $\delta^{18}O_{sw}$	Fresh	Fresh	Lund and Curry, 2006
Carolina Slopes	*G. ruber* (W) $\delta^{18}O_{sw}$	Fresh	Fresh	Saenger et al. 2011
Bermuda	*D. labyrinthiformis* $\delta^{18}O_{sw}$	Fresh	Fresh	Goodkin et al. 2008
Puerto Rico	*M. faveolata* $\delta^{18}O_{sw}$	Fresh	Fresh	Kilbourne et al. 2010
Labrador Sea	*T. quinqueloba* $\delta^{18}O_{sw}$	Fresh	Fresh	Moffa-Sanchez et al. 2014
Precipitation Proxies				
Ghana	Authigenic Carbonate $\delta^{18}O$	Dry	Dry	Shanahan et al. 2009
Cariaco Basin	Titanium Percent	Dry	Dry	Haug et al. 2001
Peruvian Andes	Authigenic Carbonate $\delta^{18}O$	Wet	Wet	Bird et al. 2011
Quelcayya Ice Cap	Ice Core $\delta^{18}O$	Wet	Wet	Thompson et al. 1986
Northern Peru	Stalagmite $\delta^{18}O$	Wet	Wet	Reuter et al. 2011
Northwestern Venezuela	*Cyperaceae* Pollen, Magnetic Susceptibility	Wet	Wet	Polissar et al. 2006

Note: Table 5 is o

Table 5. continued next page.

Central Mexico	Stalagmite $\delta^{18}O$	Wet	Wet	Lachniet et al. 2012
Central Mexico	Authigenic Carbonate $\delta^{18}O$	Wet	Wet	Bhattacharya et al. 2015
Yucatan	Stalagmite $\delta^{18}O$	Wet	Wet	Medina-Elizade et al. 2012
Southwest US	Tree-rings	Wet	Wet	Cook et al. 2007
New Mexico	Stalagmite Width	Wet	Wet	Polyak and Asmerom, 2001
Southeast US	Tree-rings	Dry	Dry	Cook et al. 2007

Table 5. List of proxies utilized in Figure 1. LIA-mean calculated based on mean state during LIA (1450-1850 AD) relative to the modern era. Expectation during LIA is based on Figure 16.

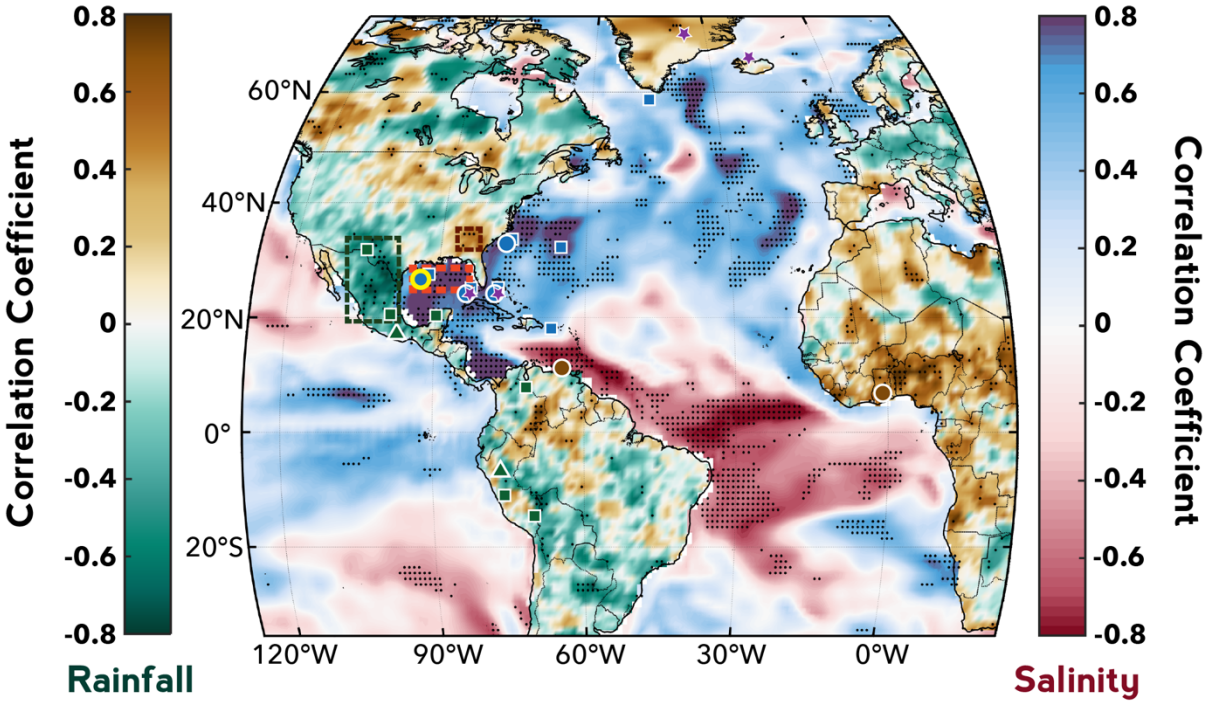

Figure 16. Correlation map between northern Gulf of Mexico SSS (dashed red box) and 1) global oceanic SSS (ORA-S4 dataset; red-blue scale) and 2) continental precipitation (GPCC dataset; green-brown) with locations of proxy records used in the study. Proxy locations are marked with circles (sedimentary records), triangles (speleothems), dashed boxes (tree-ring compilations), stars (circulation proxies), and squares (additional proxies; see Table 5) with color fill indicating sign (fresh – blue; dry/wet – brown/green; purple – weakened poleward transport) during the LIA. Correlations were performed with 8 year lowpass filters to reduce sensitivity to interannual variability, where black stippling indicates significance at the 95% level.

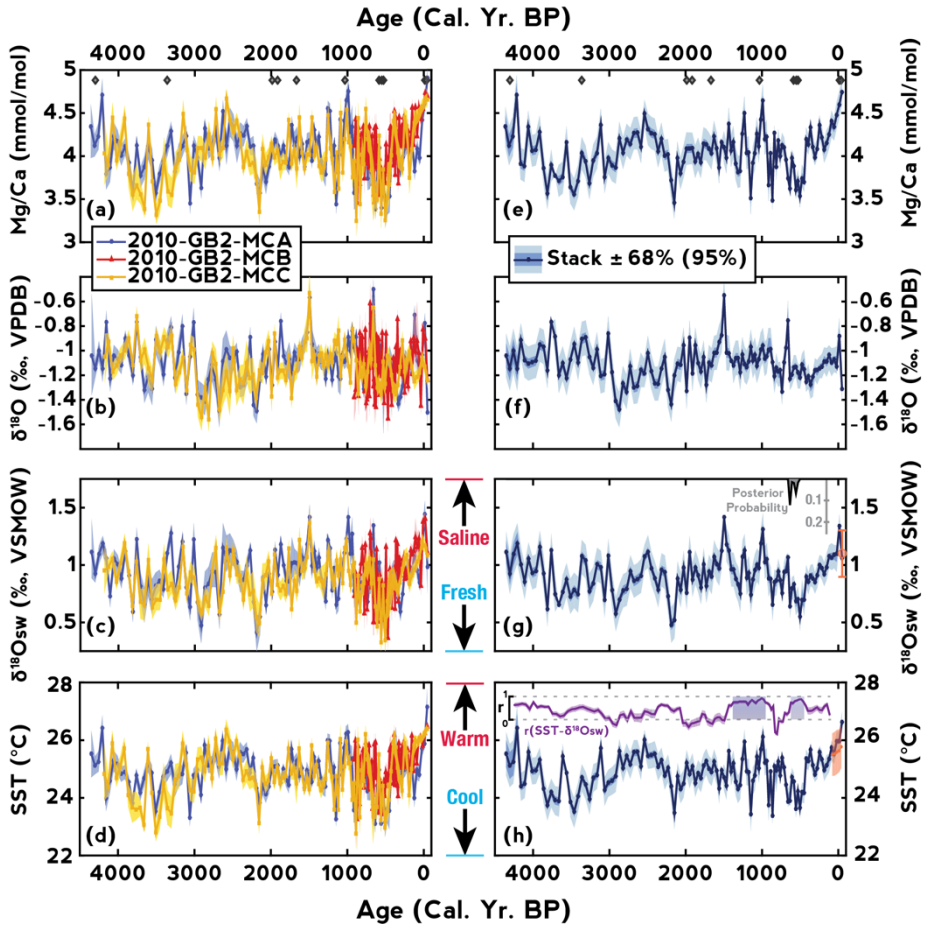

Figure 17. Garrison Basin multicore reconstructions (left) and corresponding stacked records (right). Individual core Mg/Ca (mmol/mol) and $\delta^{18}O_c$ data (‰, VPDB), and $\delta^{18}O_{sw}$ (‰, VSMOW) and SST (°C) reconstructions (blue – MCA, red, MCB, yellow – MCC) plotted with median and 68% uncertainty envelope incorporating age, analytical, calibration, and sampling errors (left) along with corresponding median stacked records with 68% and 95% uncertainty envelopes (right). Diamonds in (a) and (e) indicate stratigraphic points sampled for radiocarbon. Grey histogram in (g) is the probability distribution for a changepoint in the $\delta^{18}O_{sw}$ time series. Orange circle in (g) is the mean of available $\delta^{18}O_{sw}$ measurements in the GOM and orange line and uncertainty envelope in (h) is instrumental monthly mean SST data processed with foraminiferal sampling procedures (supplementary materials). Purple line in (g) is the 100-year running correlation between SST and $\delta^{18}O_{sw}$ with corresponding uncertainty with shaded boxes indicating correlations with $r>0.7$ ($p<0.001$).

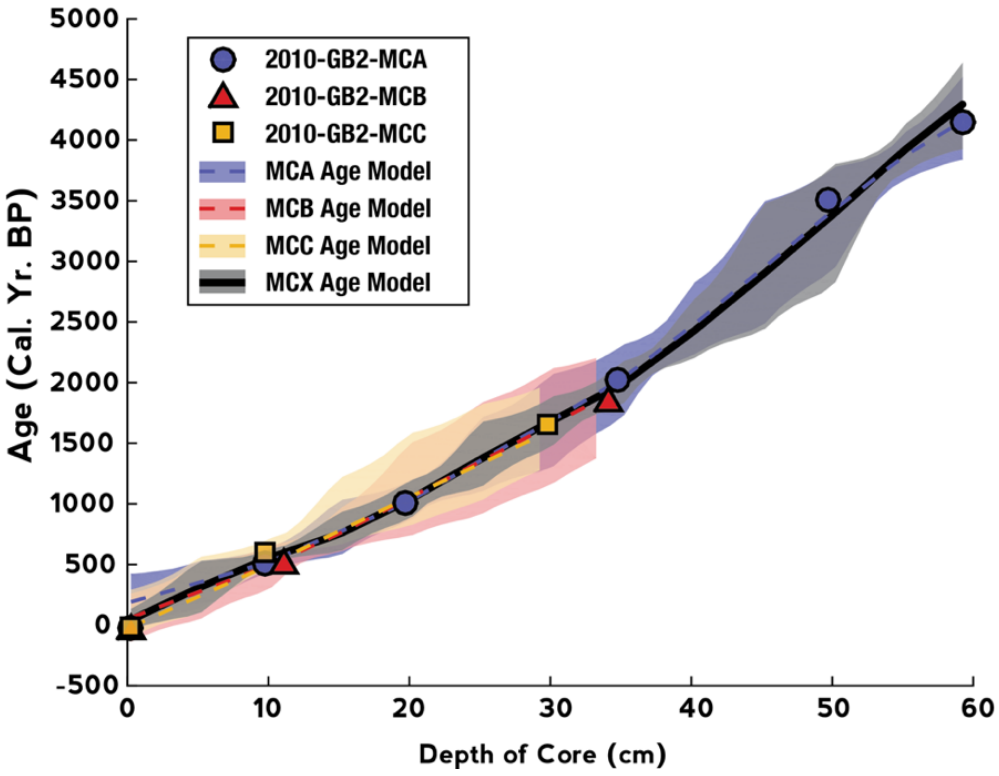

Figure 18. Bayesian posteriors of calibrated ages versus depth for MCA (purple), MCB (red), MCC (yellow), and the overall age model (MCX; black) using BACON [*Blaauw and Christen*, 2011]. The full uncertainty envelopes have been plotted.

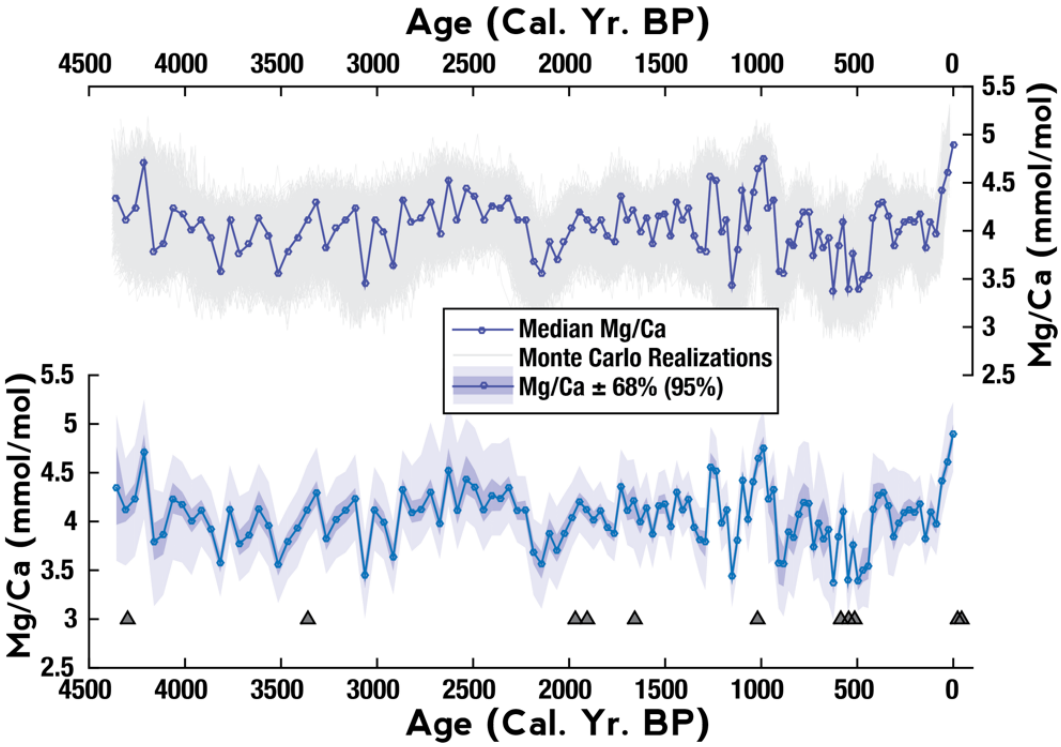

Figure 19. A demonstration of our uncertainty modeling algorithm where 5000 Mg/Ca time series from MCA are plotted using a bootstrap Monte Carlo framework. We plot the median value and associated 68% and 95% confidence bounds in the second panel. Dates are plotted in grey triangles below.

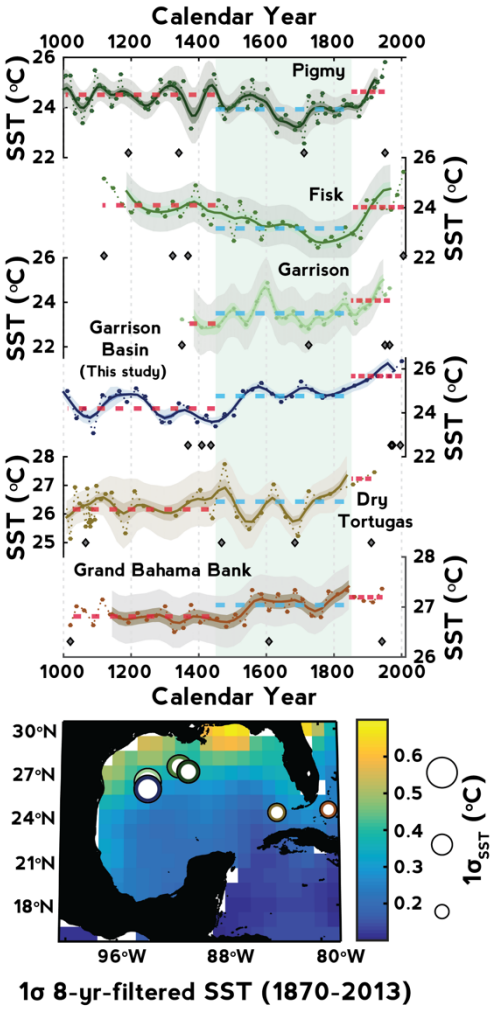

Figure 20. (a). Regional comparison of SST records from the Gulf of Mexico over the last millennium. Reconstructed SST data (circles connected by dotted lines) and 100-year filtered data (thick lines) with 68%, 95% uncertainty envelopes are plotted for each record. Previously published records are all reprocessed using the same calibration and uncertainty calculations as for the Garrison Basin records. Light green box highlights the Little Ice Age (1450-1850 C.E.) and blue and red dashed lines indicate the mean SST during the respective intervals. 3 (b). Proxy locations in the Gulf of Mexico with instrumental multidecadal SST variability. Standard deviations of 10-year filtered SST from the monthly HadISST dataset with proxy records overlain as white circles with border colors corresponding to above time series, scaled to indicate 1σ variability over the last millennium. Note proxy SST variability (northern GOM vs. Florida Straits) in line with instrumental SST variability.

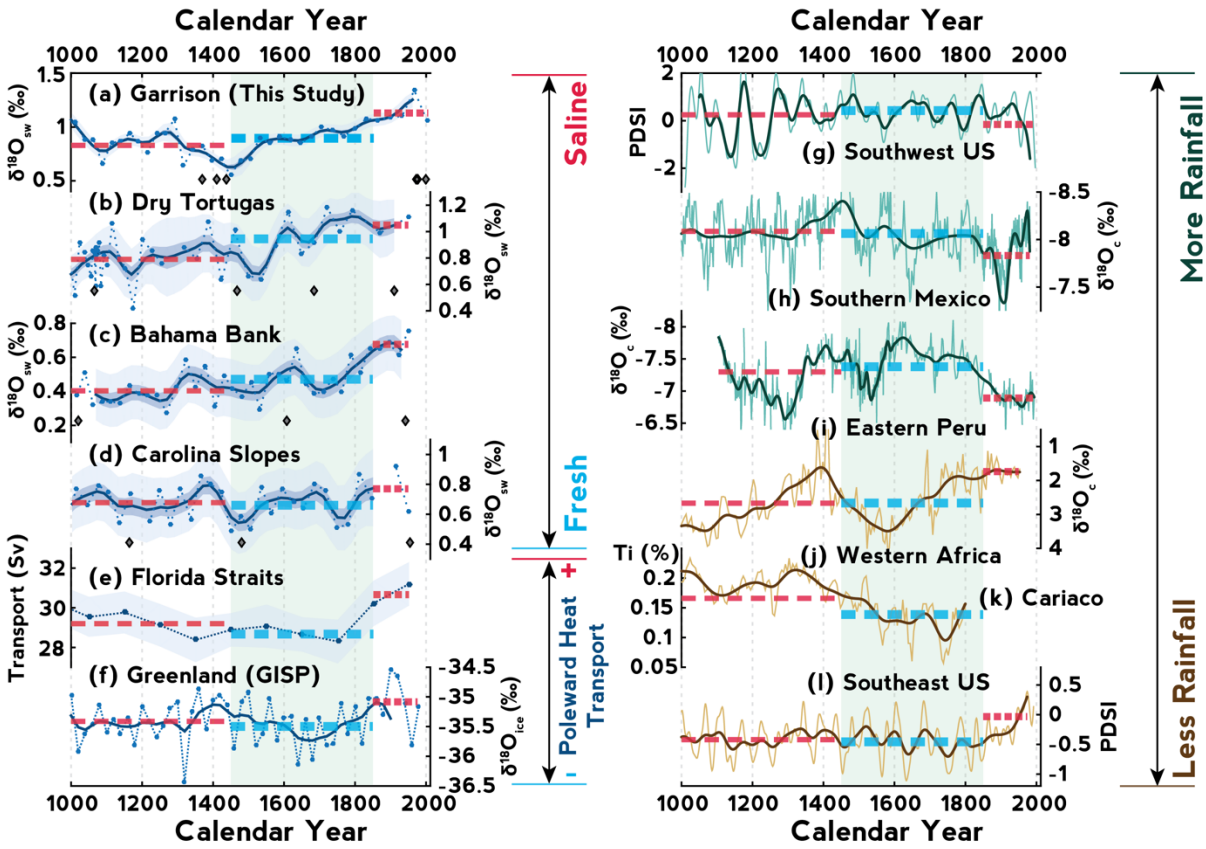

Figure 21. Comparison of proxies of SSS, precipitation, and poleward heat transport over the last millennium. Reconstructed $\delta^{18}O_{sw}$ data (circles connected by dotted lines) and 100-year filtered data (thick lines) with 68%, 95% uncertainty envelopes are plotted for the $\delta^{18}O_{sw}$ proxies (a-d). 100-year filtered data (thick lines) is plotted for the other records (f-l). Light green box in both panels highlights the Little Ice Age (1450-1850 C.E.) and blue and red dashed lines indicate the mean of the respective intervals. Previously published records are all reprocessed using the same calibration and uncertainty calculations as for the Garrison Basin records. All proxy locations are displayed as circles (sedimentary), triangles (speleothems), dashed boxes (tree-rings) or stars (poleward heat transport) in Figure 16.

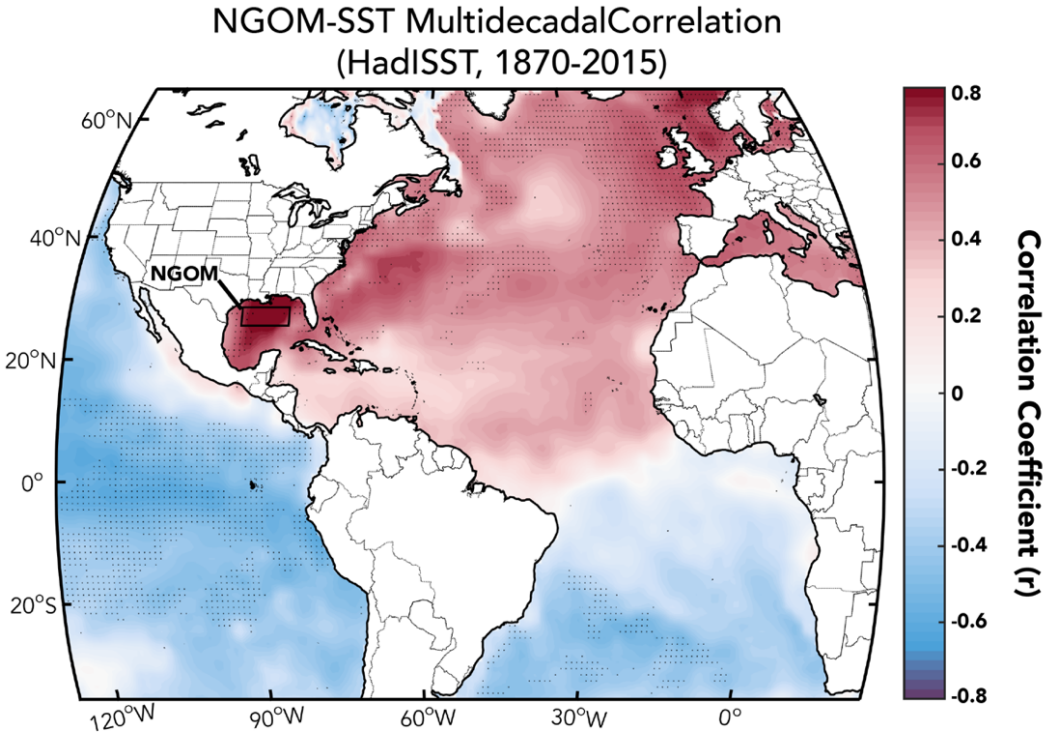

Figure 22. Correlation map between northern Gulf of Mexico SSTs (black box) and global oceanic SST using the gridded HadISST monthly dataset. The data were filtered using an 8-year Gaussian filter and detrended prior to correlation to reduce sensitivity to interannual variability. Stippling indicates significance at the 95% level.

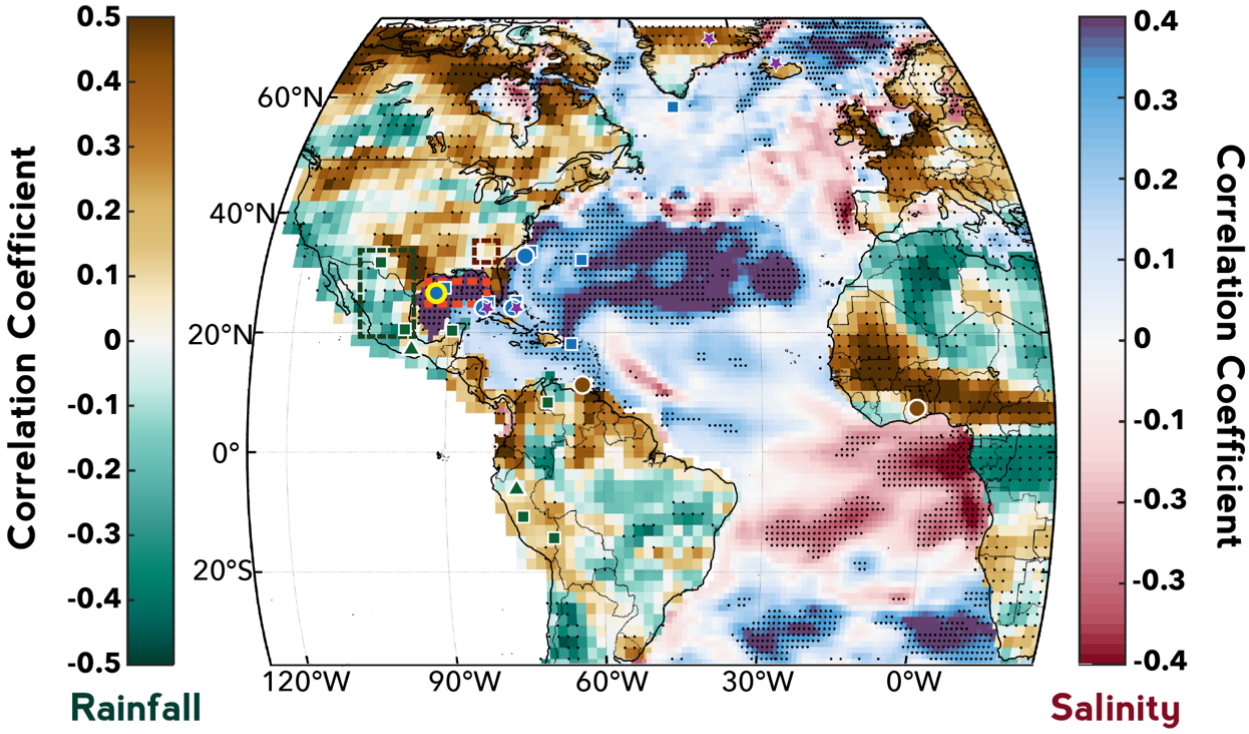

Figure 23. Model-based correlation map between northern Gulf of Mexico SSS (dashed red box) and 1) global oceanic SSS and 2) continental precipitation with locations of proxy records used in the study. Proxy locations are marked as in Figure 1. Correlations were performed with 50-150 year bandpass filters to isolate centennial scale variability, where black stippling indicates significance at the 95% level.

Conclusions

The central aim of this dissertation was to reconstruct and investigate natural climate variability of the Gulf of Mexico (GOM) surface-ocean on multidecadal and centennial timescales. I have used marine sediments in three multicores from the Garrison Basin, northern GOM, to reconstruct sea-surface temperature (SST) and salinity (SSS) variability over the late Holocene. Using the stable oxygen isotopic composition ($\delta^{18}O$) and magnesium-to-calcium ratios (Mg/Ca) of *Globigerinoides ruber* (White variety), I have produced a continuous, high-resolution record of SST and SSS variability in the GOM spanning the last 4,400 years.

Chapter 1 examined the fidelity of *G. ruber* (W) and its various morphotypes in recording mean-annual SST and SSS changes using sediment trap, core-top, and downcore samples. Using abundance data, geochemical measurements, and through statistical data-model comparisons I have shown that:

1. *G. ruber* (W) calcifies in the upper mixed-layer of the ocean and lives throughout the year in the GOM.
2. *G. ruber* (W) geochemistry is insensitive to the effect of morphotypical variability and it is dominantly controlled by climate variability.

The observations and modeling results in Chapter 1 unequivocally indicate that *G. ruber* (W)-based Holocene records, regardless of morphotype, reflect annual surface water conditions in the GOM.

In Chapter 2, I constructed a new algorithm that characterizes the overall uncertainty in temperature and salinity reconstructions generated from paired Mg/Ca-$\delta^{18}O$ data in foraminifera. The algorithm, entitled Paleo-Seawater Uncertainty Solver (PSU Solver), incorporates multiple sources of error in a bootstrap Monte Carlo framework to produce median estimates of temperature and salinity along with corresponding uncertainty constraints as output. PSU Solver has the capability to accept user-specified calibration equations and sea-level curves, and can be applied to paleoceanographic records of any resolution. By applying PSU Solver to several published datasets, I demonstrate how the underlying paleoclimate reconstructions can be altered by incorporating the influence of salinity on Mg/Ca variability or by using different sea-level curves to correct for ice-volume effects on $\delta^{18}O$ variability. Using the ecological findings inferred from Chapter 1, I apply the methodology behind the PSU Solver algorithm to assess the robustness of the Garrison Basin SST and SSS reconstructions. High confidence is placed in the accuracy of these reconstructions and their uncertainties based on core-top agreement with instrumental measurements.

I focus on the northern GOM SST and SSS reconstructions over the past 4,400 years in Chapter 3. The three Garrison Basin multicores display excellent replication on centennial timescales. The resultant stacked records generated from these records indicate marked centennial-scale variability in SST and SSS (up to 1°C and 0.3 PSU) with gradual (~600-800 yrs) and abrupt (~100-200 yrs) swings throughout the late Holocene. To place these new paleodata in context of global processes, I have analyzed observations, reanalysis datasets, and model simulations to investigate the multidecadal-to-centennial-scale controls

on GOM SST and SSS. These exercises not only confirm the integral link between the GOM and Atlantic Ocean circulation via SST and SSS, but also establish a linkage between Western Hemisphere precipitation and Atlantic Ocean circulation. Using a transient simulation of the last millennium conducted with a fully-coupled general circulation model, I find that this centennial-scale linkage appears to be a robust feature of model output as well. Multiproxy synthesis including oceanic and terrestrial proxies, including the new Garrison Basin records, provide further support for such an ocean-atmosphere linkage over the last millennium. I hypothesize that such a hydroclimate phenomena occurred during the Little Ice Age (1450-1850 CE) where weakened Atlantic Ocean circulation associated with reduced Gulf Stream transport caused anomalous droughts and pluvials across the Western Hemisphere. Thus, the newly generated records of SST and SSS variability from the northern GOM offer a fresh perspective into late Holocene climate change that may help us understand what could be possible for the future.

In summary, this dissertation has produced a continuous, high-resolution record of SST and SSS variability in the northern GOM over the late Holocene and has advanced the foundation for utilizing *G. ruber* (W) as a proxy in the GOM. Using sediment trap core-top, and downcore samples we have explored the utility of *G. ruber* (W) morphotypes in reconstructing SST and SSS signals. I have characterized uncertainty in these reconstructions by developing a generalized algorithm based on a bootstrap Monte Carlo methodology. Finally, I posit a hypothesis involving the linkage between Atlantic Ocean circulation and Western Hemisphere precipitation changes on centennial timescales based on the Garrison Basin reconstructions. Future work may focus on testing this

hypothesis by generating additional, high-resolution paleoceanographic records during the late Holocene and by analyzing additional transient model simulations. This will contribute significantly towards characterizing natural climate variability on centennial timescales.

References

Ahmed, M. et al. (2013), Continental-scale temperature variability during the past two millennia, *Nature Geosci.*, *6*(5), 339–346, doi:10.1038/ngeo1797.

Anand, P., D. Kroon, A. D. Singh, R. S. Ganeshram, G. M. Ganssen, and H. Elderfield (2008), Coupled sea surface temperature-seawater $\delta^{18}O$ reconstructions in the Arabian Sea at the millennial scale for the last 35 ka, *Paleoceanography*, *23*(4), PA4207, doi:10.1029/2007PA001564.

Anand, P., H. Elderfield, and M. H. Conte (2003), Calibration of Mg/Ca thermometry in planktonic foraminifera from a sediment trap time series, *Paleoceanography*, *18*(2), 1050, doi:10.1029/2002PA000846.

Anchukaitis, K. J., and J. E. Tierney (2012), Identifying coherent spatiotemporal modes in time-uncertain proxy paleoclimate records, *Clim. Dyn.*, *41*(5-6), 1291–1306, doi:10.1007/s00382-012-1483-0.

Arbuszewski, J. A., P. B. deMenocal, A. Kaplan, and E. C. Farmer (2010), On the fidelity of shell-derived $\delta^{18}O_{seawater}$ estimates, *Earth Planet. Sci Lett.*, 1–12, doi:10.1016/j.epsl.2010.10.035.

Arbuszewski, J. A., P. B. deMenocal, C. Cléroux, L. Bradtmiller, and A. C. Mix (2013), Meridional shifts of the Atlantic intertropical convergence zone since the Last Glacial Maximum, *Nature Geosci.*, *6*(11), 1–4, doi:10.1038/ngeo1961.

Balmaseda, M. A., K. Mogensen, and A. T. Weaver (2012), Evaluation of the ECMWF ocean reanalysis system ORAS4, *Quat. J. Roy. Meteorol. Soc.*, *139*(674), 1132–1161, doi:10.1002/qj.2063.

Barker, S., M. Greaves, and H. Elderfield (2003), A study of cleaning procedures used for foraminiferal Mg/Ca paleothermometry, *Geochem. Geophys. Geosyst.*, *4*(9), 8407, doi:10.1029/2003GC000559.

Beck, C., J. Grieser, and B. Rudolf (2005), A new monthly precipitation climatology for the global land areas for the period 1951 to 2000, *Geophys. Res. Abst.*, *7*(07154).

Bemis, B. E., H. J. Spero, J. Bijma, and D. W. Lea (1998), Reevaluation of the oxygen isotopic composition of planktonic foraminifera: Experimental results

and revised paleotemperature equations, *Paleoceanography*, *13*(2), 150–160, doi:10.1029/98pa00070.

Biasutti, M., A. H. Sobel, S. J. Camargo, and T. T. Creyts (2011), Projected changes in the physical climate of the Gulf Coast and Caribbean, *Climatic Change*, *112*(3-4), 819–845, doi:10.1007/s10584-011-0254-y.

Bigg, G. R., and E. J. Rohling (2000), An oxygen isotope data set for marine waters, *J. Geophys. Res. Oceans*, *105*(C4), 8527–8535, doi:10.1029/2000jc900005.

Billups, K., and D. P. Schrag (2003), Application of benthic foraminiferal Mg/Ca ratios to questions of Cenozoic climate change, *Earth Planet. Sci Lett.*, *209*(1-2), 181–195, doi:10.1016/S0012-821X(03)00067-0.

Blaauw, M., and J. A. Christen (2011), Flexible Paleoclimate Age-Depth Models Using an Autoregressive Gamma Process, *Bayesian Analysis*, *6*, 457–474, doi:10.1214/11-BA618.

Böhm, E., J. Lippold, M. Gutjahr, M. Frank, P. Blaser, B. Antz, J. Fohlmeister, N. Frank, M. B. Andersen, and M. Deininger (2014), Strong and deep Atlantic meridional overturning circulation during the last glacial cycle, *Nature*, 1–17, doi:10.1038/nature14059.

Braconnot, P., S. P. Harrison, M. Kageyama, P. J. Bartlein, V. Masson-Delmotte, A. Abe-Ouchi, B. L. Otto-Bliesner, and Y. Zhao (2012), Evaluation of climate models using palaeoclimatic data, *Nature Clim. Change*, *2*(6), 417–424, doi:10.1038/nclimate1456.

Bretherton, C. S., M. Widmann, V. P. Dymnikov, J. M. Wallace, and I. Bladé (1999), The effective number of spatial degrees of freedom of a time-varying field, *J. Climate*, *12*(7), 1990–2009, doi:10.1175/1520-0442(1999)012<1990:tenosd>2.0.co;2.

Bryden, H. L., H. R. Longworth, and S. A. Cunningham (2005), Slowing of the Atlantic meridional overturning circulation at 25°N, *Nature*, *438*(7068), 655–657, doi:10.1038/nature04385.

Caley, T., and D. M. Roche (2015), Modeling water isotopologues during the last glacial: Implications for quantitative paleosalinity reconstruction, *Paleoceanography*, *30*(6), 739–750, doi:10.1002/2014PA002720.

Chang, P., R. Zhang, W. Hazeleger, C. Wen, X. Wan, L. Ji, R. J. Haarsma, W.-P.

Breugem, and H. Seidel (2008), Oceanic link between abrupt changes in the North Atlantic Ocean and the African monsoon, *Nature Geosci.*, *1*(7), 444–448, doi:10.1038/ngeo218.

Chang, Y.-L., and L. Y. Oey (2013), Loop Current Growth and Eddy Shedding Using Models and Observations: Numerical Process Experiments and Satellite Altimetry Data, *J. Phys. Oceanogr.*, *43*(3), 669–689, doi:10.1175/JPO-D-12-0139.1.

Cheng, W., J. C. H. Chiang, and D. Zhang (2013), Atlantic Meridional Overturning Circulation (AMOC) in CMIP5 Models: RCP and Historical Simulations, *J. Climate*, *26*(18), 7187–7197, doi:10.1175/JCLI-D-12-00496.1.

Clemens, S. C., W. L. Prell, and Y. Sun (2010), Orbital-scale timing and mechanisms driving Late Pleistocene Indo-Asian summer monsoons: Reinterpreting cave speleothem δ18O, *Paleoceanography*, *25*(4), PA4207–19, doi:10.1029/2010PA001926.

Conroy, J. L., K. M. Cobb, J. Lynch-Stieglitz, and P. J. Polissar (2014), Constraints on the salinity–oxygen isotope relationship in the central tropical Pacific Ocean, *Mar. Chem.*, *161*(C), 26–33, doi:10.1016/j.marchem.2014.02.001.

Cook, E. R., and K. Peters (1981), The smoothing spline: a new approach to standardizing forest interior tree-ring width series for dendroclimatic studies, *Tree-Ring Bulletin*, *41*.

Cook, E. R., K. J. Anchukaitis, B. M. Buckley, R. D. D'Arrigo, G. C. Jacoby, and W. E. Wright (2010), Asian Monsoon Failure and Megadrought During the Last Millennium, *Science*, *328*(5977), 486–489, doi:10.1126/science.1185188.

d'Orbigny, A. (1826), Tableau méthodique de la classe des Céphalopodes, *Annales des Sciences Naturelles*, *7*, 245–314.

Dekens, P. S., D. W. Lea, D. K. Pak, and H. J. Spero (2002), Core top calibration of Mg/Ca in tropical foraminifera: Refining paleotemperature estimation, *Geochem. Geophys. Geosyst.*, *3*(4), 1–29, doi:10.1029/2001GC000200.

Deuser, W. G. (1987), Seasonal Variations in Isotopic Composition and Deep-Water Fluxes of the Tests of Perennially Abundant Planktonic Foraminifera of the Sargasso Sea: Results From Sediment-Trap Collections and Their Paleoceanographic Significance, *J. Foraminiferal Res.*, *17*(1), 14–27,

doi:10.2113/gsjfr.17.1.14.

Dueñas-Bohórquez, A., R. E. da Rocha, A. Kuroyanagi, L. J. de Nooijer, J. Bijma, and G.-J. Reichart (2011), Interindividual variability and ontogenetic effects on Mg and Sr incorporation in the planktonic foraminifer Globigerinoides sacculifer, *Geochim. Cosmochim. Acta*, *75*(2), 520–532, doi:10.1016/j.gca.2010.10.006.

Ebisuzaki, W. (1997), A method to estimate the statistical significance of a correlation when the data are serially correlated, *J. Climate*, *10*(9), 2147–2153, doi:10.1175/1520-0442(1997)010<2147:amtets>2.0.co;2.

Efron, B. (1979), Bootstrap methods: another look at the jackknife, *Ann. Stat.*, *7*(1), 1–26, doi:10.1214/aos/1176344552.

Elderfield, H., and G. M. Ganssen (2000), Past temperature and δ18O of surface ocean waters inferred from foraminiferal Mg/Ca ratios, *Nature*, *405*, 442–445.

Elderfield, H., P. Ferretti, M. Greaves, S. Crowhurst, I. N. McCave, D. A. Hodell, and A. M. Piotrowski (2012), Evolution of ocean temperature and ice volume through the Mid-Pleistocene climate transition, *Science*, *337*, 704–709, doi:10.1594/PANGAEA.786205.

Enfield, D. B., A. M. Mestas-Nuñez, and P. J. Trimble (2001), The Atlantic Multidecadal Oscillation and its relation to rainfall and river flows in the continental U.S, *Geophys. Res. Lett.*, *28*(10), 2077–2080, doi:10.1029/2000gl012745.

Epstein, S., and T. Mayeda (1953), Variation of O-18 Content of Waters From Natural Sources, *Geochim. Cosmochim. Acta*, *4*(5), 213–224, doi:10.1016/0016-7037(53)90051-9.

Evans, M. N., S. E. Tolwinski-Ward, D. M. Thompson, and K. J. Anchukaitis (2013), Applications of proxy system modeling in high resolution paleoclimatology, *Quat. Sci. Rev.*, *76*(C), 16–28, doi:10.1016/j.quascirev.2013.05.024.

Ezat, M. M., T. L. Rasmussen, and J. Groeneveld (2014), Persistent intermediate water warming during cold stadials in the southeastern Nordic seas during the past 65 k.y, *Geol.*, *42*(8), 663–666, doi:10.1130/G35579.1.

Fairbanks, R. G., M. Sverdlove, R. Free, and P. H. Wiebe (1982), Vertical distribution and isotopic fractionation of living planktonic foraminifera from

the Panama Basin, *Nature*, *298*(5877), 841–844, doi:10.1038/298841a0.

Farmer, E. C., A. Kaplan, P. B. de Menocal, and J. Lynch-Stieglitz (2007), Corroborating ecological depth preferences of planktonic foraminifera in the tropical Atlantic with the stable oxygen isotope ratios of core top specimens, *Paleoceanography*, *22*(3), PA3205, doi:10.1029/2006PA001361.

Ferguson, J. E., G. M. Henderson, M. Kucera, and R. E. M. Rickaby (2008), Systematic change of foraminiferal Mg/Ca ratios across a strong salinity gradient, *Earth Planet. Sci Lett.*, *265*(1-2), 153–166, doi:10.1016/j.epsl.2007.10.011.

Galloway, J. J., and S. G. Wissler (1927), Pleistocene Foraminifera from the Lomita Quarry, Palos Verdes Hills, California, *J. Paleontol.*, *1*(1), 35–87, doi:10.2307/1298073?ref=search-gateway:d45cc7e1d484928c8161a3d53bdd613e.

Ganssen, G. M., F. J. C. Peeters, B. Metcalfe, P. Anand, S. J. A. Jung, D. Kroon, and G.-J. A. Brummer (2010), Quantifying sea surface temperature ranges of the Arabian Sea for the past 20 000 years, *Clim. Past Discuss.*, *6*(6), 2795–2814, doi:10.5194/cpd-6-2795-2010.

Goff, J. A., L. Lugrin, S. P. Gulick, Y. M. Okumura, and K. Thirumalai (2015), Oyster reef die-offs in stratigraphic record of Corpus Christi Bay, Texas, possibly caused by drought-driven extreme salinity changes, *The Holocene*, 1–9, doi:10.1177/0959683615612587.

Goodkin, N. F., K. A. Hughen, W. B. Curry, S. C. Doney, and D. R. Ostermann (2008), Sea surface temperature and salinity variability at Bermuda during the end of the Little Ice Age, *Paleoceanography*, *23*(3), PA3203, doi:10.1029/2007PA001532.

Gopalakrishnan, G., B. D. Cornuelle, I. Hoteit, D. L. Rudnick, and W. B. Owens (2013), State estimates and forecasts of the loop current in the Gulf of Mexico using the MITgcm and its adjoint, *J. Geophys. Res. Oceans*, *118*(7), 3292–3314, doi:10.1002/jgrc.20239.

Grant, K. M., E. J. Rohling, M. Bar-Matthews, A. Ayalon, M. Medina-Elizalde, C. B. Ramsey, C. Satow, and A. P. Roberts (2012), Rapid coupling between ice volume and polar temperature over the past 150,000 years, *Nature*, *491*(7426), 744–747, doi:10.1038/nature11593.

Greaves, M. et al. (2008), Interlaboratory comparison study of calibration

standards for foraminiferal Mg/Ca thermometry, *Geochem. Geophys. Geosyst.*, *9*(8), 1–27, doi:10.1029/2008GC001974.

Hall, P., and M. A. Martin (1988), On bootstrap resampling and iteration, *Biometrika*, *75*(4), 661–671, doi:10.2307/2336307.

Hathorne, E. C. et al. (2013), Interlaboratory study for coral Sr/Ca and other element/Ca ratio measurements, *Geochem. Geophys. Geosyst.*, *14*(9), 3730–3750, doi:10.1002/ggge.20230.

Haug, G. H., K. A. Hughen, D. M. Sigman, L. C. Peterson, and U. Röhl (2001), Southward Migration of the Intertropical Convergence Zone Through the Holocene, *Science*, *293*(5533), 1304–1308, doi:10.1126/science.1059725.

Hertzberg, J. E., and M. W. Schmidt (2013), Refining Globigerinoides ruber Mg/Ca paleothermometry in the Atlantic Ocean, *Earth Planet. Sci Lett.*, *383*(C), 123–133, doi:10.1016/j.epsl.2013.09.044.

Holloway, M. D., L. C. Sime, J. S. Singarayer, J. C. Tindall, and P. J. Valdes (2016), Reconstructing paleosalinity from $\delta^{18}O$: Coupled model simulations of the Last Glacial Maximum, Last Interglacial and Late Holocene, *Quat. Sci. Rev.*, *131*(Part B), 350–364, doi:10.1016/j.quascirev.2015.07.007.

Hönisch, B., K. A. Allen, D. W. Lea, H. J. Spero, S. M. Eggins, J. A. Arbuszewski, P. B. deMenocal, Y. Rosenthal, A. D. Russell, and H. Elderfield (2013), The influence of salinity on Mg/Ca in planktic foraminifers – Evidence from cultures, core-top sediments and complementary $\delta^{18}O$, *Geochim. Cosmochim. Acta*, *121*, 196–213, doi:10.1016/j.gca.2013.07.028.

Huybers, P., and C. Wunsch (2004), A depth-derived Pleistocene age model: Uncertainty estimates, sedimentation variability, and nonlinear climate change, *Paleoceanography*, *19*(1), PA1028, doi:10.1029/2002PA000857.

Jungclaus, J. H., K. Lohmann, and D. Zanchettin (2014), Enhanced 20th-century heat transfer to the Arctic simulated in the context of climate variations over the last millennium, *Clim. Past*, *10*(6), 2201–2213, doi:10.5194/cp-10-2201-2014.

Jungclaus, J. H., N. Fischer, H. Haak, K. C. Lohmann, J. Marotzke, D. Matei, U. Mikolajewicz, D. Notz, and J. S. von Storch (2013), Characteristics of the ocean simulations in the Max Planck Institute Ocean Model (MPIOM) the ocean component of the MPI-Earth system model, *J. Adv. Model. Earth Syst.*, *5*(2), 422–446, doi:10.1002/jame.20023.

Kawahata, H. (2005), Stable isotopic composition of two morphotypes of Globigerinoides ruber (white) in the subtropical gyre in the North Pacific, *Paleontol. Res.*, *9*(1), 27–35, doi:10.2517/prpsj.9.27.

Kawahata, H., A. Nishimura, and M. K. Gagan (2002), Seasonal change in foraminiferal production in the western equatorial Pacific warm pool: evidence from sediment trap experiments, *Deep Sea Res. Part II*.

Khider, D., G. Huerta, C. Jackson, L. D. Stott, and J. Emile-Geay (2015), A Bayesian, multivariate calibration for Globigerinoides ruber Mg/Ca, *Geochem. Geophys. Geosyst.*, *16*, 1–17, doi:10.1002/2015GC005844.

Kilbourne, K. H., T. M. Quinn, R. Webb, T. P. Guilderson, J. Nyberg, and A. Winter (2008), Paleoclimate proxy perspective on Caribbean climate since the year 1751: Evidence of cooler temperatures and multidecadal variability, *Paleoceanography*, *23*, PA3220, doi:10.1029/2008PA001598.

Killingley, J. S., R. F. Johnson, and W. H. Berger (1981), Oxygen and carbon isotopes of individual shells of planktonic foraminifera from Ontong-Java Plateau, equatorial Pacific, *Palaeogeogr. Palaeoclim. Palaeoecol.*, *33*(1-3), 193–204, doi:10.1016/0031-0182(81)90038-9.

Krebs, U., and A. Timmermann (2007), Tropical Air–Sea Interactions Accelerate the Recovery of the Atlantic Meridional Overturning Circulation after a Major Shutdown, *J. Climate*, *20*(19), 4940–4956, doi:10.1175/JCLI4296.1.

Kuroyanagi, A., and H. Kawahata (2004), Vertical distribution of living planktonic foraminifera in the seas around Japan, *Mar. Micropaleontol.*, *53*(1-2), 173–196, doi:10.1016/j.marmicro.2004.06.001.

Kushnir, Y., R. Seager, M. Ting, N. Naik, and J. Nakamura (2010), Mechanisms of Tropical Atlantic SST Influence on North American Precipitation Variability*, *J. Climate*, *23*(21), 5610–5628, doi:10.1175/2010JCLI3172.1.

Kısakürek, B., A. Eisenhauer, F. Böhm, D. Garbe-Schönberg, and J. Erez (2008), Controls on shell Mg/Ca and Sr/Ca in cultured planktonic foraminiferan, Globigerinoides ruber (white), *Earth Planet. Sci Lett.*, *273*(3-4), 260–269, doi:10.1016/j.epsl.2008.06.026.

Lachniet, M. S., J. P. Bernal, Y. Asmerom, V. J. Polyak, and D. R. Piperno (2012), A 2400 yr Mesoamerican rainfall reconstruction links climate and cultural change, *Geol.*, *40*(3), 259–262, doi:10.1130/G32471.1.

Laepple, T., and P. Huybers (2014), Ocean surface temperature variability: Large model–data differences at decadal and longer periods, *Proc. Nat. Acad. Sci.*, *111*(47), 16682–16687, doi:10.1073/pnas.1412077111.

Lambeck, K., H. Rouby, A. Purcell, Y. Sun, and M. Sambridge (2014), Sea level and global ice volumes from the Last Glacial Maximum to the Holocene, *Proc. Nat. Acad. Sci.*, *111*(43), 15296–15303, doi:10.1073/pnas.1411762111.

Landrum, L., B. L. Otto-Bliesner, E. R. Wahl, A. Conley, P. J. Lawrence, N. Rosenbloom, and H. Teng (2013), Last Millennium Climate and Its Variability in CCSM4, *J. Climate*, *26*(4), 1085–1111, doi:10.1175/JCLI-D-11-00326.1.

Lea, D. W. (2004), The 100 000-yr cycle in tropical SST, greenhouse forcing, and climate sensitivity, *J. Climate*, doi:10.1175/1520-0442(2004)017%3C2170:TYCITS%3E2.0.CO%3B2.

Lea, D. W., D. K. Pak, and H. J. Spero (2000), Climate Impact of Late Quaternary Equatorial Pacific Sea Surface Temperature Variations, *Science*, *289*(5485), 1719–1724, doi:10.1126/science.289.5485.1719.

Lea, D. W., T. A. Mashiotta, and H. J. Spero (1999), Controls on magnesium and strontium uptake in planktonic foraminifera determined by live culturing, *Geochim. Cosmochim. Acta*, *63*(16), 2369–2379, doi:10.1016/s0016-7037(99)00197-0.

Lear, C. H., H. Elderfield, and P. A. Wilson (2000), Cenozoic deep-sea temperatures and global ice volumes from Mg/Ca in benthic foraminiferal calcite, *Science*, *287*(5451), 269–272, doi:10.1126/science.287.5451.269.

Lear, C. H., H. K. Coxall, G. L. Foster, D. J. Lunt, E. M. Mawbey, Y. Rosenthal, S. M. Sosdian, E. Thomas, and P. A. Wilson (2015), Neogene ice volume and ocean temperatures: Insights from infaunal foraminiferal Mg/Ca paleothermometry, *Paleoceanography*, *30*(11), 1437–1454, doi:10.1002/2015PA002833.

Leduc, G., L. Vidal, K. Tachikawa, F. Rostek, C. Sonzogni, L. Beaufort, and E. Bard (2007), Moisture transport across Central America as a positive feedback on abrupt climatic changes, *Nature*, *445*(7130), 908–911, doi:10.1038/nature05578.

LeGrande, A. N., and G. A. Schmidt (2006), Global gridded data set of the oxygen isotopic composition in seawater, *Geophys. Res. Lett.*, *33*(12), L12604–5, doi:10.1029/2006GL026011.

Lin, H.-L., W.-C. Wang, and G.-W. Hung (2004), Seasonal variation of planktonic foraminiferal isotopic composition from sediment traps in the South China Sea, *Mar. Micropaleontol.*, *53*(3-4), 447–460, doi:10.1016/j.marmicro.2004.08.004.

Liu, H., C. Wang, S.-K. Lee, and D. B. Enfield (2012a), Atlantic Warm-Pool Variability in the IPCC AR4 CGCM Simulations, *J. Climate*, *25*(16), 5612–5628, doi:10.1175/JCLI-D-11-00376.1.

Liu, Q., Y. Jia, P. Liu, Q. Wang, and P. C. Chu (2001), Seasonal and intraseasonal thermocline variability in the central south China Sea, *Geophys. Res. Lett.*, *28*(23), 4467–4470, doi:10.1029/2001gl013185.

Liu, Y., S.-K. Lee, B. A. Muhling, J. T. Lamkin, and D. B. Enfield (2012b), Significant reduction of the Loop Current in the 21st century and its impact on the Gulf of Mexico, *J. Geophys. Res.*, *117*(C5), C05039–8, doi:10.1029/2011JC007555.

LoDico, J. M., B. P. Flower, and T. M. Quinn (2006), Subcentennial-scale climatic and hydrologic variability in the Gulf of Mexico during the early Holocene, *Paleoceanography*, *21*(3), PA3015, doi:10.1029/2005PA001243.

Löwemark, L., W.-L. Hong, T.-F. Yui, and G.-W. Hung (2005), A test of different factors influencing the isotopic signal of planktonic foraminifera in surface sediments from the northern South China Sea, *Mar. Micropaleontol.*, *55*(1-2), 49–62, doi:10.1016/j.marmicro.2005.02.004.

Lund, D. C., and W. B. Curry (2006), Florida Current surface temperature and salinity variability during the last millennium, *Paleoceanography*, *21*(2), PA2009–15, doi:10.1029/2005PA001218.

Lund, D. C., J. Lynch-Stieglitz, and W. B. Curry (2006), Gulf Stream density structure and transport during the past millennium, *Nature*, *444*(7119), 601–604, doi:10.1038/nature05277.

Mahajan, S., R. Zhang, and T. L. Delworth (2011), Impact of the Atlantic Meridional Overturning Circulation (AMOC) on Arctic Surface Air Temperature and Sea Ice Variability, *J. Climate*, *24*(24), 6573–6581, doi:10.1175/2011JCLI4002.1.

Mann, H. B., and D. R. Whitney (1947), On a test of whether one of two random variables is stochastically larger than the other, *Ann. Math. Stat.*, *18*(1), 50–60, doi:10.1214/aoms/1177730491.

Marcott, S. A., P. U. Clark, and L. Padman (2011), Ice-shelf collapse from subsurface warming as a trigger for Heinrich events, *Proc. Nat. Acad. Sci.*, *108*(33), 13415–13419, doi:10.1073/pnas.1104772108/-/DCSupplemental/pnas.1104772108_SI.pdf.

Marino, G., E. J. Rohling, L. Rodríguez-Sanz, K. M. Grant, D. Heslop, A. P. Roberts, J. D. Stanford, and J. Yu (2015), Bipolar seesaw control on last interglacial sea level, *Nature*, *522*(7555), 197–201, doi:10.1038/nature14499.

Marino, G., R. Zahn, M. Ziegler, C. Purcell, G. Knorr, I. R. Hall, P. Ziveri, and H. Elderfield (2013), Agulhas salt-leakage oscillations during abrupt climate changes of the Late Pleistocene, *Paleoceanography*, *28*(3), 599–606, doi:10.1002/palo.20038.

Masson-Delmotte, V. et al. (2013), *Information from Paleoclimate archives In Climate Change 2013: the Physical Science Basis. Contribution of Working Group I to the Fifth Assessment Report of the Intergovernmental Panel on Climate Change*, edited by T. F. Stocker, D. Qin, G.-K. Plattner, M. Tignor, S. K. Allen, J. Boschung, A. Nauels, Y. Xia, V. Bex, and P. Midgley, Cambridge University Press, Cambridge, United Kingdom and New York, NY, USA.

McGregor, H. V. et al. (2015), Robust global ocean cooling trend for the pre-industrial Common Era, *Nature Geosci.*, *8*(9), 671–677, doi:10.1038/ngeo2510.

Medina-Elizalde, M., D. W. Lea, and M. S. Fantle (2008), Implications of seawater Mg/Ca variability for Plio-Pleistocene tropical climate reconstruction, *Earth Planet. Sci Lett.*, *269*(3-4), 585–595, doi:10.1016/j.epsl.2008.03.014.

Mignot, J., and C. Frankignoul (2004), Interannual to interdecadal variability of sea surface salinity in the Atlantic and its link to the atmosphere in a coupled model, *J. Geophys. Res.*, *109*(C4), C04005–14, doi:10.1029/2003JC002005.

Miller, G. H. et al. (2012), Abrupt onset of the Little Ice Age triggered by volcanism and sustained by sea-ice/ocean feedbacks, *Geophys. Res. Lett.*, *39*(2), L02708, doi:10.1029/2011GL050168.

Mix, A. C., A. E. Morey, N. G. Pisias, and S. W. Hostetler (1999), Foraminiferal faunal estimates of paleotemperature: Circumventing the No-analog problem yields cool Ice Age tropics, *Paleoceanography*, *14*(3), 350–359, doi:10.1029/1999pa900012.

Mix, A. C., and W. F. Ruddiman (1984), Oxygen-isotope analyses and Pleistocene ice volumes, *Quat. Res.*, *21*(1), 1–20, doi:10.1016/0033-5894(84)90085-1.

Moffa-Sanchez, P., A. Born, I. R. Hall, D. J. R. Thornalley, and S. Barker (2014a), Solar forcing of North Atlantic surface temperature and salinity over the past millennium, *Nature Geosci.*, *7*(4), 275–278, doi:10.1038/ngeo2094.

Moffa-Sanchez, P., I. R. Hall, S. Barker, D. J. R. Thornalley, and I. Yashayaev (2014b), Surface changes in the eastern Labrador Sea around the onset of the Little Ice Age, *Paleoceanography*, *29*(3), 160–175, doi:10.1002/2013PA002523.

Mohtadi, M., M. Prange, D. W. Oppo, R. De Pol-Holz, U. Merkel, X. Zhang, S. Steinke, and A. Lückge (2014), North Atlantic forcing of tropical Indian Ocean climate, *Nature*, *509*(7498), 76–80, doi:10.1038/nature13196.

Mohtadi, M., S. Steinke, J. Groeneveld, H. G. Fink, T. Rixen, D. Hebbeln, B. Donner, and B. Herunadi (2009), Low-latitude control on seasonal and interannual changes in planktonic foraminiferal flux and shell geochemistry off south Java: A sediment trap study, *Paleoceanography*, *24*, PA1201, doi:10.1029/2008PA001636.

Moreno-Chamarro, E., D. Zanchettin, K. Lohmann, and J. H. Jungclaus (2015), Internally generated decadal cold events in the northern North Atlantic and their possible implications for the demise of the Norse settlements in Greenland, *Geophys. Res. Lett.*, *42*(3), 908–915, doi:10.1002/2014gl062741.

Moreno-Chamarro, E., D. Zanchettin, K. Lohmann, and J. H. Jungclaus (2016), An abrupt weakening of the subpolar gyre as trigger of Little Ice Age-type episodes, *Clim. Dyn.*, 1–18, doi:10.1007/s00382-016-3106-7.

Morimoto, M., O. Abe, H. Kayanne, N. Kurita, E. Matsumoto, and N. Yoshida (2002), Salinity records for the 1997–98 El Niño from Western Pacific corals, *Geophys. Res. Lett.*, *29*(11), 1540–4, doi:10.1029/2001GL013521.

Nürnberg, D., A. Müller, and R. R. Schneider (2000), Paleo-sea surface temperature calculations in the equatorial east Atlantic from Mg/Ca ratios in planktic foraminifera: A comparison to sea surface temperature estimates from $U^{k'}_{37}$, oxygen isotopes, and foraminiferal transfer function, *Paleoceanography*, *15*(1), 124–134, doi:10.1029/1999pa000370.

Nürnberg, D., J. Bijma, and C. Hemleben (1996), Assessing the reliability of

magnesium in foraminiferal calcite as a proxy for water mass temperatures, *Geochim. Cosmochim. Acta*, *60*(5), 803–814, doi:10.1016/0016-7037(95)00446-7.

Nürnberg, D., M. Ziegler, C. Karas, R. Tiedemann, and M. W. Schmidt (2008), Interacting Loop Current variability and Mississippi River discharge over the past 400 kyr, *Earth Planet. Sci Lett.*, *272*(1-2), 278–289, doi:10.1016/j.epsl.2008.04.051.

Okumura, Y. M., D. Schneider, C. Deser, and R. Wilson (2012), Decadal–Interdecadal Climate Variability over Antarctica and Linkages to the Tropics: Analysis of Ice Core, Instrumental, and Tropical Proxy Data, *J. Climate*, *25*(21), 7421–7441, doi:10.1175/JCLI-D-12-00050.1.

Olesik, J. W. (1991), Elemental analysis using ICP-OES and ICP/MS, *Anal. Chem.*, *63*(1), 12A–21A, doi:10.1021/ac00001a001.

Oppo, D. W., Y. Rosenthal, and B. K. Linsley (2009), 2,000-year-long temperature and hydrology reconstructions from the Indo-Pacific warm pool, *Nature*, *460*(7259), 1113–1116, doi:10.1038/nature08233.

O'Brien, C. L., G. L. Foster, M. A. Martínez-Botí, R. Abell, J. W. B. Rae, and R. D. Pancost (2014), High sea surface temperatures in tropical warm pools during the Pliocene, *Nature Geosci.*, *7*(8), 606–611, doi:10.1038/ngeo2194.

Palter, J. B. (2015), The Role of the Gulf Stream in European Climate, *Annu. Rev. Marine. Sci.*, *7*(1), 113–137, doi:10.1146/annurev-marine-010814-015656.

Park, W., and M. Latif (2008), Multidecadal and multicentennial variability of the meridional overturning circulation, *Geophys. Res. Lett.*, *35*(22), L22703–5, doi:10.1029/2008GL035779.

Peeters, F. J. C., E. Ivanova, S. Conan, G.-J. A. Brummer, G. M. Ganssen, S. Troelstra, and J. van Hinte (1999), A size analysis of planktic foraminifera from the Arabian Sea, *Mar. Micropaleontol.*, *36*(1), 31–63, doi:10.1016/s0377-8398(98)00026-7.

Poore, R. Z., H. J. Dowsett, S. Verardo, and T. M. Quinn (2003), Millennial- to century-scale variability in Gulf of Mexico Holocene climate records, *Paleoceanography*, *18*(2), 26–1 – 26–11, doi:10.1029/2002PA000868.

Poore, R. Z., K. A. Tedesco, and J. W. Spear (2013), Seasonal Flux and Assemblage Composition of Planktic Foraminifers from a Sediment-Trap

Study in the Northern Gulf of Mexico, *J. Coastal. Res.*, *63*, 6–19, doi:10.2112/SI63-002.1.

Qu, T., H. Mitsudera, and T. Yamagata (2000), Intrusion of the North Pacific waters into the South China Sea, *J. Geophys. Res.*, *105*(C3), 6415, doi:10.1029/1999jc900323.

Ravelo, A. C., K. T. Lawrence, A. Fedorov, and H. L. Ford (2014), Comment on "A 12-million-year temperature history of the tropical Pacific Ocean," *Science*, *346*(6216), 1467–1467, doi:10.1126/science.1257618.

Rayner, N. A., D. E. Parker, E. B. Horton, C. K. Folland, L. V. Alexander, D. P. Rowell, E. C. Kent, and A. Kaplan (2003), Global analyses of sea surface temperature, sea ice, and night marine air temperature since the late nineteenth century, *J. Geophys. Res.*, *108*(D14), 4407–37, doi:10.1029/2002JD002670.

Reimer, P. J. et al. (2013), Intcal13 and Marine13 Radiocarbon Age Calibration Curves 0-50,000 Years Cal Bp, *Radiocarbon*, *55*(4), 1869–1887.

Reuter, J., L. D. Stott, D. Khider, A. Sinha, H. Cheng, and R. L. Edwards (2009), A new perspective on the hydroclimate variability in northern South America during the Little Ice Age, *Geophys. Res. Lett.*, *36*(21), L21706–5, doi:10.1029/2009GL041051.

Richey, J. N., R. Z. Poore, B. P. Flower, and T. M. Quinn (2007), 1400 yr multiproxy record of climate variability from the northern Gulf of Mexico, *Geol.*, *35*(5), 423–4, doi:10.1130/G23507A.1.

Richey, J. N., R. Z. Poore, B. P. Flower, T. M. Quinn, and D. J. Hollander (2009), Regionally coherent Little Ice Age cooling in the Atlantic Warm Pool, *Geophys. Res. Lett.*, *36*(21), L21703–5, doi:10.1029/2009GL040445.

Robbins, J. A., E. L. Grossman, J. Morales, R. Thompson, and A. O'Dea (2012), Seasonal oxygen isotopic variations in marine waters from the Caribbean and Pacific coasts of Panama, p. 2063, San Francisco.

Robbins, L. L., and N. Healy-Williams (1991), Toward a classification of planktonic foraminifera based on biochemical, geochemical, and morphological criteria, *J. Foraminiferal Res.*, *21*(2), 159–167, doi:10.2113/gsjfr.21.2.159.

Rohling, E. J. (2000), Paleosalinity: confidence limits and future applications,

Mar. Geol., *163*(1-4), 1–11, doi:10.1016/s0025-3227(99)00097-3.

Rohling, E. J., and G. R. Bigg (1998), Paleosalinity and $\delta^{18}O$: A critical assessment, *J. Geophys. Res.*, *103*(C1), 1307, doi:10.1029/97jc01047.

Rohling, E. J., G. L. Foster, K. M. Grant, G. Marino, A. P. Roberts, M. E. Tamisiea, and F. Williams (2014), Sea-level and deep-sea-temperature variability over the past 5.3 million years, *Nature*, *508*(7497), 1–15, doi:10.1038/nature13230.

Ruggieri, E. (2012), A Bayesian approach to detecting change points in climatic records, *Int. J. Climatol.*, *33*(2), 520–528, doi:10.1002/joc.3447.

Ruxton, G. D. (2006), The unequal variance t-test is an underused alternative to Student's t-test and the Mann-Whitney U test, *Behavioral Ecology*, *17*(4), 688–690, doi:10.1093/beheco/ark016.

Ryu, J.-H., and K. Hayhoe (2014), Regional and large-scale influences on seasonal to interdecadal variability in Caribbean surface air temperature in CMIP5 simulations, *Clim. Dyn.*, *45*(1-2), 455–475, doi:10.1007/s00382-014-2351-x.

Saenger, C., R. E. Came, D. W. Oppo, L. D. Keigwin, and A. L. Cohen (2011), Regional climate variability in the western subtropical North Atlantic during the past two millennia, *Paleoceanography*, *26*, PA2206, doi:10.1029/2010PA002038.

Schiffelbein, P., and S. Hills (1984), Direct assessment of stable isotope variability in planktonic foraminifera populations, *Palaeogeogr. Palaeoclim. Palaeoecol.*, *48*(2-4), 197–213, doi:10.1016/0031-0182(84)90044-0.

Schmidt, G. A. (1999a), Error analysis of paleosalinity calculations, *Paleoceanography*, *14*(3), 422–429, doi:10.1029/1999pa900008.

Schmidt, G. A. (1999b), Forward modeling of carbonate proxy data from planktonic foraminifera using oxygen isotope tracers in a global ocean model, *Paleoceanography*, *14*(4), 482–497, doi:10.1029/1999pa900025.

Schmidt, G. A. et al. (2011), Climate forcing reconstructions for use in PMIP simulations of the last millennium (v1.0), *Geosci. Model Dev.*, *4*(1), 33–45, doi:10.5194/gmd-4-33-2011.

Schmidt, G. A., and S. Mulitza (2002), Global calibration of ecological models for

planktic foraminifera from coretop carbonate oxygen-18, *Mar. Micropaleontol.*, *44*(3-4), 125–140, doi:10.1016/s0377-8398(01)00041-x.

Schmidt, M. W., H. J. Spero, and D. W. Lea (2004), Links between salinity variation in the Caribbean and North Atlantic thermohaline circulation, *Nature*, *428*(6979), 1–4, doi:10.1038/nature02346.

Schneider, R. (2014), Climate science: Sea levels from ancient seashells, *Nature*, *508*(7497), 465–466, doi:10.1038/nature13328.

Schneider, T., T. Bischoff, and G. H. Haug (2014), Migrations and dynamics of the intertropical convergence zone, *Nature*, *513*(7516), 45–53, doi:10.1038/nature13636.

Schrag, D. P. (1999), Rapid analysis of high-precision Sr/Ca ratios in corals and other marine carbonates, *Paleoceanography*, *14*(2), 97–102.

Shackleton, N. J. (1967), Oxygen isotope analyses and Pleistocene temperatures re-assessed, *Nature*, *215*(5096), 15–17, doi:10.1038/215015a0.

Shackleton, N. J. (1987), Oxygen isotopes, ice volume and sea level, *Quat. Sci. Rev.*, *6*(3-4), 183–190, doi:10.1016/0277-3791(87)90003-5.

Shanahan, T. M., J. T. Overpeck, K. J. Anchukaitis, J. W. Beck, J. E. Cole, D. L. Dettman, J. A. Peck, C. A. Scholz, and J. W. King (2009), Atlantic Forcing of Persistent Drought in West Africa, *Science*, *324*(5925), 1–4, doi:10.1126/science.1166352.

Shapiro, S. S., and M. B. Wilk (1965), An analysis of variance test for normality (complete samples), *Biometrika*, *52*(3/4), 591, doi:10.2307/2333709.

Spear, J. W., and R. Z. Poore (2011), *Seasonal Flux and Assemblage Composition of Planktic Foraminifera from the Northern Gulf of Mexico, 2008-2009*.

Spero, H. J., and D. F. Williams (1989), Opening the carbon isotope “vital effect” black box 1. Seasonal temperatures in the euphotic zone, *Paleoceanography*, *4*(6), 593–601, doi:10.1029/pa004i006p00593.

Spero, H. J., J. Bijma, D. W. Lea, and B. E. Bemis (1997), Effect of seawater carbonate concentration on foraminiferal carbon and oxygen isotopes, *Nature*, *390*.

Spero, H. J., K. M. Mielke, E. M. Kalve, D. W. Lea, and D. K. Pak (2003), Multispecies approach to reconstructing eastern equatorial Pacific thermocline hydrography during the past 360 kyr, *Paleoceanography*, *18*(1), 1022, doi:10.1029/2002PA000814.

Spero, H. J., S. M. Eggins, A. D. Russell, L. Vetter, M. R. Kilburn, and B. Hönisch (2015), Timing and mechanism for intratest Mg/Ca variability in a living planktic foraminifer, *Earth Planet. Sci Lett.*, *409*(C), 32–42, doi:10.1016/j.epsl.2014.10.030.

Srinivasan, M. S., J. P. Kennett, and A. W. H. Bé (1974), Globorotalia menardii neoflexuosa new subspecies from the northern Indian Ocean, *Deep-Sea Res.*, *21*(4), 321–324, doi:10.1016/0011-7471(74)90103-x.

Srokosz, M. A., and H. L. Bryden (2015), Observing the Atlantic Meridional Overturning Circulation yields a decade of inevitable surprises, *Science*, *348*(6241), 1255575–1255575, doi:10.1126/science.1255575.

Steinke, S., H.-Y. Chiu, P.-S. Yu, C.-C. Shen, L. Löwemark, H.-S. Mii, and M.-T. Chen (2005), Mg/Ca ratios of two *Globigerinoides ruber* (white) morphotypes: Implications for reconstructing past tropical/subtropical surface water conditions, *Geochem. Geophys. Geosyst.*, *6*(11), Q11005, doi:10.1029/2005GC000926.

Thirumalai, K., A. Singh, and R. Ramesh (2011), A MATLAB™ code to perform weighted linear regression with (correlated or uncorrelated) errors in bivariate data, *J. Geol. Soc. India*, *77*(4), 377–380, doi:10.1007/s12594-011-0044-1.

Thirumalai, K., J. N. Richey, T. M. Quinn, and R. Z. Poore (2014), *Globigerinoides ruber* morphotypes in the Gulf of Mexico: A test of null hypothesis, *Sci. Rep.*, *4*, 1–7, doi:10.1038/srep06018.

Thirumalai, K., J. W. Partin, C. S. Jackson, and T. M. Quinn (2013), Statistical constraints on El Niño Southern Oscillation reconstructions using individual foraminifera: A sensitivity analysis, *Paleoceanography*, *28*(3), 401–412, doi:10.1002/palo.20037.

Thirumalai, K., T. M. Quinn, and G. Marino (2016), Constraining past seawater $\delta^{18}O$ and temperature records developed from foraminiferal geochemistry, *Paleoceanography*.

Tierney, J. E., F. S. R. Pausata, and P. B. deMenocal (2015a), Deglacial Indian monsoon failure and North Atlantic stadials linked by Indian Ocean

surface cooling, *Nature Geosci.*, 1–6, doi:10.1038/ngeo2603.

Tierney, J. E., N. J. Abram, K. J. Anchukaitis, M. N. Evans, C. Giry, K. H. Kilbourne, C. P. Saenger, H. C. Wu, and J. Zinke (2015b), Tropical sea surface temperatures for the past four centuries reconstructed from coral archives, *Paleoceanography*, 1–27, doi:10.1002/(ISSN)1944-9186.

Timmermann, A., J. Sachs, and O. E. Timm (2014), Assessing divergent SST behavior during the last 21 ka derived from alkenones and G. ruber-Mg/Ca in the equatorial Pacific, *Paleoceanography*, doi:10.1002/(ISSN)1944-9186.

Tindall, J. C., and A. M. Haywood (2015), Modeling oxygen isotopes in the Pliocene: Large-scale features over the land and ocean, *Paleoceanography*, *30*(9), 1183–1201, doi:10.1002/2014PA002774.

Trauth, M. H. (2013), TURBO2: A MATLAB simulation to study the effects of bioturbation on paleoceanographic time series, *Computers & Geosciences*, *61*(C), 1–10, doi:10.1016/j.cageo.2013.05.003.

Trauth, M. H., M. Sarnthein, and M. Arnold (1997), Bioturbational mixing depth and carbon flux at the seafloor, *Paleoceanography*, *12*(3), 517–526, doi:10.1029/97pa00722.

Van den Broeck, E. (1876), Etude sur les Foraminiferes de la Barbade (Antilles), *Ann. Soc. Belge. Microsc.*, *1*, 55–152.

Vellinga, M., and R. A. Wood (2002), Global climatic impacts of a collapse of the Atlantic thermohaline circulation, *Climatic Change*, *54*(3), 251–267, doi:10.1023/A:1016168827653.

Vinther, B. M. et al. (2006), A synchronized dating of three Greenland ice cores throughout the Holocene, *J. Geophys. Res.*, *111*(D13), D13102–11, doi:10.1029/2005JD006921.

Waelbroeck, C. et al. (2009), Constraints on the magnitude and patterns of ocean cooling at the Last Glacial Maximum, *Nature Geosci.*, *2*(2), 127–132, doi:10.1038/ngeo411.

Waelbroeck, C., L. Labeyrie, E. Michel, J.-C. Duplessy, J. F. McManus, K. Lambeck, E. Balbon, and M. Labracherie (2001), Sea-level and deep water temperature changes derived from benthic foraminifera isotopic records, *Quat. Sci. Rev.*, *21*(1-3), 1–11, doi:10.1016/s0277-3791(01)00101-9.

Wagner, A. J., T. P. Guilderson, and N. C. Slowey (2009), Pre-bomb surface water radiocarbon of the Gulf of Mexico and Caribbean as recorded in hermatypic corals, *Radiocarbon*, *51*(3), 947–954.

Wanamaker, A. D., P. G. Butler, J. D. Scourse, J. Heinemeier, J. Eiríksson, K. L. Knudsen, and C. A. Richardson (2012), Surface changes in the North Atlantic meridional overturning circulation during the last millennium, *Nature Commun.*, *3*, 899–7, doi:10.1038/ncomms1901.

Wang, J., J. Emile-Geay, D. Guillot, N. P. McKay, and B. Rajaratnam (2015), Fragility of reconstructed temperature patterns over the Common Era: Implications for model evaluation, *Geophys. Res. Lett.*, *42*, 1–9, doi:10.1002/2015GL065265.

Wang, L. (2000), Isotopic signals in two morphotypes of *Globigerinoides ruber* (white) from the South China Sea: implications for monsoon climate change during the last glacial cycle, *Palaeogeogr. Palaeoclim. Palaeoecol.*, *161*(3-4), 381–394, doi:10.1016/s0031-0182(00)00094-8.

Welch, B. L. (1947), The Generalization of “Student's” Problem When Several Different Population Varlances Are Involved, *Biometrika*, *34*(1-2), 28–35, doi:10.1093/biomet/34.1-2.28.

Weldeab, S., D. W. Lea, H. Oberhänsli, and R. R. Schneider (2014), Links between southwestern tropical Indian Ocean SST and precipitation over southeastern Africa over the last 17kyr, *Palaeogeogr. Palaeoclim. Palaeoecol.*, *410*(C), 1–13, doi:10.1016/j.palaeo.2014.06.001.

Weldeab, S., D. W. Lea, R. R. Schneider, and N. Andersen (2007), 155,000 Years of West African Monsoon and Ocean Thermal Evolution, *Science*, *316*(5829), 1303–1307, doi:10.1126/science.1140461.

Wicks, T. Z., K. Thirumalai, T. M. Shanahan, and C. J. Bell (2015), The use of δ13C values of leporid teeth as indicators of past vegetation, *Palaeogeogr. Palaeoclim. Palaeoecol.*, *418*(C), 245–260, doi:10.1016/j.palaeo.2014.11.017.

Williams, C., B. P. Flower, and D. W. Hastings (2012), Seasonal Laurentide Ice Sheet melting during the “Mystery Interval” (17.5-14.5 ka), *Geol.*, *40*(10), 955–958, doi:10.1130/G33279.1.

Williams, C., B. P. Flower, D. W. Hastings, T. P. Guilderson, K. A. Quinn, and E. A. Goddard (2010), Deglacial abrupt climate change in the Atlantic Warm Pool: A Gulf of Mexico perspective, *Paleoceanography*, *115*(4), PA4221,

doi:10.1029/2010PA001928.

Wunsch, C. (2003), Determining paleoceanographic circulations, with emphasis on the Last Glacial Maximum, *Quat. Sci. Rev.*, *22*(2-4), 1–15, doi:10.1016/s0277-3791(02)00177-4.

Wunsch, C. (2010), Towards understanding the Paleocean, *Quat. Sci. Rev.*, *29*(17-18), 1960–1967, doi:10.1016/j.quascirev.2010.05.020.

York, D., N. M. Evensen, M. L. Martínez, and J. De Basabe Delgado (2004), Unified equations for the slope, intercept, and standard errors of the best straight line, *Am. J. Phys.*, *72*(3), 367–9, doi:10.1119/1.1632486.

Zachos, J. C., M. W. Wara, S. M. Bohaty, and M. L. Delaney (2003), A transient rise in tropical sea surface temperature during the Paleocene-Eocene thermal maximum, *Science*, *302*(5650), 1551–1554, doi:10.1126/science.1090110.

Zhang, Y. G., M. Pagani, and Z. Liu (2014), A 12-Million-Year Temperature History of the Tropical Pacific Ocean, *Science*, *344*(6179), 1–4, doi:10.1126/science.1246172.